Prediction and Control of Transient Instability Using Wide Area Phasor Measurements

By

Francisco Ramon Gomez Lezama

A Thesis submitted to the Faculty of Graduate Studies of
The University of Manitoba
in partial fulfillment of the requirements of the degree of

DOCTOR OF PHILOSOPHY

Department of Electrical and Computer Engineering

University of Manitoba

Winnipeg, Manitoba

September 2011

Abstract

This thesis presents a novel technique for prediction of the transient stability status of a power system following a large disturbance such as a fault, and application of the technique for subsequent emergency control. The prediction is made based on the synchronously measured samples of the magnitudes of fundamental frequency voltage phasors at major generation/load centers. The voltage samples are taken immediately after a fault is cleared and used as inputs to a binary classifier based on support vector machines to identify the transient stability condition. The classifier is trained using examples of the post-fault recovery voltages (inputs) obtained through simulations and the corresponding stability status (output) determined using a power angle-based stability index. Studies with the New England 39-bus test system indicate that the proposed algorithm can correctly recognize when the power system is approaching transient instability. The proposed system is then applied to Venezuelan power system and Manitoba Hydro power grid to demonstrate the applicability for large practical power systems. Performance of the proposed transient stability prediction scheme under the presence of asymmetrical faults, voltage sensitive loads, unlearned network topologies and measurement noise was found to be satisfactory.

Once an impending transient instability situation has been detected, appropriate emergency control strategies are triggered to minimize the impact of this on the safe operation of the network and reduce the possibility of a blackout. This thesis examines two differ-

ent emergency control schemes: a) A fuzzy logic based emergency load and generator shedding scheme and b) A high voltage direct current (HVdc) power order reduction scheme based on synchronized phasors measurements. These strategies were developed for two power systems with contrasting characteristics: one for the Venezuelan power system which is a conventional power system completely based on alternating current (AC) transmission, and the other for the Manitoba Hydro network which heavily depend on long HVdc transmission for power transfer. The proposed wide area control systems demonstrated good performance on the Venezuelan and Manitoba Hydro power grids.

Acknowledgments

I would like to express my special gratitude to Dr. Athula Rajapakse for his support, guidance and for sharing his experiences for the successful completion of this research work. It was a privilege to work under his supervision.

I am also grateful to Dr. Udaya Annakkage for his advice and valuable discussions on practical aspects on transient stability assessment and control.

I wish to thank Dr. Ioni Fernando, Mr. David Diakiw and the personnel of the Transmission Planning Department of Manitoba Hydro for their useful inputs, and practical discussions on stability and modeling of networks with HVdc links.

I must also thank the academic and technical staff at the Department of Electrical and Computer Engineering, especially Dr. Ani Gole and Mr. Erwin Dirks for their support and technical discussions.

I would like to express my gratitude to Mr. Andrew Isaacs and the staff of Electranix Corporation for their support in system modeling along my research work.

Thanks to the administrative staff of the University of Manitoba, for their support in each step of this study, especially to Traci Hofer and Amy Dario.

Also, I would like to thank all my friends at the Power Group of the Department of Electrical and Computer Engineering of the University of Manitoba for their continuous en-

couragement and for making my studies at the University of Manitoba one of the best experiences of my life.

Thanks to my family for their great support and encouragement finalizing this important step in my professional life.

Over all the things, I would like to thank God; the foundation of this research work and my whole life. He is the inspiration and motivation of my life.

Francisco Gomez

September 2011

Dedication

To my dear wife and lovely family.

Contents

List of Tables

List of Figures

List of Symbols

t	Time
δ	Generator Rotor Angle
Y	Bus Admittance Matrix
n	Number of busses in the System
v, θ	Bus Voltage magnitude and angle respectively
P_G, Q_G	Generator bus active power injection and set point voltage respectively
P_L, Q_L	Load bus active and reactive power consumptions respectively
ω	Synchronous angular speed of the rotor
K_D, H	Damping and inertia constants of a generator respectively
P_m, P_e	Generator input mechanical power and electrical output respectively

List of Abbreviations

AC	Alternating Current
ADC	Analogue-to-digital Converter
ANN	Artificial Neural Networks
COI	Center of Inertia
CCT	Critical Clearing Time
DT	Decision Trees
DAE	Differential and Algebraic Equations
DFT	Discrete Fourier Transform
EMTP	Electromagnetic Transient Simulation Program
EAC	Equal-Area criterion
EEAC	Extended Equal Area Criterion
FACTS	Flexible AC Transmission Systems
FIS	Fuzzy Inference System
GT	Generator Tripping
GPS	Global Positioning System
HVdc	High Voltage Direct Current transmission system
LS	Load Shedding

MF	Membership Function
MAPP	Midcontinent Area Power Pool
NCS	Northern Collector System
PDC	Phasor Data Concentrator
PMU	Phasor Measurement Unit
RAS	Remedial Action Schemes
SIME	Single Machine Equivalent Method
SMIB	Single Machine Infinite Bus
SPS	Special Protection Systems
SVC	Static Reactive Power Compensation
SCADA	Supervisory Control and Data Acquisition system
SVM	Support Vector Machines
SMT	Synchronized Measurement Technology
SIPS	System Integrity Protection Systems
TDS	Time Domain Simulations
TVE	Total Vector Error
TSAT	Transient Stability Assessment Tool
WACS	Wide Area Control Systems

List of Appendices

Appendix A

Chapter 1

Introduction

This chapter presents the background, motivation, and objectives of the research. A short review of the concepts of power systems stability, operating states and the wide area measurement is also included to reinforce the background necessary to formulate the thesis objectives. The chapter ends with a short introduction to the organization of thesis.

1.1 Background

Power systems are designed to be able to adjust to various disturbances such as faults, sudden and large changes in loads or loss of generation, and continue to operate satisfactorily within the desired bounds of voltage and frequency. However, unexpected events can happen in the system leading to rotor angle, frequency or voltage instability [1]. Economic incentives and other factors have led to increased electric transmission system usage, power transfer, and changes in historic usage patterns, both among regions and within individual utilities. New transmission construction has often lagged behind these changes, resulting in lower operating margins, increasing the probability of system-wide instabilities [2].

Among the measures that can be undertaken to minimize the impact of such system-wide instabilities include the implementation of Remedial Action Schemes (RAS), also known as Special Protection Systems (SPS) or System Integrity Protection Systems (SIPS). These schemes have become more common primarily because they are less costly and quicker to permit, design, and build than other alternatives such as constructing major transmission lines and power plants[3]. Equipment-specific protection schemes that are traditionally present in power systems are not adequate for providing solutions to system-wide problems, and remedial action schemes usually require system wide measurements [4]. Modern technologies such as synchronized phasor measurement and fast and secure telecommunication capabilities allow the development of hitherto unexplored solutions against voltage, frequency or angular instability due to these large disturbances.

1.2 Power system stability

Power System Stability is defined as the ability of the system to regain an equilibrium state after being subjected to a physical disturbance. Power system stability can be divided into:

a) rotor (or power) angle stability;

b) frequency stability; and

c) voltage stability [5].

This classification is presented in Figure 1.1. Power systems are nonlinear dynamic systems. Thus the stability of a power system depends on the size of the disturbance as well as the initial conditions. As a consequence, rotor angle and voltage stability can be divided into two subcategories: small- and large-disturbance stability.

The stability of a power system is mainly related to the electromechanical phenomena of the elements interacting in the system, being also affected by the fast electromagnetic and slow thermodynamic phenomena. Therefore, depending of the phenomena being studied, the stability could be referred to as short-term stability and long-term stability.

This thesis studies the *large disturbance rotor angle stability* phenomena and proposes monitoring and control strategies to mitigate the consequences of large disturbances. The *large disturbance rotor angle stability* is also commonly referred to as the *transient stability*, and in this thesis, both these terms are used.

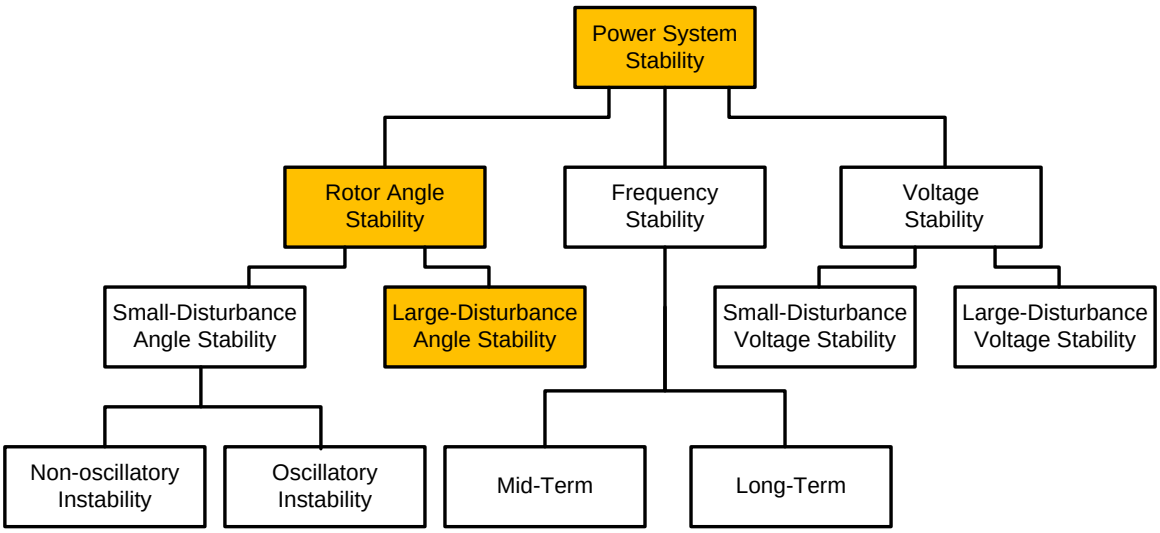

Figure 1.1 Stability classification [5].

1.3 Power system operating states

Clear definition of the power system operating states helps understanding the objectives of transient stability prediction and control schemes developed later in this thesis. A conceptual classification of different states of operation was first proposed by DyLiacco [6] in 1967. DyLiacco classified operating states into three categories as normal, emergency

and restorative states. This classification was extended by Fink and Carlsen [7] in 1978 using five states, namely: normal, alert, emergency, in extremis, and restorative. Figure 1.2, from reference [8], shows these operating states and how the transition from one state to other can take place.

In general, a power system can be represented using a set of differential equations that describe the system dynamics, a set of equality constraints that describe the power balances (noted as **E** in Figure 1.2), and a set of inequality constraints that describe the equipment capacity limits and acceptable ranges of variables such as bus voltages (noted as **I** in Figure 1.2). In the *normal operating state*, all system variables are within the normal range and both the equality and inequality constraints are satisfied. Normally, a power system operates with an adequate security margin and is able to withstand the impact of a single contingency without violating system constraints. The security margin in the above sentence generally means a measure of the distance to an event that may cause the system to become unstable, and it is also referred to as the stability margin [9].

A power system enters to the *alert state* when the level of adequacy of the system security margin has decreased but the system is still not violating the constraints. When a power system is in *alert state*, an occurrence of another disturbance might lead to overloading of equipment taking the system to the *emergency state* or the *in extremis state* depending on the severity of the disturbance.

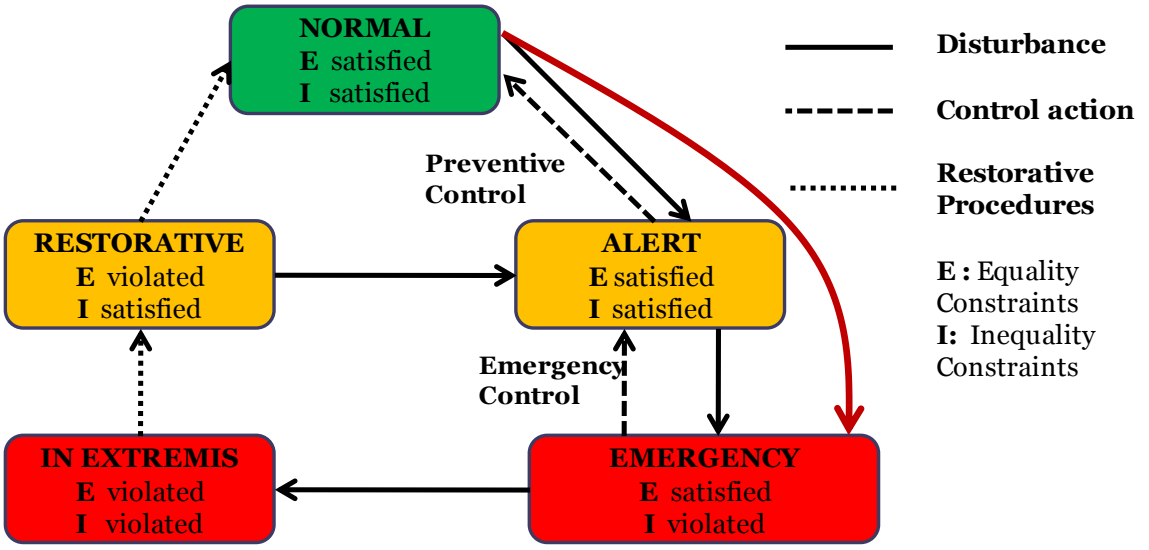

Figure 1.2 Classification of the power systems states [8]

When in the *alert state*, the power system can be restored to the *normal state* by taking preventive control actions like generation rescheduling. This action will redistribute the power flow to prevent overloading of equipment under certain contingencies. In cases where the generation reserve is not enough to take preventive control action, the system will remain in *alert state* until the condition that promotes the risk of failure disappears, for example due to improved weather or completion of some special maintenance.

When the voltage levels decrease below the minimum permissible limit for safe operation and/or some equipment are overloaded, the system is considered to be in *emergency state*. During this condition emergency control actions like load/generation rejection, HVdc supplementary control, dynamic braking, fast-valving, among others needs to be engaged. If appropriate control actions are not taken, then the system will move to the *in extremis state* where partial or total blackout will occur.

The *restorative state* comprises of the moment when control actions or sequence of actions are taken to re-establish the energy supply to the loads across the system.

The focus of this research work is on the early detection of the occurrence of an *emergency state*, and fast activation of suitable emergency control measures to restore the normal operation of the grid after critical disturbances.

1.4 Wide area measurement technology

Modern power systems are complex and spread over a large geographical area. Therefore, effective monitoring requires measurements at different locations and communication of the measurements to a central location. The correct time alignment of the measurements taken at different locations was always a challenge. Proper time alignment is particularly important when performing post-mortem analysis after a severe disturbance, validating simulation models or in real time monitoring, protection and control. The recent advent of the wide-area measurements technology based on synchronized phasor measurements has provided a solution to this problem [4].

Synchronized phasor measurement provides voltage and current phasors synchronized with high precision to a common time reference. This is achieved by time synchronizing the sampling of signals and time tagging the phasors using the global positioning system (GPS) [10]. Time synchronized phasors, referred to as *Synchrophasors*, together with modern communication and computation technology facilitate the monitoring of the state of a power system, including the phase angles of bus voltages and line currents.

A generic representation of a wide area measurement system is shown in Figure 1.3. Measurements provided by the Phasor Measurement Units (PMU's) are usually collected by a local computer and transmitted at a high speed over a local-area communication network to a host computer known as Phasor Data Concentrator (PDC) [10]. The function

of PDC is to gather the data from several PMUs installed in different geographical locations of the network, verify its integrity, and create a coherent stream of simultaneously recorded data for utilization in different applications.

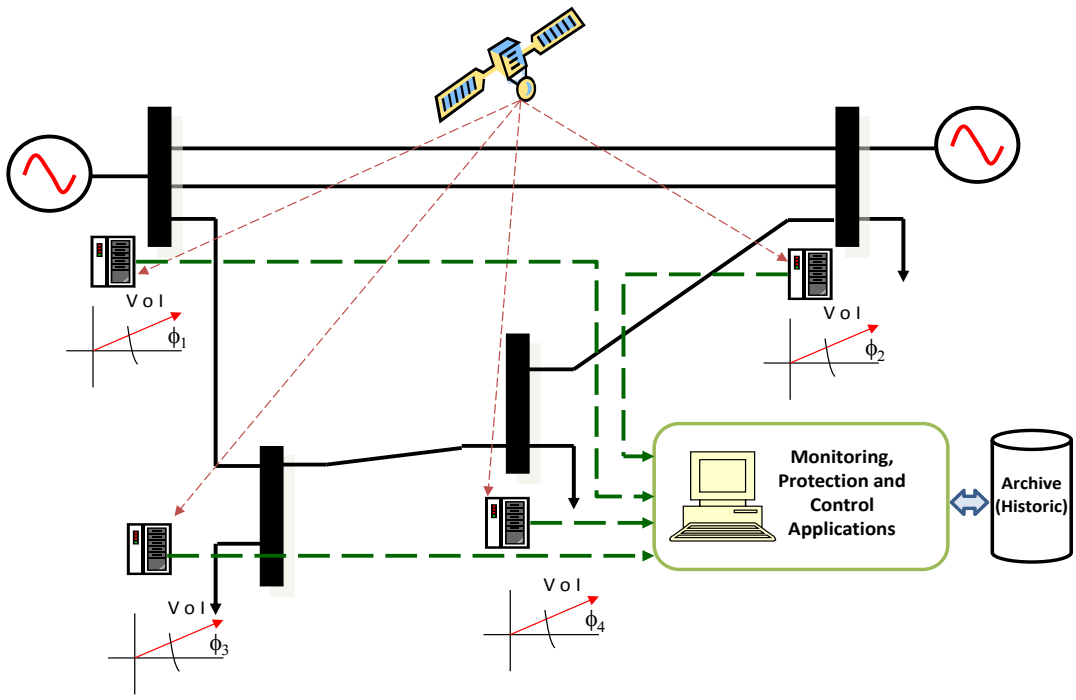

Figure 1.3 Wide area measurement technology

1.4.1 Phasors

A phasor represents a periodic waveform as a rotating vector in a complex plane. An Alternating Current (AC) waveform can be mathematically represented as:

$$x(t) = X_m \cos(\omega t + \phi) \tag{1.1}$$

Where: X_m is the magnitude of the sinusoidal waveform

ω is the instantaneous angular frequency

ϕ is the angular starting point of the waveform

In phasor notation, this signal is typically represented as in (1.2).

$$\bar{X} = X_m \angle\phi \tag{1.2}$$

where X_m is the magnitude of the phasor, and ϕ is the position of rotating phasor against the real axis Re as illustrated in Figure 1.4.

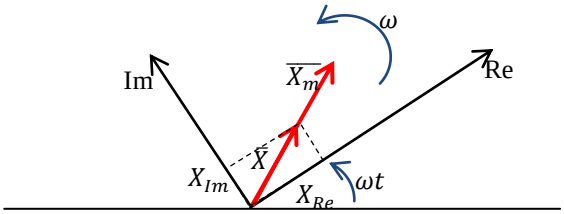

Figure 1.4 Illustration of a rotating phasor

Since the correlation with the equivalent RMS quantity is desired in the synchrophasor definition, a scale factor of $1/\sqrt{2}$ must be applied to the magnitude. The resulting phasor representation is:

$$\bar{X} = \frac{X_m}{\sqrt{2}} \angle\phi \tag{1.3}$$

IEEE Standard C37.118-2005 [11] defines synchrophasor as the magnitude and angle of a cosine signal as referenced to an absolute point in time and provides other details such as accuracy limits and format for presenting synchrophasor data.

1.4.2 Phasor measurement unit (PMU)

A Phasor Measurement Unit is a device that computes the voltage and current phasors using the analogue signals from the system. Voltage and current waveforms for which the phasors are to be determined are measured using current and voltage transformers and delivered to the PMU as three-phase analogue signals. Each signal is filtered using an anti-aliasing filter and sent to an analogue-to-digital converter (ADC) where the signal is

sampled. The sampling instances are synchronized with the GPS clock to an accuracy of less than 1μs. This is achieved using an oscillator phase-locked with the one pulse per second signal received from a GPS receiver. Then, the orthogonal components of each phasor are computed, typically using the Discrete Fourier Transform (DFT). Finally, a time stamp that defines the boundary of the power frequency period is attached to the phasor. The functional diagram of a PMU is presented in Figure 1.5.

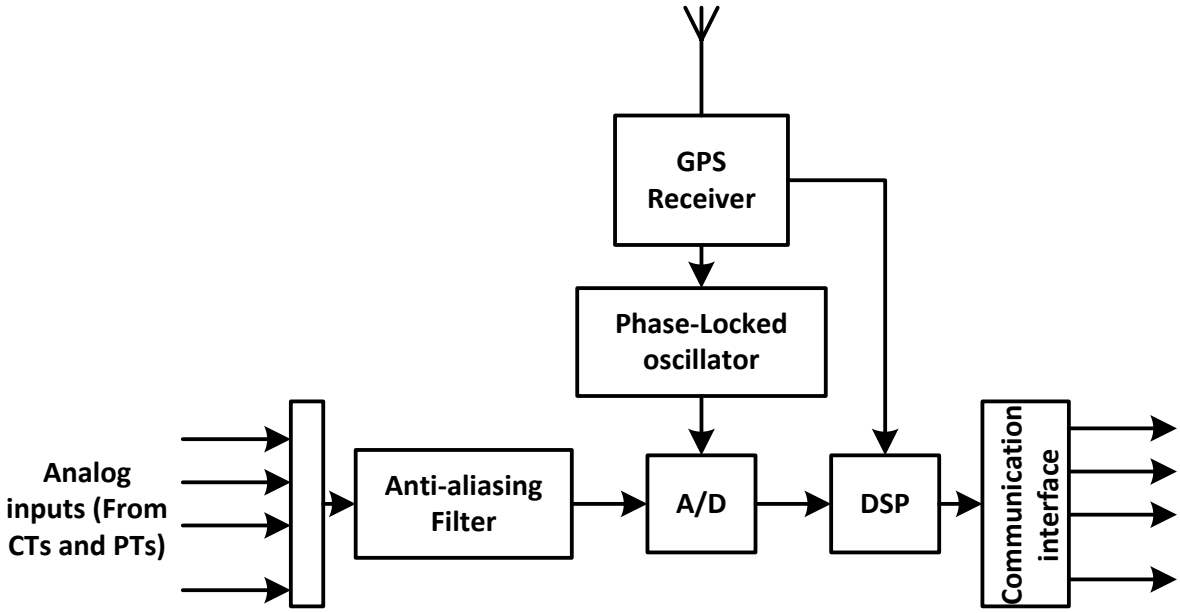

Figure 1.5 Functional diagram of a PMU

1.5 Motivation behind the research

Power systems in North America and Europe experienced a number of blackouts in the recent past. The impact of these blackouts was massive: tens of millions of customers were affected and billions of dollars were lost to the economy [1]. Although investment in network infrastructure is imperative to improve the grid reliability, it is extremely expensive to design a power system to completely prevent rare multiple disturbances. On

the other hand, an increase in the transmission network capacity alone does not inherently enhance the security of the power system nor eliminate the probability of blackouts [12].

As stated in the previous section, special protection systems provide less costly and faster to implement solutions to minimize the impact of rare disturbances that could lead to blackouts or partial collapses. Fast recognition of evolving transient instability conditions is very crucial to allow effective control and protection actions [13]. A typical power system could exhibit transient instability within a period as short as one second after a severe disturbance despite the large inertia of the synchronous generators connected to it. Thus any emergency control system designed to prevent transient instability should respond within a few hundreds of milliseconds. Although several attempts have been made to develop methods for detecting transient instabilities in near real-time (within several tens of milliseconds) [10, 13-15], more research is needed to develop practically applicable methods that can be used in emergency control systems. The possibility of monitoring the entire power system is indispensable for successfully predicting the transient stability behaviour. Availability of Phasor Measurement Units and the related communication infrastructure enable near real-time measurement of the essential variables of a power system spread on a wide geographic area. The Synchronized Measurement Technology (SMT) based on the Phasor Measurement Units (PMUs), telecommunication technology, and the capability of computers to process a large amount of real-time data are approaching a level that is acceptable for implementing response-based protection and control against transient instability [10]. Furthermore, the recent advances in machine learning techniques such as Artificial Neural Networks (ANN), Decision Trees (DT), Kernel Regression (KR) and Support Vector Machines (SVM) [16-23] have opened up new avenues

for developing more sophisticated and intelligent solutions to difficult problems such as early prediction of impending instabilities in a power system. These factors motivated the exploration of machine learning-based methods to predict the transient stability states of a power system using wide area phasor measurements and use such early predictions to determine and activate appropriate emergency control actions. Although there are some previous attempts [13-15] to develop similar emergency control algorithms, most of them are demonstrated on small test systems. However, testing of such methods on large-scale (> 1000 buses) real power systems is imperative to comprehend the practicality of applying sophisticated control algorithms on real power systems.

1.6 Research objective and contributions

The main goal of this research was to investigate techniques for quick determination of the transient stability state of a power system after subjecting it to a large disturbance such as a fault. The underlying hypothesis of the investigation is that the measurements obtained through phasor measurements units installed at different locations of the power system provides sufficient information to ascertain the transient stability status. The research also investigated how early prediction of stability status can be used to design emergency control against transient instability. During the course of the research, the following contributions were made.

Literature pertaining to previous research which investigated the problem of predicting the transient stability status of a power system was reviewed. These methods were studied in detail categorizing them based on the approach used. The suitability of each ap-

proach for near real-time applications was evaluated based on information available. The results of this literature review are presented in Chapter 2.

A new method that utilizes the post-disturbance measurements to predict the system transient stability status was proposed. The method involves use of a Support Vector Machine (SVM) classifier to determine the future stability status based on the wide area synchronized phasor measurements obtained immediately after a disturbance. The transient stability status prediction referred to in this thesis is different from the well known and widely investigated online dynamic security assessment where a stability margin is calculated for an anticipated set of credible contingencies (usually pre-defined) starting from a known operating point (usually obtained through supervisory control and data acquisition (SCADA) system) [24]. The aim of online dynamic security assessment is *preventive control*, if the stability margin is unacceptable for a specific contingency. In contrast, the aim of the transient stability status prediction method developed in this is to trigger *emergency control* after occurrence of a severe disturbance if an impending instability is detected through measurements; as such it is fundamentally different in its potential application. Furthermore, no prior knowledge of the nature of the actual contingency is assumed in predicting the transient stability status.

There are a number of different measurable power system variables such as frequency, voltage magnitudes, and voltage phase angles which can be used as primary inputs for predicting the transient stability status. The research investigated the effectiveness of these variables as predictors of the transient stability status, as well as indicators of the required for emergency control actions. One major contribution of this research was the identification of the importance of synchronously measured voltage phasor magnitudes,

which are directly available from phasor measurement units, as an early indicator of the transient instability.

The method of designing the transient stability prediction scheme and its applicability was demonstrated using a number of test power systems. The concept was first proved using a 39-bus power system, and then applied to two real power systems: the Manitoba Hydro power system and the Venezuelan power system. The accuracy of prediction and its sensitivity to different factors such as the operating point, nature of loads, noisy data, and the network topology changes were studied.

The possibility of detecting impending transient instability conditions at early stage allows designing appropriate emergency control schemes focused on preserving the transient stability and the integrity of the power system. Emergency control actions are usually system dependent and make use of specific characteristics of the particular power system. Thus the emergency control systems investigated in this thesis used the Manitoba Hydro power system and the Venezuelan power system as examples. The two systems have contrasting characteristics: Manitoba Hydro system is characterized by its high voltage direct current (HVdc) transmission system whereas the Venezuelan power grid is characterized by its 765 kV ac transmission system. The thesis develops a fuzzy logic based approach for designing an emergency load and generator shedding scheme for the Venezuelan power system, and a rule-based approach for designing an emergency HVdc power order control scheme for the Manitoba Hydro power system. The performance of the developed emergency control schemes were demonstrated using simulations.

1.7 Thesis overview

The thesis is organized as follows. In Chapter 2, the results of the survey of transient stability analysis methods commonly found in the literature are presented. The review includes examination of the suitability of various transient stability analysis methods for near real-time applications.

The concept of the transient stability status prediction scheme proposed in this thesis is introduced in Chapter 3. The algorithm as well as a brief explanation of the machine learning technique used in the algorithm, Support Vector Machine (SVM), is presented. Chapter 3 also includes a comparison of the performance of various transient stability status predictors.

In Chapter 4, the proposed transient stability status prediction algorithm is applied to two real power system networks, the Venezuelan power grid and Manitoba Hydro power network. Detailed results of the prediction accuracy tests and the sensitivity studies are presented.

Application of the transient stability status prediction for initiating emergency control actions to mitigate transient instability is presented in Chapter 5. In this chapter, the development and testing of two example SPSs are presented. The first SPS is based on a fuzzy logic based controller to minimize the consequences of harmful disturbances in conventional ac power system. The second SPS is a rule based scheme for HVdc power order reduction to stabilize the system once a transient instability condition is detected.

Chapter 6 presents the major conclusions, highlights the main contributions, and makes several suggestions for future research in the area of power systems transient stability prediction and emergency control using synchrophasors.

Chapter 2

Transient stability of power systems

2.1 Introduction

The objective of this chapter is to introduce the essential background information and review the existing work related to the research. The existing transient stability assessment methods and their suitability for real-time applications based on synchronized phasor measurement technology are reviewed. The advantages and drawbacks of each method are discussed. Finally, the performance expected from the phasor measurement units as specified in the relevant standards are briefly examined.

2.2 Power system stability

2.2.1 Stability theory

A power system, as any dynamic system, is represented by a set of differential and algebraic equations. These equations have the general structure given by:

$$\dot{\boldsymbol{x}}(t) = f(t, \boldsymbol{x}(t)) \tag{2.1}$$

$$0 = g(t, \boldsymbol{x}(t)) \tag{2.2}$$

where $\boldsymbol{x}$ is the vector of state variables. The power system has an equilibrium point $\boldsymbol{x_o}$ at time t_o if $f(t, \boldsymbol{x_o}) \equiv 0$ for all $t \geq t_o$. After subjecting to a disturbance, if the trajectory of $\boldsymbol{x}$ remains in the vicinity of the equilibrium point as $t \to \infty$ then the system is referred as stable. The system is referred as asymptotically stable if the trajectory returns to an equilibrium point as $t \to \infty$.

The set of equations represented by (2.1) comprises the differential equations that model the generators, motors, including their control schemes, and all other devices whose dynamics are considered in the stability analysis [9]. The state vector $\boldsymbol{x}(t)$ typically include generator rotor angles, angular speeds, field voltages, damping winding currents, and the state variables associated with controllers and other equipment such as FACTS devices. A power network has much faster response compared to the electrical machines and controllers connected to it, and therefore, the network response is assumed instantaneous. Thus, the network and the static loads are represented using set of algebraic equations as in (2.2).

The system is initially assumed to be at a pre-disturbance steady-state condition governed by the equations

$$\dot{x}(t) = f^{pre}\big(x(t)\big) \qquad -\infty < t \leq 0 \tag{2.3}$$

The superscript pre indicates predistubance. At this condition the system is at equilibrium, and the initial conditions are obtained from the classical power flow solution. At $t = 0$ the fault or the disturbance in the systems is initiated. At this point the conditions of the system change and therefore, the dynamics of the power system is represented by:

$$\dot{x}(t) = f^{f}\big(x(t)\big) \qquad 0 < t \leq t_{cl} \tag{2.4}$$

In (2.4) the superscript f highlights the faulty condition or the period of time when the disturbance is present in the system. This fault or disturbance is eventually removed by the protection devices at time t_{cl}, known as the clearing time. The removal of the faulted path of the system results in a topology change, and consequently the right hand side of the initial differential equation (2.1) is altered. Finally, the post disturbance dynamics is expressed as:

$$\dot{x}(t) = f^{post}(x(t)) \qquad t_{cl} < t \leq \infty \tag{2.5}$$

The stability analysis usually takes place during the post disturbance period.

2.2.2 Transient stability: time domain approach

In large disturbance rotor angle stability or the transient stability, variations of the synchronous machine rotor angles are the main focus. Time domain simulation (TDS) approach solves the Differential and Algebraic Equations (DAE) given by and (2.1) and (2.2) using step-by-step numerical integration, and obtains the machine rotor angle variation along the time. The application of this approach to assess the transient stability of an electric power system has been extensively reported in the literature [8, 9, 25]. Initially, it was restricted to systems with small number of generators due to the complexity involved in solving the set of differential equations that represents the dynamic of the electric machines. The enormous evolution of the digital computers made possible the utilization of time domain simulation as a tool to analyze the transient stability of a large power system. The modern commercial transient stability simulation software programs not only handle power systems with a large number of generators, but also use sophisticated

models to represent the power system elements, enabling accurate transient stability assessment [26, 27].

During the assessment of the stability of the system, the differential and algebraic equations are solved separately. First the algebraic equations (2.2) are solved following a disturbance to calculate the bus voltages, bus current injections, and the remaining non-state variables. Once this initial step is achieved, the time dependant variables given by (2.1), are calculated using the known values of state variables obtained in the initial stage. Finally, an explicit integration method is used to calculate the values of state variables for the next time step [8, 25].

Integration methods as predictor-corrector, Runge-Kutta are known as explicit methods. They use the dependent variable values computed in the previous step to obtain the next step values. These methods are easy to implement even when a complex set of system state equations need to be solved [8]. In order to capture the proper dynamics and preserve the simulation stability it is necessary to keep the integration time-step smaller than the lowest time constant of the system. On the other hand, there are integration methods known as implicit integration methods. The classical and simplest is the trapezoidal rule. This method is based on the linear interpolation and uses trapezoids to obtain the area under the curve.

The simultaneous solution schemes that use implicit integration methods transform the differential equations (2.1) into a set of state variables equations (x) and bus voltages (V) for the current and following time step. These sets of state variables equations are solved together with the algebraic equations representing the electrical network to obtain the values of the state variables and other non-state variables at the next time step.

Time domain simulation programs use a single line representation of a balanced three phase network. Unbalanced networks caused by unbalanced faults are simulated by combining balanced sequence networks derived by symmetrical components analysis [28].

Although, time domain simulation programs provide accurate and reliable assessment of system information following a disturbance, it can only be used to numerically calculate the time evolution of power system variables following a known disturbance for a given pre-disturbance operating condition.

2.2.3 Equal-Area criterion and its extensions

The Equal-Area criterion (EAC) is a graphical method used to assess the transient stability of an electric power system. The origin of the method is not well known yet but some publications explaining this technique has been presented, specially analyzing one-machine connected to an infinite bus [8, 9, 25]. The principle of EAC is developed considering a single-machine connected to an infinite bus through a transmission network. The electromechanical behaviour of such a single machine infinite bus (SMIB) power system could be represented using the motion or swing equation:

$$M\frac{d^2\delta}{dt^2} = P_m - P_e = P_a \tag{2.6}$$

Where

M = Inertia coefficient of the machine

δ = Angle between the machine's rotor and the infinite bus system

P_m = Mechanical power input to the machine

P_e = Electric power output from the machine

P_a = Accelerating power

Multiplication of both sides of the swing equation by$(d\delta/dt)$ and integration gives

$$\left[\frac{d\delta}{dt}\right]^2 = \int_{\delta_0}^{\delta} \frac{\omega_0(P_m - P_e)}{H} d\delta \tag{2.7}$$

where δ_0 is the rotor angle before the start of disturbance. The process that happens after a network fault on this system can be illustrated on a $P - \delta$ diagram as shown in Figure 2.1. At the initial operating point, $P_m = P_e$, and the corresponding power angle is δ_0. The relationships between the electric power output P_e and the power angle δ before the fault, during the fault, and after clearing the fault are shown in the red, green and blue curves. When a fault occurs, the electric power output of the generator almost instantaneously drops to a point "b" on the blue curve. Due to the slow electromechanical response of the generator, the rotor cannot accelerate instantaneously, but gradually traces the blue curve up to point "c" due to increase of rotor speed beyond the synchronous speed. At point "c", the fault is removed and the electrical power jumps to point "d" on the green curve, making $P_e > P_m$. Thus the rotor starts to decelerate, but δ keeps increasing until reaching a maximum value δ_{max}. After that, the rotor angle should start to return, otherwise the generator will be moving to loss of synchronism [9]. In Figure 2.1, A_1 represents the accelerating area and shows the net kinetic energy gained during the fault-on period and A_2 represents the decelerating area showing the potential energy absorbed by the system.

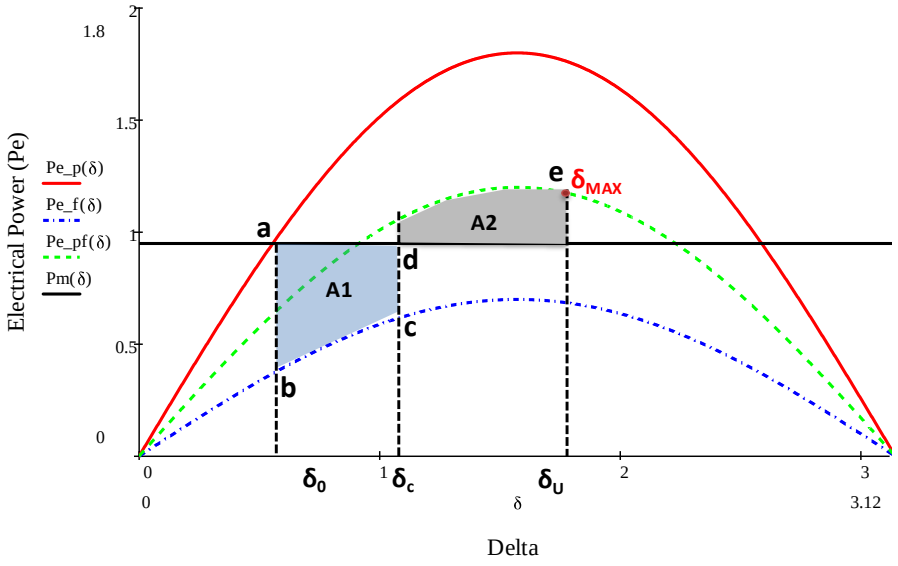

Figure 2.1 Power–angle curve showing the areas defined in the Equal Area Criterion

At the initial point, $\frac{d\delta}{dt} = 0$, and after the disturbance $\frac{d\delta}{dt}$ become positive and δ increases. As mentioned earlier, if the system is stable, the rotor angle δ should change the direction after reaching δ_{max} and, thus $\frac{d\delta}{dt}$ should become zero again when $\delta = \delta_{max}$ [29]. Therefore, the stability criterion could be written as:

$$\left[\frac{d\delta}{dt}\right]^2 = \int_{\delta_0}^{\delta_{max}} \frac{\omega_0(P_m - P_e)}{H} d\delta = 0 \tag{2.8}$$

The integral in (2.8) represents the difference between the areas A_1 and A_2 in Figure 2.2 [29], where two cases are compared in terms of their power-angle curve. Both cases were generated considering a three-phase fault in the system with only difference being the fault clearing times. The curve on the left corresponds to a stable case and if carefully analysed, it is possible to observe that $A_1 = A_2$. This means that the energy gained during the rotor acceleration is equal to the energy absorbed during the deceleration area. On

the other hand, for the unstable case (presented on the right) the accelerating area is much bigger than decelerating area ($A_1 > A_2$) , meaning that the energy gained during the rotor acceleration is greater than the energy absorbed during the deceleration area. Thus no feasible δ_{max} and the generator looses synchronism.

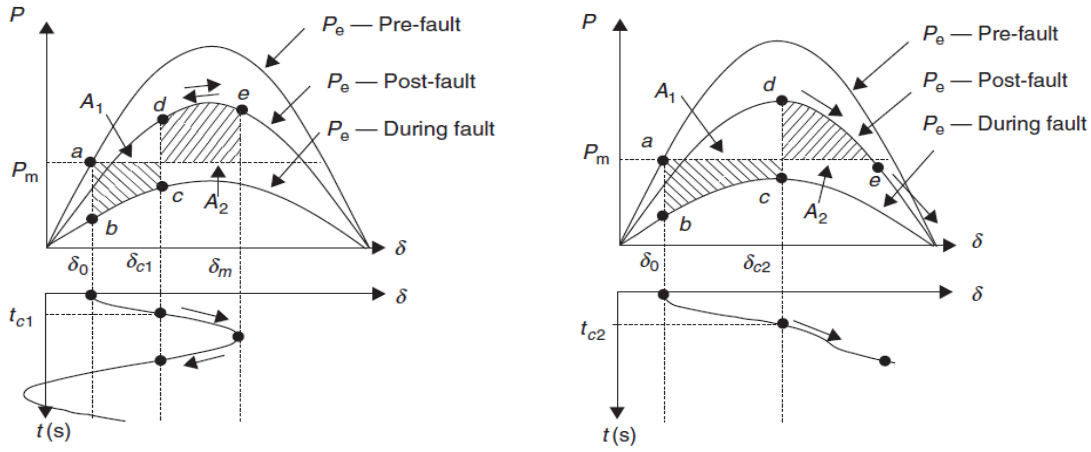

Figure 2.2 Rotor response (defined by the swing equation) superimposed on the power–angle curve for a stable case (left) and an unstable case (right) [29]

The disadvantage of this approach is the simplicity of the models used to assess the stability. The generator is represented by the classical model and the speed governor and excitation controller effects are neglected [30].

The applicability of the original version of Equal Area Criterion is limited to the ideal case of a single machine interconnected to an infinite-bus. The concept of EAC was extended to multi-machine power systems in the late eighties by two separate research groups led by Rahimi [31] , and Xue [32] through the introduction of the Extended Equal Area Criterion (EEAC).

The EEAC is based on the principle that transient instability is a result of the separation of generator rotor angles into two clusters after being subjected to a severe transient dis-

turbance. These two groups of generators are called the critical cluster and the remaining cluster of machines. Each group of machines is replaced by an equivalent machine reducing the multi-machine system to a two machines system. One of the two equivalent machines represents the dynamic behaviour associated with the critical cluster of machines promoting the instability of the system. The other equivalent machine represents the dynamics of the remaining cluster of machines.

Finally, the equivalent two-machine system is further reduced to a one machine connected to an infinite bus (OMIB) system for which the conventional EAC can be applied to estimate the transient stability margin [33]. The main assumption in the EEAC is that during the study period, the rotor angles of each cluster are represented by the center of angles is calculated just before the fault occurs. The centre of angles or centre of inertia angle for each cluster is given by:

$$\delta_{COI} = \frac{\sum_{i=1}^{n} H_i \delta_i}{H_i} \tag{2.9}$$

where δ_i and H_i are the generator rotor angle and inertia constant of the i^{th} generator and n is the number of generators in the cluster. Similar to the EAC, the EEAC formulation also uses the classical model of generator representing the mechanical dynamics of the generators. Thus errors due to ignoring the electrical dynamics of the rotor circuit and the controllers are still present.

2.2.4 Transient energy based methods

Energy criterion for transient stability analysis was the earliest of all direct methods of multi-machine power system transient stability assessment. These techniques were exten-

sions of the equal area criterion to power systems with more than two generators represented by the classical model [34].

A typical analogy used to explain this method is the kinetic and potential energy associated with a ball rolling in a bowl. Once a disturbance occurs, the power system gains kinetic and potential energy that makes the system move away from the initial equilibrium point [8]. After removing the fault, the kinetic energy is converted into potential energy and the power system tries to absorb this energy to bring the system back to a new equilibrium point. The amount of power that the system is able to absorb depends on the post-disturbance network configuration. In Figure 2.3, the energy-angle relationship is presented. At $\delta_{0,}$ the system is in equilibrium. After the disturbance, the system gains kinetic and potential energy until the disturbance is removed at δ_c. After this, the kinetic energy transform into potential energy which should be absorbed afterwards to prevent this energy level reaching the critical energy level where the loss of synchronism is imminent.

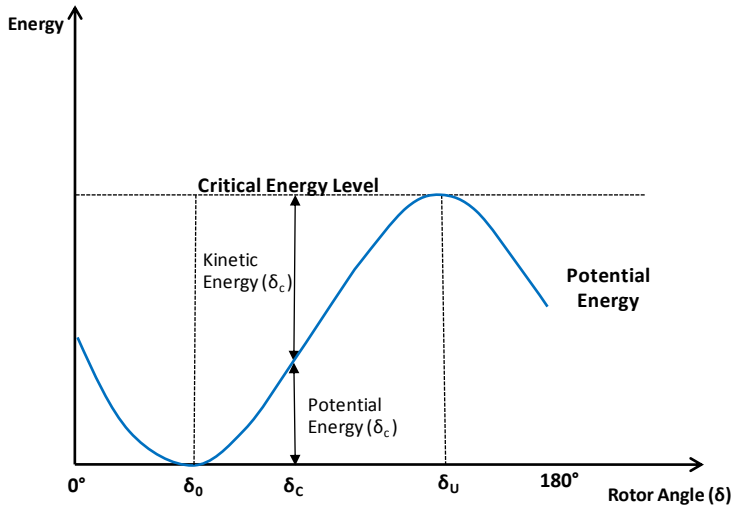

Figure 2.3 Energy-angle relationship to illustrate the transient energy method

2.2.5 Hybrid methods

Transient stability assessment techniques that combine time domain simulations with transient energy based methods have also been proposed. These methods are less accurate than the original time domain simulations. However, the hybrid methods gain a significant reduction of the computational requirement and extract important information such as stability margins from time domain simulations [30]. Computation of a stability margin allows determination of whether the system is moving toward instability or not. Some of these techniques have been used for dynamic security assessment. The most relevant hybrid transient stability assessment methods are explained briefly in the following sections.

2.2.5.1. Time domain transient energy function methods

Time domain transient energy function methods determine the stability of a power system without solving the differential equations that governs the dynamic behaviour of the system. This method is based on the Lyapunov's second method or Lyapunov's direct method. The avoidance of solving the differential equations is translated as ignoring the effects of the excitation system and controllers, as well the governing systems. The transient stability analysis is calculated by ignoring the slow transient and representing the generators using the classical model [8]. During the analysis, all the formulations are done relative to the center of inertia (COI) angle [8, 9, 25].

If the admittance matrix of the system is given by:

$$Y = G + jB \tag{2.10}$$

The transient energy function is expressed as

$$W = \frac{1}{2}\sum_{i=1}^{n} M_i \widetilde{\omega_i}^2 - \sum_{1}^{n} P_i(\theta_i - \theta_i{}^s) - \sum_{i=1}^{n-1}\sum_{j=j+1}^{n}\left(C_{ij}cos\left(\theta_{ij} - \theta_{ij}{}^s\right) - \int_{\theta_i{}^{s2}+\theta_j{}^{s2}}^{\theta_i+\theta_j} D_{ij}cos\theta_{ij}d(\theta_i - \theta_i{}^s)\right) \quad (2.11)$$

Where $\theta_{ij} = \theta_i - \theta_j$

$\theta_i = \delta_i - \delta_0 =$ Generator angle respect to COI angle

$i, j =$ Indices for generators;

$s =$ Indicates the reference;

$\widetilde{\omega} =$ Angular speed of generator rotor with respect to the COI

$C_{ij} = E_i E_j B_{ij}$;

$D_{ij} = E_i E_j G_{ij}$;

$E_i =$ Constant voltage behind the direct axis reactance of the generator i;

$M_i =$ Inertia constant of generator i ;

$B_{ij} =$ Transfer susceptance between generators *i* and *j* in the bus admittance matrix

$G_{ij} =$ Transfer conductance between generators *i* and *j* in the bus admittance matrix

The transient energy level of the system is the sum of the kinetic energy gained by the generators during the disturbance (W_{KE}) and the potential energy (W_{PE}) absorbed by the electric system to keep the generator inside the stability region.

$$W = W_{KE}(\widetilde{\omega}) + W_{PE}(\theta) \quad (2.12)$$

The transient energy present during the post-disturbance period (W^{pd}) is compared against a transient energy threshold or reference value (W_c).

If $W^{pd} < W_c$, the system is assessed as stable. When $W^{pd} > W_c$, the system is considered as unstable. The sensitivity is analyzed by computing the energy margin ΔW obtained by

$$\Delta W = W_c - W^{pd} \tag{2.13}$$

A detailed explanation of the method and its computation steps can be found in [8, 9, 25]. The values of phase angles and generator speeds required to calculate the kinetic and potential energy functions can be obtained from phasor measurements, but knowledge of the post disturbance system topology and accurate system impedance parameters are still required to calculate the transfer admittances.

2.2.5.2. SIME (Single Machine Equivalent) method

This method successfully combines the computational efficiency of the direct methods and the modeling accuracy of time-domain simulation [35]. The concept is based on the ideas used in the extended equal area criterion. The generators are divided into two coherent groups called the critical group and the remaining group. The group of generators that have rotor angles with larger deviation from the COI angle are the critical cluster. The rest of the generators form the remaining group. Proper identification of these two coherent groups allows reducing the multi-machine power system to an equivalent one-machine infinite bus (OMIB) system as pointed out earlier. The equal area criterion is then applied by comparing the accelerating and decelerating areas to obtain a stability status [30].

Time-domain simulation is used in this method to classify machines into two groups. During the simulation, the rotor angles are compared and organized in the decreasing order of the deviation of rotor angles from their adjacent machines. The machines with the largest deviations are considered as candidate critical machines.

Once, the critical group is identified, the corresponding OMIB parameters are computed using the procedure described below:

1. Transform the two clusters previously identified into two equivalent machines, using their partial centre of angles.

$$\begin{gathered}\delta_{critical} \cong M_{critical}^{-1} \sum_{k\in\ critical} M_k\delta_k(t) \\ M_{critical} = \sum_{k\in\ critical} M_k \\ \delta_{remaining} \cong M_{remaining}^{-1} \sum_{k\in\ reamining} M_k\delta_k(t) \\ M_{remaining} = \sum_{k\in\ \text{remaining}} M_k\end{gathered} \tag{2.14}$$

where M_k is the inertia coefficient of the k^{th} machine.

2. Reduce this two machine system into an equivalent OMIB whose rotor angle and mechanical power are given by:

$$\delta(t) \cong \delta_{critical}(t) - \delta_{remaining}(t) \tag{2.15}$$

$$P_m(t) = M\left(M_{critical}^{-1} \sum_{k\in\ critical} P_{m\_critical}(t) - M_{remaining}^{-1} \sum_{j\in\ remaining} P_{m\_j}(t) \right) \tag{2.16}$$

$$M = M_{critical}M_{remaining}\,/\left(M_{critical}+M_{remaining}\right)$$

where M is the equivalent OMIB inertia coefficient. This methods is explain in further detail in the literature [30].

Finally, a stability margin is obtained using the classical equal area criterion, where:

$$\eta = A_{dec} - A_{acc} \tag{2.17}$$

For a given scenario the, the system is unstable if $\eta < 0$ and it is stable when $\eta > 0$. The condition where $\eta = 0$ is considered the boundary. Moreover, two stability margins (unstable margin and stable margin) are computed.

$$\eta_u = -\frac{1}{2}M\omega_u^2 \tag{2.18}$$

$$\eta_{st} = \int_{\delta_c}^{\delta_u} |P_a| d\delta \tag{2.19}$$

Where η_u and η_{st} are the unstable and stable stability margins respectively. δ_c and δ_u are the clearing and instability angles. This method has been applied mainly for contingency filtering in transient stability assessment to minimize time domain simulation efforts.

2.2.6 Machine learning based methods

Machine learning and intelligent techniques have made rapid progress in the recent decades. The potential of artificial intelligence techniques such as Artificial Neural Networks (ANN), Fuzzy Systems, Decision Trees (DT), Kernel Regression and Support Vector Machines for application in solving difficult power system problems has been well recognized [16-23].

ANNs can be used for function approximation as well as for classification problems. One of the relevant early application of ANNs was for regression in transient stability assessment [22]. In this work, an ANN was trained to calculate the critical clearing time for different loading conditions in a small power system. After the initial success, the focus of the research shifted to the development of online applications [18] such as online dynamic security assessment.

Those ANN implementations used off-line generated transient stability data for the purposes such as input feature selection, training of ANN, and finally for performance evaluation tests. One of the limitations that researchers faced when using ANN based methods was the possibility of having many local solutions and the slow rate of convergence during the training [36].

Decision trees (DT) have also been applied to assess the transient stability condition of power systems [17, 19]. DT obtains a linear mapping function after splitting the training data in a sequential manner. The training or the building of decision rules involves determining a threshold margin that accomplishes certain criteria [37]. DT is considerably easy and fast to implement [38] and especially suitable for classification problems. They

work best for the applications that require a small number of outputs. The main drawback is the lack of accuracy due to the non-optimized methods used for training the classifiers.

In 1995, a new classification method known as Support Vector Machine (SVM) was proposed [39]. The advantage of this new approach over traditional ANNs is the calculation of a globally optimum solution. Some applications of SVM for transient stability assessment is reported in [21, 23] and shown to provide high accuracy and smaller training time compared to conventional ANN and other machine learning based methods. However, the studies reported in [21, 23] required a large number of inputs to achieve sufficient classification accuracy.

Most of the methods described above were developed to compute some form of stability margin for a known contingency. This is the main objective of dynamic security assessment, which could be performed offline or online. The research reported in this thesis investigates a slightly different problem, which is to predict the transient stability status after a disturbance using the post-fault measurements. No knowledge of the contingency is assumed. Thus many of the transient stability assessment methods found in the literature cannot be directly applied.

2.3 Special protection systems against transient instability

Special Protection Systems (SPS) are specialized schemes designed to detect a particular conditions in the power systems that may cause unusual stress to the power system, and

subsequently trigger particular actions to counteract the observed condition in a controlled manner [40].

In some cases, SPSs are designed to detect a system condition that is known to cause instability, overload, or voltage collapse. The actions to improve the condition of the system may require the opening of one or more lines, tripping of generators, control of the HVdc power transfers, intentional shedding of load, or other measures that will alleviate the problem of concern.

2.3.1 Examples of existing SPS

In one of the earliest schemes of wide area out-of-step protection, Tokyo Electric Power Co. (TEPCO) used the measured phase angle difference between two groups of generators to predict the future phase angle difference. If a prescribed angle difference threshold is exceeded, a controlled system separation scheme is implemented [41]. The Western Area stability and voltage Control System (WACS) implemented on the Bonneville Power Administration (BPA) system uses the time integral of the weighted average of 12 voltage magnitude measurements on the 500 kV network as a measure of instability. Control actions such as capacitor or reactor bank switching and generator tripping are taken when this integral exceeds certain preset thresholds [42]. An alternative algorithm of the same system uses generator reactive power measurements as additional inputs to the controller and uses a fuzzy logic system to determine final control actions [42].

Another algorithm is suggested in[43], which does not require knowledge of the system and uses only the on-line measurements of generator's rotor angles and power mismatches to predict the transient angular stability of the generator. It implies that there

would not be any need for tuning/adaptation procedure when applied this method on another power system. The valve affecting the mechanical input of a generator is controlled in order to stabilize the generator.

A general separation scheme was proposed in [44]; the authors apply the Normal Form method to the Manitoba-Hydro power system to determine groups of machines that swing coherently against each other following a small perturbation. The boundaries separating coherent generator groups are identified and tripped to form islands [44]. If these islands are deemed to be not stable, then various techniques such as load shedding, generation curtailment, relay tripping, are implemented.

In summary, special protection schemes installed so far by many utilities are costly and require the implementation of complex schemes for the near real-time enhancement of the transient stability of the grid. Consequently, there is a need for the development of simpler and more effective methods based on the current technology such as PMU measurements. Therefore, the research work presented in this thesis focuses in presenting novel wide area control schemes to improve the transient stability condition of the system after being subjected to a critical disturbance.

2.3.2 Proposals in literature

Use of machine learning techniques to predict the transient stability status of a power system after a fault has been previously studied in [45-47]. The measured resistance based method in [47] only aims to predict the out of step conditions in a tie line. The decision tree/rule based method in [45] is able to predict the system wide stability status but requires 1-2 sec after fault clearance to make accurate predictions. In [48] an array of neu-

ral networks (NNs) has been used to predict unstable oscillations between two groups of generators. These NNs take phase angle difference between the two generator buses and its rate of change as inputs. The outputs of the NNs are processed through a voting procedure to determine the transient stability status of the system. The method requires training of a large number of NNs depending on the number of generators in the system. In the approach propose in [49], oscillations after the clearance of a sever fault are modeled using an autoregressive (AR) model for which the input is the voltage phase differences between the substations. The stability of the system is determined by analyzing the roots of the pulse transfer function of the AR model.

Reference [46] proposed a SVM classifier and a set of pre-identified voltage variation trajectory templates to predict the transient stability status. The measured bus voltages are compared with the templates to evaluate a fuzzy membership that indicate the similarity between the measured voltage variations and the templates. The similarity values are input to the trained SVM make the classification. Investigations made during this research found that identification of smooth voltage trajectory templates as used in [46] becomes difficult for some cases due to characteristics specific the given power systems.

In reference [50], Kernel Ridge Regression, which is somewhat similar to SVM has been used to estimate a transient stability boundary (TSB) as a nonlinear function of power system variables. This work could be classified in the broad area of dynamic security assessment and has applications in other areas such as dynamic security constrained optimal power flow and re-dispatch of generation for preventive control.

2.3.3 Event based SPSs vs response based SPSs

Most special protection systems that control power grids are event based systems that activate in response to a selected set of contingencies. These event based systems continuously monitor the status signals from various elements in the power system via telecommunication links. A change in the status signals would indicate a contingency and the SPS logic is programmed to take a pre-determined remedial action based on the particular combination of status signals. Although such event based protection systems are extremely fast their complexity grows as the system changes [51]. Another concern with the event based systems is the response to unforeseen situations.

Alternative to event based special protection systems are the response based special protection systems. These systems rather than responding to specific events, take actions in response to abnormal situations detected through system variables such as voltages and power flows [52]. It is well known that abnormal situations could lead to transient instability within a few seconds [9]. For this reason, the speed of gathering the data is critical in the response based special protection systems to enhance the transient stability. Furthermore, effective monitoring requires measurements at the different geographical locations [53] and communication of the measurements to a central location. The correct alignment of these measurements in time is particularly important in real-time stability assessment for emergency control after a severe disturbance. The wide-area measurements technology based on synchronized phasor measurements provides a potential solution to this problem [4].

2.4 Synchrophasors performance criteria

The constant development PMUs technology is allowing higher measurement accuracy and time resolution, increasing the capability of perceiving different phenomena in the power system. The accuracy of the phasors computed by a PMU is affected during the transients due to deviations in the frequency and the distortion of waveform. The phasor is concept defined for a particular frequency, and assuming perfectly sinusoidal waveform. But in practice the frequency deviations are unavoidable. Algorithms have being developed for applying corrections during off-nominal frequencies. However, in control and protection applications, the accuracy of measurement matters most in when there is a disturbance in the system. The problem investigated in this thesis, that is early prediction of transient stability status after a disturbance and emergency control requires measurements taken during transient periods where it is susceptible to the errors emanating from the off-nominal frequency and waveform distortion. The IEEE Standard C37.118-2005 on Synchrophasors [11] defines PMU performance under steady conditions. A new IEEE Synchrophasors standard is being developed where the PMU performance under transient conditions is addressed [54]. Some of the important considerations relevant to the application of synchrophasor technology are discussed in the following subsections.

2.4.1 Measurement accuracy

The accuracy of a synchrophasor depends both on the accuracy of the phase and the magnitude over a range of operating conditions. Thus the accuracy of a synchrophasor is measured by a quantity defined as "Total Vector Error (TVE)". TVE is defined as [11]:

$$TVE = \left(\sqrt{\frac{(X_r(n) - X_r)^2 + (X_i(n) - X_i)^2}{X_r{}^2 + X_i{}^2}} \right) * 100 \quad (2.20)$$

where X_r and X_i represents the real and imaginary components of the theoretical exact synchrophasor and $X_r(n)$ and $X_i(n)$ represent the components of the estimated synchrophasor.

In the most demanding accuracy class (Level 1), the PMU must maintain less than 1% TVE under conditions of ±5 Hz of off-nominal frequency, according to the Synchrophasor standard [11]. A TVE of 1% amounts to maximum of 1% error in the magnitude with zero error in phase, or 0.573^o error in phase with zero error in the magnitude.

A PMU also measures the frequency (and the rate of change of frequency), however a frequency measurement accuracy is not specified in the standard. Nevertheless, it has documented in the literature that PMUs are among the best frequency transducers available, delivering accuracy of a few millihertz (typically 1–3 mHz) [11] .

2.4.2 Synchrophasors during transients

It is known that power system voltage and current waveforms are not steady state sinusoids, particularly during system disturbances. They frequently contain sustained harmonic and non-harmonic components. In addition, because of faults and other switching transients, there may be step changes in the magnitude and phase angles of the waveforms. Other disturbances result in relatively slow changes in phase angles and magnitudes due to electromechanical oscillations of machine rotors. Anti-aliasing filters used in the PMUs attenuate the high frequency signals to insignificant values [4].

The estimation of phasors is typically performed over one period of the nominal system frequency. During this transient period, there are changes in the magnitude and phase of the waveforms. Generally, the phasor computations can be accurately estimated within a range of ± 5Hz around the nominal frequency. Step changes in the input signals due to electromagnetic transients may occur within the data window, in which case, one needs to consider whether the phasor estimate obtained in that window is valid [4].

Some effective techniques ("Transient Monitors") to verify the validity of the computed phasors has been developed and are being used in the commercially available PMUs [55]. More detailed specifications and testing methods to evaluate PMU performance under transient conditions will be included in the new version of the standard under development [56].

2.4.3 Communication of PMU data

The communication facilities are a key element to the phasors data acquisition and application, especially for transient stability prediction and control which require fast detection and remedial actions. There are two key elements to be considered during the design process of a wide area based application: the channel capacity and the latency. The amount of data generated by a PMU will depend on the resolution required (number of phasor per second) for a specific application. But it is considered not a limitation for the conventional communication infrastructure available in most utilities due to the modest amount of data transmitted by a PMU.

On the other hand, the latency will rely on the type of communication infrastructure being used. Leased telephone circuits were among the first communication media used for

PMU data acquisition. They can still be used for post-disturbance analysis, system benchmarking or other applications where latency is not of importance.

Currently, most of the utilities use microwave links but shifting towards the fiber-optic cables when the communication links are upgraded. Fiber-optic links allow faster data transfer rates that require for the protection and control applications. In early applications the phasor measurements are communicated to the control center data concentrator over analog microwave links and modems, but currently the digital fiber-optics is the most preferred media [57].

The latency of fiber optic digital communication is around 20-50 ms, while latency using modems over analog microwave channels is over 80 ms [58]. Depending on the communication infrastructure used for an application, these time delays plus an additional time delay due to the phasor-data correlation carried out in the PDC should be taken into consideration.

Other important issues that need to be addressed during the development and implementation of Wide Area application is the consideration of the case of missing PMUs or erroneous data. The reliability of the deployed applications will rely on the quality of the communication platform as well as the measurement devices. The redundancy in the communication links will increase the cost of the implementation considerably. An alternative to tackle this situation is placing PMUs in different buses inside the same coherent area. Some buses are electrically close and they respond similarly under contingencies in the grid. They capture almost the same dynamic behaviour of that particular section of the grid. In case of losing the measurement of one of those PMUs, the remaining unit continues to monitor that section of the grid and the application could continue in service.

In the case of erroneous data, this could be detected by comparing subsequent measurements. The Phasor Data Concentrator (PDC) detects late data arrival or lost packets and requests a new packet to the PMU. This may add an additional delay in the measurement. In cases where the PDC is not able to detect erroneous measurements, some interpolation techniques could be implemented to replace the missing measurement.

2.5 Concluding remarks

The main aim of this research is the system protection against large disturbance rotor angle instability, which is also commonly referred to as the transient instability. In the case of a disturbance leading to transient instability, fast recognition of the potentially dangerous conditions is very crucial for allowing sufficient time to take control actions [14]. This chapter presented a short survey of early transient stability assessment methods which are predominantly developed for dynamic security assessment, their advantages and limitations in near real-time applications based on the wide area measurement technology. Recently published research related to predicting the transient stability based on measurements was reviewed. Many of these methods apply machine learning techniques for learning complex relationships between the measured power system variables and the transient stability. Accuracy of phasor measurements as well as the speed and reliability of telecommunication infrastructure are important preconditions required for implementing wide area measurement based control and protections schemes.

Chapter 3

Early prediction of transient stability status

3.1 Introduction

The basic framework of the transient stability status prediction scheme proposed in this thesis is presented in this chapter. The generic structure of the proposed scheme consists of a classifier which uses system measurements taken after a disturbance as inputs to classify the future transient stability status as *stable* or *unstable*. The performance of the proposed scheme was systematically evaluated with different candidate predictor sets to select the most suitable inputs. The tests were carried out using a test power system that is commonly used for power systems dynamic research.

3.2 Definition of transient stability status prediction and its objectives

In this thesis, the term *transient stability status prediction* means progressive monitoring of power system variables after a disturbance and determining whether the transient

swings arising from the disturbance are stable or not. The aim of such exercise is to activate suitable emergency control actions such as system separation, generation shedding, load shedding, dynamic breaking, generator fast valving, and HVdc terminal control, if an instability condition is detected. Since the time frame associated with transient stability phenomena is in the order of a second, the prediction of transient stability status has to be extremely fast, in order to allow sufficient time for taking a remedial action. Transient stability status prediction explored in this thesis differs from the *online dynamic security assessment* which usually focuses on the determination of a stability margin such as the critical clearing time (CCT) in response to a given contingency. In contrast to dynamic security assessment, transient stability prediction does not focus on a particular fault or disturbance, and primarily involves monitoring of the post disturbance period.

Generator rotor angles and speeds are directly affected by the electromechanical changes that occur during an external disturbance. The transient instability generally manifests as separation of generator rotor angles. Thus the most direct indicators of the transient stability status are the generator rotor angles. Deviation of the generator rotor angles from their pre-fault steady state values is a result of the acceleration or deceleration of the rotors due to transient imbalance between the mechanical power and the electrical power output. Therefore, the rate of change of rotor angles or the frequency deviations are another potential set of indicators. However, generator voltages are also indirectly affected as the electrical power output of the generators could vary during the post-fault period. Figure 3.1 shows an example of the typical variations of the voltage magnitudes, rotor angles and the speeds of the generators in a power system after being subjected to a three phase short circuit. These waveforms are obtained by simulating a fault in the 39-bus test

system [34]. The fault is applied at 0.1 seconds and cleared after 5 cycles. The plotted curves are the voltage magnitudes, rotor angles and the rotor speeds of the 10 generators connected to the test network. This fault leads to a transient instability which is clearly indicated by the separating generator rotor angles.

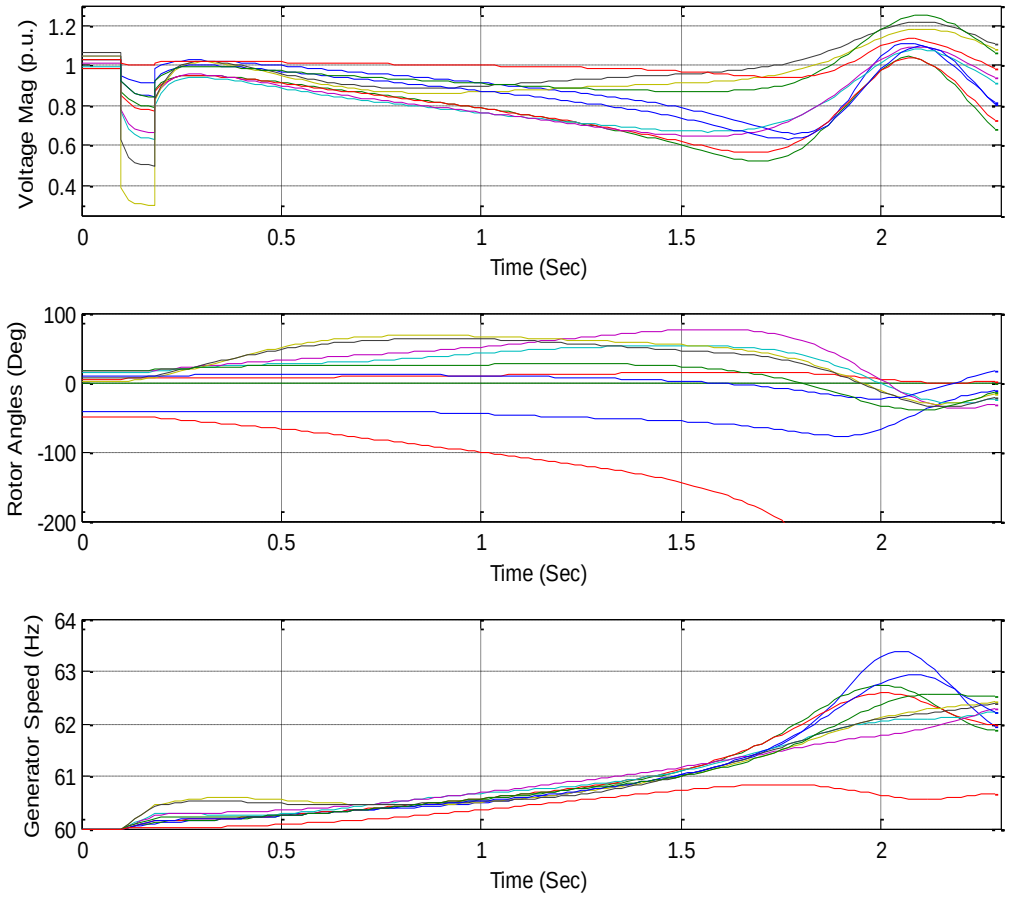

Figure 3.1 Variations of the voltage magnitudes, rotor angles and generator speeds during a contingency leading to instability

In Figure 3.2, the variations of the voltage magnitudes, rotor angles and generator speed corresponding to a case of fault that is not leading to transient instability is presented. The contingency applied is similar to the previous case, but at a different location on the 39 bus New England test system. The same variables corresponding to the 10 generators are shown in the graphs.

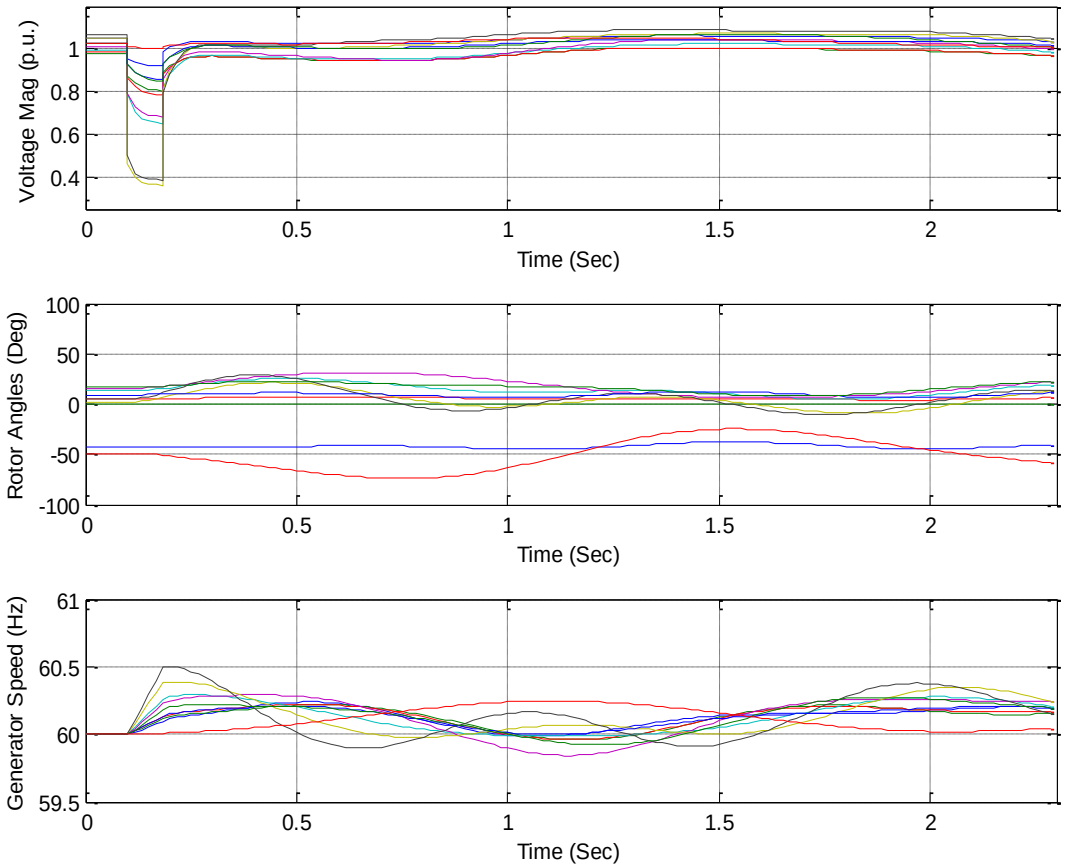

Figure 3.2 Variations of the voltage magnitudes, rotor angles and generator speeds during a contingency not leading to instability

During and after clearing the fault, all three variables (voltage magnitude, rotor angle and rotor speed) show some change and those changes are somewhat different for the stable and unstable cases. The proposed investigation is based on the hypothesis that subtle differences existing in the trajectories of these variables following the clearing of a fault can indicate whether the system is going to be transient stable after the disturbance or not. For example, the generator voltage variations shown on the two graphs in Figure 3.3 have some subtle differences during the interested period shown in boxes. The top graph corresponds to a case where the system is stable after a fault and the bottom graph is for a fault that leads to system instability. Such differences should help predicting the stability status

after a fault. Based on the hypothesis stated above, we must be able to find a relationship between the observed variations in the rotor angle, frequency or voltages and the transient stability status. However, for a multi-machine system this relationship is not straightforward, but can be learned from examples using a machine learning technique.

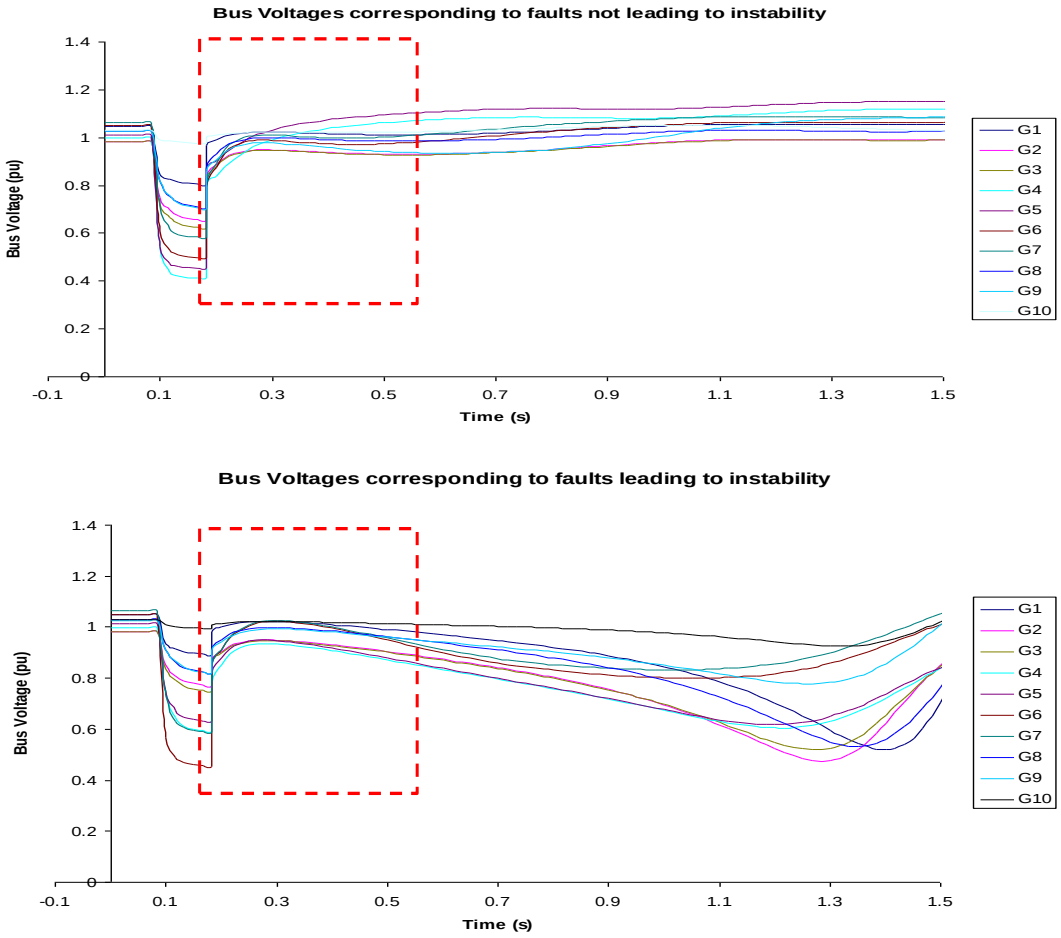

Figure 3.3 Variations of the generator voltages following a fault that is not leading transient instability (top) and a fault that is leading to transient instability (bottom)

3.3 Approach for transient stability status prediction

The problem of predicting the future transient stability status based on the present measurements can be formulated as a classification problem as shown in Figure 3.4. The inputs to the classifier, $x_i(k)$, are the sampled values of the predictor variables, which could

be the generator rotor angles, speeds or the voltage magnitudes, while the output, $y(k)$, is the stability status with k being the sample number and i being the measurement point. The complex relationship between the post-fault variations of the power system variables and the system stability status is learned by the classifier during the training process.

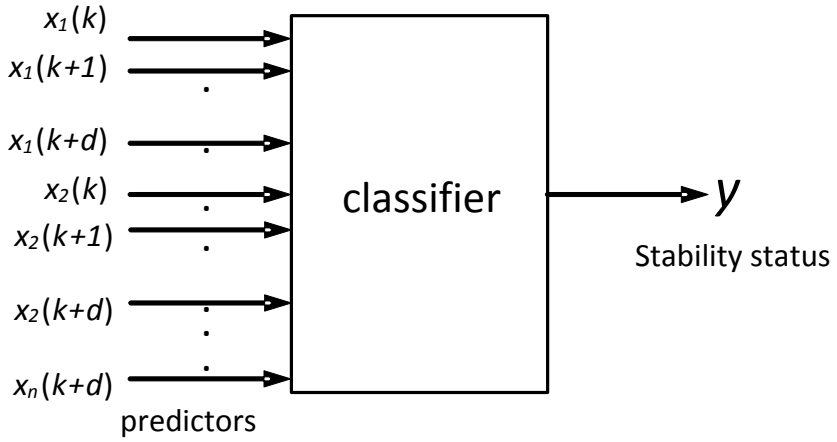

Figure 3.4 Arrangement of the transient stability prediction scheme

It is assumed that all input variables, for example the voltages of different generators which could be located geographically far from each other, are sampled simultaneously as shown in Figure 3.5. This type of synchronized sampling can be achieved using phasor measurement units. The sampled values of the different variables need to be communicated to a central location where the transient stability status prediction is performed. Thus this thesis assumes availability of suitable wide area measurement infrastructure. The performance requirements expected from the wide area measurement infrastructure was briefly discussed in Chapter 2.

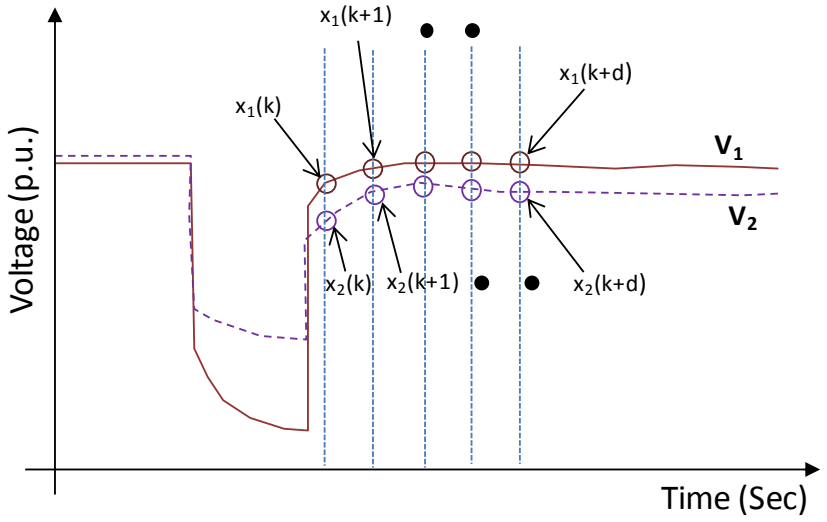

Figure 3.5 Synchronized sampling of two signals

The general procedure for designing the classifier of the proposed transient stability status prediction scheme is illustrated in Figure 3.6. The classifier needs to be trained using example data. The training data are generated through simulation of various credible contingencies in the considered power system. Then the features for the classification are extracted from the simulation outputs and a class label is attached to each set of inputs features depending on the stability status observed after the contingency. A part of this database is then used for training the classifier. The rest is used for verification of the trained classifier.

Two important factors for the success of this scheme are the selection of appropriate set of inputs (or predictors), and the accuracy of classification. After a careful review of various techniques, Support Vector Machines (SVMs) was selected for implementation of the classifier. The technique is described in Section 3.4. The procedure used for the selection of predictors and the results of this investigation are presented in Section 3.5.

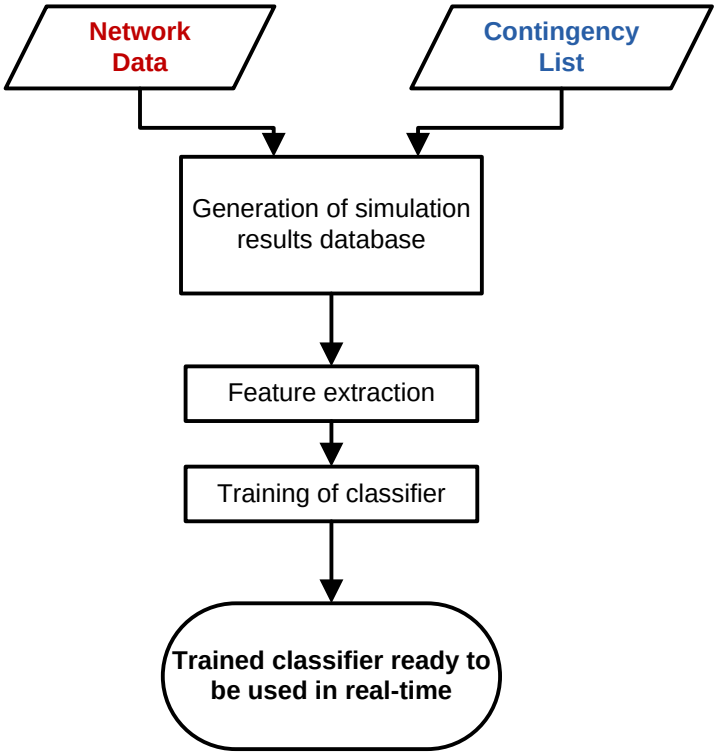

Figure 3.6 Process of designing the transient stability prediction scheme

3.4 Support Vector Machine (SVM) classification

The Support Vector Machines are a general method to solve classification, regression and estimation problems. Given a set of input-output (possibly noisy) examples, training of an SVM classifier involves finding an optimal decision function $f(\mathbf{x})$ that accurately predicts unseen data into different classes and minimizes the classification error [39]. Given a set of training data $\{(\boldsymbol{x_1}, y_1), \ldots, (\boldsymbol{x_N}, y_N)\}$, where $\boldsymbol{x_i} \in \mathfrak{R}^{\boldsymbol{D}}$ are the input vectors and $y_i \in \{-1,1\}$ are the corresponding class labels, an SVM seeks to construct a hyperplane that separates the data with the maximum margin of separability [38]. N is the number of observations, and D is the dimension of the input vectors.

Traditional neural network and other machine learning approaches have suffered difficulties with generalization, producing models that can over-fit the used data. The reason for

this effect is the type of optimization algorithms used during the parameter selection stage and the statistical principles used to obtain the best possible model [39]. In 1995 Vapnik proposed the foundation of what is known as Support Vector Machines (SVM). Since then, this technique has been used to solve different problems due to its attractive features and promising empirical performance [37]. The main attractive feature of SVM is the generalization capability which is less affected by the number of input features. The SVM classifiers keep a high performance under changes in the input signals due to variations in the system analyzed. This is a key factor in power system applications due to wide range of operating conditions and topology changes undergoing in a power grid. It is also less affected by variations in the input signals due to noisy measurements.

The problem formulation relies on the Structural Risk Minimization (SRM) principle, which has been shown to be superior to traditional Empirical Risk Minimization (ERM) principle employed by the conventional neural networks.

The decision function of a SVM binary classifier can be written as

$$f(\mathbf{x}) = sign\left\{\sum_{\mathrm{j}=1}^{\mathrm{N^{SV}}} \alpha_{\mathrm{j}}\, y_{\mathrm{j}}^{\mathrm{SV}} \left(\mathbf{\Phi}(\mathbf{x}) \cdot \mathbf{\Phi}(\mathbf{x}_{\mathbf{j}}^{\mathbf{SV}})\right) + \mathrm{b}\right\} \tag{3.1}$$

Where $\boldsymbol{x_j^{SV}}$ are the support vectors, $\Phi(\cdot)$ is a nonlinear vector function that maps the input vector onto a higher dimensional feature space [38], $y_{\mathrm{j}}^{\mathrm{SV}}$ is the label corresponding to the j^{th} support vector, N^{sv} is the number of support vectors, b is a bias term, and α_j are the Lagrange multipliers obtained from solving the dual optimization problem that minimizes the objective function

$$\frac{1}{2}\|\mathbf{w}\|^2 + C\sum_{i=1}^{N}\xi_i \tag{3.2}$$

subject to

$$\xi_i \geq 0 \qquad \forall\, i = 1, \ldots, N \tag{3.3}$$

$$y_i(\mathbf{w}\cdot\mathbf{x_i} + b) \geq 1 - \xi_i \qquad \forall\, i = 1, \ldots, N \tag{3.4}$$

This optimization is the process that trains the SVM by selecting the support vectors from the training data set. The parameter C(>0) in the objective function given in (3.2) is a factor that controls the trade-off between the separation margin and training errors, $\|\mathbf{w}\|$ is the norm of a vector perpendicular to the separation hyperplane and ξ_i are the slack variables which measure degree of misclassification [38]. The inner product $\left(\boldsymbol{\Phi}(\mathbf{x})\cdot\boldsymbol{\Phi}(\mathbf{x_j^{SV}})\right)$ is called the kernel function and denoted by $K\left(\mathbf{x}, \mathbf{x_j^{SV}}\right)$. In Figure 3.7, the process of mapping the input vector onto the higher dimensional space is shown. Among, the common kernel functions are the polynomials, radial basis functions and sigmoid functions. The kernel function used in this thesis is the radial basis function (3.5). This is most widely used function due to its outstanding performance for most scientific applications and overcomes the drawback of polynomial functions which requires the selection of the optimal order of the function that maximizes the classification accuracy for the stability prediction.

$$K\left(\boldsymbol{x}, \boldsymbol{x_j^{SV}}\right) = e^{\left(-\frac{\|x - x_j^{SV}\|}{2\sigma^2}\right)} \tag{3.5}$$

where σ is the width of the Gaussian. This was selected because it gave the most satisfactory results when compared to the other alternative such as linear and polynomial functions.

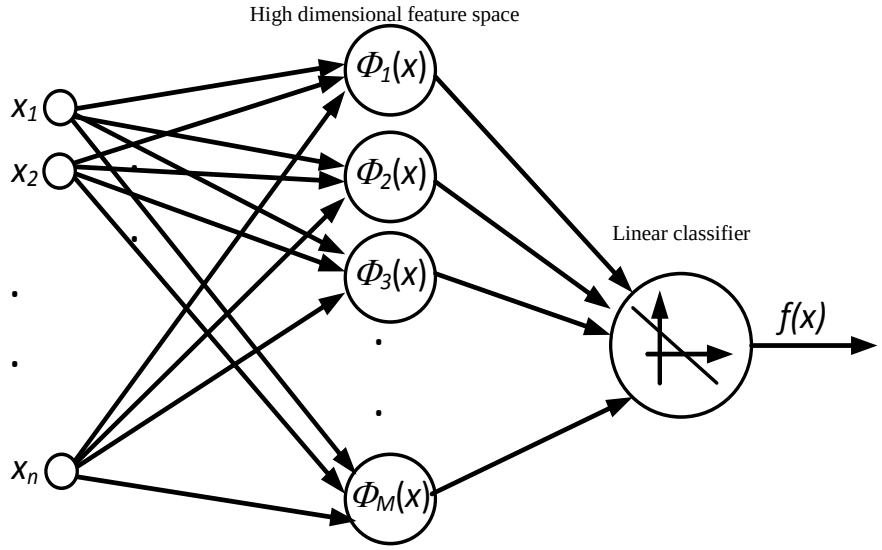

Figure 3.7 Nonlinear SVM classification by mapping the input vector into a high dimensional feature space

3.5 Comparison of different transient stability status predictors

As discussed in Section 3.2, transient instability of a power system is directly related to the angular separation between generators, and therefore, the generator rotor angles or the terminal voltage phase angles have been used for deriving indicators of transient instability. Most of the previously reported transient instability assessment and prediction algorithms use measured rotor angles (or voltage phase angels) as the inputs [8, 9, 25, 30, 34]. Nevertheless, to observe an angular separation that is large enough to assess the system stability, a considerable window of time needs to be passed after the fault. Additionally, in order to be meaningful, the rotor angle measurements should be expressed relative to a common reference frame called the centre of angles. The reference or the centre of angles

is not a constant and it has to be evaluated for each time instant considering the rotor angles of all the generators connected to the system as that instant using (2.1). Computation of the reference and expressing all angles relative to it involves an extra processing step that should be taken into consideration [8, 9, 25].

Although the transient stability is a phenomenon associated with rotor angles, variations of the rotor speed (as indicated by the frequency) and the voltage magnitudes after a fault can provide some useful information about the subsequent stability status of the system. For example, the Bonneville Power Administration's (BPA) Wide Area Stability and Voltage Control System (WACS) uses voltage magnitudes as measurement inputs [42]. In this research, use of two alternatives, namely (i) the generator speeds and (ii) the terminal voltage magnitudes, for predicting the transient stability of the system are examined. All three quantities can be easily obtained through a PMU based Wide Area Measurement System.

3.5.1 Test system

The IEEE 39-bus system (New England power system) was used as a test system to generate the data required for training and evaluating the performance of the proposed transient stability status prediction scheme. This test system comprises 39 buses, 10 generating units, 19 loads, and 46 transmissions lines [34]. The System is shown in Figure 3.8. This system has been popularly used for testing stability enhancement applications [34].

3.5.2 Training data generation

Data required for training the classifier were generated through off-line dynamic simulations [59]. The commercial software Transient Stability Assessment Tool (TSAT) was used for this purpose. The contingencies considered were three-phase to ground faults on each bus and three locations (at 25%, 50% and 75% of the length) on each transmission line. A standard clearing time of 5 cycles was assumed for all the contingencies. The above contingencies were repeated at four different operating levels (base case, base load plus 5%, 7% and 10 % increase). A total of 492 simulation cases were generated and for each case, the post-contingency variations of generator voltage magnitudes, speeds and rotor angles were recorded.

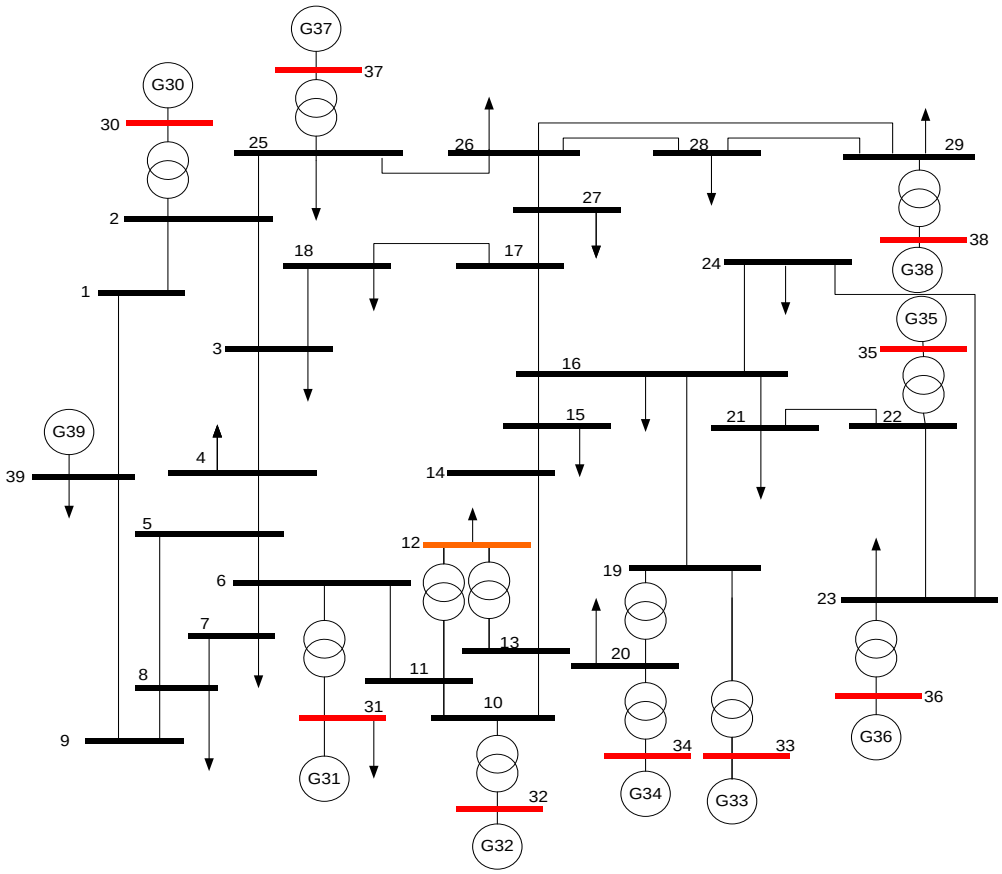

Figure 3.8 IEEE-39 bus test power system

A class label was assigned to each simulation case based on a transient stability index calculated based on generator rotor angles. This index is calculated after the time-domain simulation in TSAT [26]. The index is computed for each island in system, if the system is separated into independent power islands as a result of the contingency. The index is defined as

$$\eta = \frac{360° - |\Delta\delta|_{max}}{360° + |\Delta\delta|_{max}} \tag{3.6}$$

Where $|\Delta\delta|_{max}$ is the absolute value of the maximum angle of separation between any two generators during the post-fault period. When the transient stability index $\eta > 0$ the system is considered as stable and the class label of "1" is assigned for the simulation case; otherwise the system is transiently unstable and the class label of "-1" is assigned.

3.5.3 Cross validation

Generally, design of a classifier using machine learning requires two data sets, a learning set and a testing set. The leaning data set is used to train the classifier and the testing data set is used to evaluate the classifier accuracy for unseen cases [60]. The method used for partitioning the simulation database into training and testing sets is called K-fold cross-validation. In this method data is split into K partitions of approximately equal size. One partition is reserved for testing, and the rest of the data are used for training the classifier. This process is repeated, each time selecting a different partition for testing, until all K partitions have been used as a test set. Finally, the average of these errors is taken as the expected prediction error. The steps followed for evaluating the classifier using cross-validation are:

- Divide the data set into K partitions. In this case, K has been selected as 4.
- Leave out one of the partitions for testing the classifier.
- Use the remaining K-1 data groups for building the binary classifier.
- Use the test set in the classifier and determine the error between the observed and predicted labels.
- Repeat step 2 through 4 until all the partitions have been evaluated by the classifier.

3.5.4 Comparison of predictors

A systematic investigation to compare the prediction accuracy with different inputs was carried out and the results are presented in Figure 3.9, where the accuracy of the classifier is plotted against the number of consecutive samples of a given variable used to create the input vector (*d*) for the classification. The performance of the classifier with the three different input variables considered (voltage phasor magnitudes at the fundamental frequency, rotor angles and generator speeds) are compared in the graph. According to the results obtained, the best accuracy was always obtained with the classifier which used voltage magnitudes as inputs. Furthermore, this classifier was able to achieve over 98% accuracy just with four consecutive samples of each generator bus voltage. The maximum prediction accuracy achieved using the rotor angles was 94.1%, but that required using 12 samples of each generator rotor angle. These results confirm the observation made in [46], that is voltage magnitudes can more accurately predict the transient stability of a power system within a shorter time period when compared to conventionally used rotor angles.

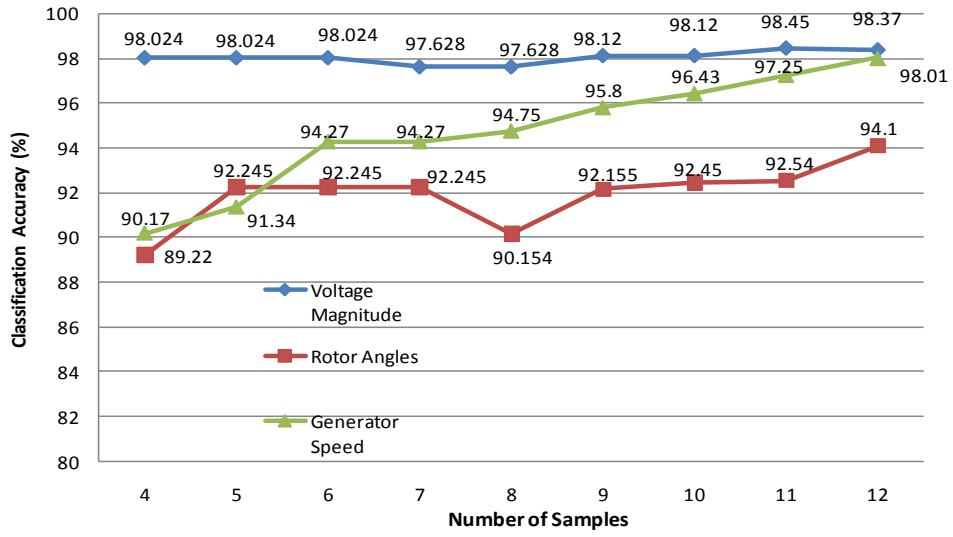

Figure 3.9 Variation of prediction accuracy with the number of samples of the input variable

The results in Figure 3.9 also indicate that the generator speeds (frequencies) are also a good predictor of transient stability. However, in order to achieve the prediction accuracy comparable to that achieved with generator voltage magnitudes, use of 12 consecutive samples of each generator speed was required. The sooner the prediction is completed the longer the time available to take control actions to avoid a possible system collapse. The response of generator speed and the rotor angle to a fault are considerably slower than that of the voltage magnitudes which has a quasi-instantaneous change after the disturbance.

Due to inertia, the generator rotor speeds and the rotor angles require longer periods of time to show a considerable deviation from their pre-fault steady state values. Use of combinations of inputs consisting of rotor angles and voltage magnitudes or generator speeds and voltage magnitudes was not much effective as a longer time window is re-

quired to observe significant improvement in the accuracy of prediction. This also leads to increase the number of inputs to the SVM rapidly without significant gain in accuracy. Based on the above observations, the stability prediction scheme that uses only four consecutive samples of voltages magnitudes as inputs was selected for further analysis in the next chapter of this thesis.

3.6 Concluding remarks

In this chapter, the framework of the new transient stability prediction scheme, which features a Support Vector Machine binary classifier, was introduced. The chapter also compared the effectiveness of three possible transient stability status predictors: sampled values of the (i) bus voltage magnitudes, (ii) generator speeds and (iii) the rotor angles, taken immediately after the fault clearance. This study, carried out using the IEEE-39 bus test system, showed that bus voltage magnitudes result in the most accurate and the fastest predictions. The other variables required a longer period of time to reliably declare the impending transient instabilities.

Chapter 4

Prediction of transient stability with voltage magnitudes

4.1 Introduction

In Chapter 3, a novel approach for fast prediction of the transient stability status of a multi-machine power system was formally presented. The novelty of the proposed approach lies in use of post-disturbance voltage magnitudes as predictors of transient stability status and application of Support Vector Machine classification theory for prediction. After evaluating the classification performance with three different input variables namely the generator rotor angles, generator speeds and the generator voltage magnitudes, it was found that voltage magnitudes is the most promising indicator for predicting the transient stability status of the system after a large disturbance. In this chapter, the performance of the transient stability status prediction system which takes the generator voltage magnitudes as inputs is thoroughly tested using simulations models of different test systems including large actual power systems.

4.2 Voltage magnitudes as transient stability predictors

When a fault occurs, the bus voltages in the system dip. Once the fault is cleared, the bus voltages attempt to recover to normal limits. The rate of recovery however, differs based on the severity of the fault. Examination of many simulation cases showed that in the case of a fault that would lead to transient instability, this rate of recovery of voltages is somewhat slower than the case of a fault that does not lead to transient instability. This difference helps the classifier to predict any impending transient instability at a very early stage.

When using the rotor angle based algorithms, the rotor angles need to be referred to the Center of Inertia (COI) angle to be meaningful. Calculation of the COI angle requires the inertia values of all connected generators. Furthermore, COI angle needs to be updated in real-time using the measurements. However, use of voltage magnitudes, which does not need such referencing except for normalizing using fixed, known base values, simplifies the required real-time processing.

In the proposed algorithm, it is assumed that a signal can be generated to trigger the transient stability status prediction algorithm using either tripping signal(s) issued by the local protection or by observing the transient dips in the voltage magnitudes due to the fault. Generation of the trigger signal will be described later in the thesis. This trigger allows identifying the instance when the fault is cleared and starting of collecting the samples of the input variables to construct the classifier input vector (**x**). The version of classifier chosen for further studies takes four consecutive synchronously measured samples of each generator bus voltage magnitude to form the input vector for the classifier. These sampled points are very close to each other in magnitude and discrimination between sta-

ble and unstable cases is not straightforward. However, in the SVM classifier, these inputs are mapped to a higher dimensional space using radial basis kernel functions making the classification achievable using a linear hyper plane.

4.3 Detailed testing on 39-Bus test system

4.3.1 Accuracy of predicting transient stability status after symmetrical faults

The training and testing data used in the investigation carried out in Chapter 3 were generated using the conventional dynamic simulation package (TSAT) [26]. These simulations provide the positive sequence voltage phasors of bus voltages and very accurate for symmetrical faults. These types of disturbances are characterized by a prominent voltage dip during the fault. In this test, the same simulation database generated in Section 3.4.4 of the previous chapter will be used.

About 75 % of the generated data was used for training the classifier and the remaining 25 % was utilized for testing the performance. During the training process the support vectors are calculated which are the parameters that define the optimal separating hyperplane. The regularization parameter C and the parameter γ associated to the RBF kernel were optimized through a grid search during the K-folded cross validation process explained previously.

After training the classifier, the classification accuracy for unseen cases was tested. The details of the results obtained are presented in Table 4.1. The classifier demonstrated a perfect accuracy in predicting the stability status for the contingencies that do not lead to

instability. For the cases where the contingency results in transient instability, the prediction accuracy was 95.45%, which corresponds to 45 out of 47 cases. The overall prediction accuracy is 126 out of 128 cases, or 98.4%.

Table 4.1 Prediction accuracy for symmetrical faults

Condition	**Prediction Accuracy on Testing Data**	
	Classified as Stable (%)	Classified as Unstable (%)
Stable Case	100 % (81/81)	0% (0/81)
Unstable Case	4.5% (2/47)	95.4% (45/47)

4.3.2 Accuracy of predicting transient stability status after asymmetrical faults

The proposed transient stability prediction technique showed good performance under symmetrical faults. Although less severe in nature, most of the faults in power systems are asymmetrical faults, and therefore it is important to ensure that the proposed system works well even under asymmetrical faults. Not only the unstable conditions should be predicted accurately, but also the stable conditions should be predicted as accurate as possible to avoid unnecessary control actions.

Stability programs use sequence impedance data to simulate asymmetrical faults but output only the positive sequence voltages. Initial investigations showed that positive sequence voltages alone do not contain sufficient information to successfully predict the post-contingency stability status under all types of faults. Beside that the post-fault bus voltages calculated in these stability programs under unbalanced conditions are only ap-

proximate. Therefore, in order to accurately test the performance under unbalanced conditions, the power system was simulated in an electromagnetic transient (EMTP) simulation program. The 39-bus New England test system was implemented in PSCAD/EMTDC. The PSCAD simulation model was cross-validated against the phasor domain model [61]. This type of simulations requires much longer computational time compared to the dynamic simulations carried out in stability programs such as TSAT.

4.3.2.1. Generation of simulation database

The model of the IEEE 39 bus test system in PSCAD/EMTDC was used to simulate various asymmetrical and symmetrical faults. The fault types simulated were: single-line to ground, line-to-line, and line-to-line to ground as well as three-phase-to ground faults. The faults were created on all transmission lines at different locations (25%, 50% and 75% of the line length). The faults were cleared at different clearing times in the range of 5 to 10 cycles. These simulations were repeated at different loading conditions ranging from 95% to 112% of the base case load. In total 8,355 simulation cases were generated to use as training and testing data.

PSCAD/EMTDC simulations produce time domains waveforms. The voltage phasors were extracted from these waveforms using Fast Fourier Transform (FFT) component available in the software program. In order to emulate the function of a PMU, output of the FFT was sampled at a rate of one sample per cycle. Phasor values of all three phase voltages were recorded. This is an additional step required in extracting the voltage phasor magnitude data when compared with TSAT simulation program which directly

gives positive sequence voltage phasors. This process extracting phasor magnitudes is illustrated in Figure 4.1.

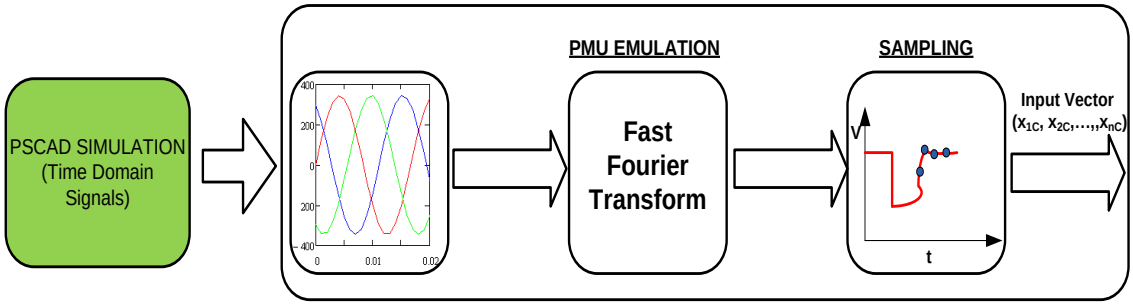

Figure 4.1 Pre-processing of PSCAD generated simulation data

4.3.2.2. Modified transient stability status prediction scheme

The structure of the transient stability prediction system was modified to accommodate asymmetrical faults. Since all three phase voltages are used, three classifiers, one per each phase, were trained using voltage magnitudes. If any one of the classifiers predicted the system to be unstable, the system is considered unstable. Thus the outputs of the three classifiers were combined using an OR logic. A modified transient status prediction scheme is shown in Figure 4.2.

The general process of developing the SVM classifier for the transient stability prediction scheme was presented in Figure 3.6. Note that if significant changes occur in the network or new disturbances need to be considered, the SVM must be retrained after modifying the simulation database accordingly. Initially, the training process comprises the calculation of the kernel parameters: γ and σ^2, the regularization parameter and the bandwidth respectively. This is achieved using a grid search method and it is the most time consuming stage of the classifier implementation. This is illustrated by the training

time required for this process when used 75% of the full database. The time required to run the SVM training program coded in MATLAB on a personal computer with an Intel Core 2 Duo @ 2.33 GHz processor and 3 GB of RAM memory was 51480.0 seconds (14 hours and 18 minutes approximately). Once, the optimal kernel parameters are obtained the support vectors that will hold the separating hyperplane need to be computed. The elapsed time for this computation was 48.0 seconds. This timing was obtained using a function available in Matlab programming language. Therefore, the total training time is approximately 51,528.0 seconds.

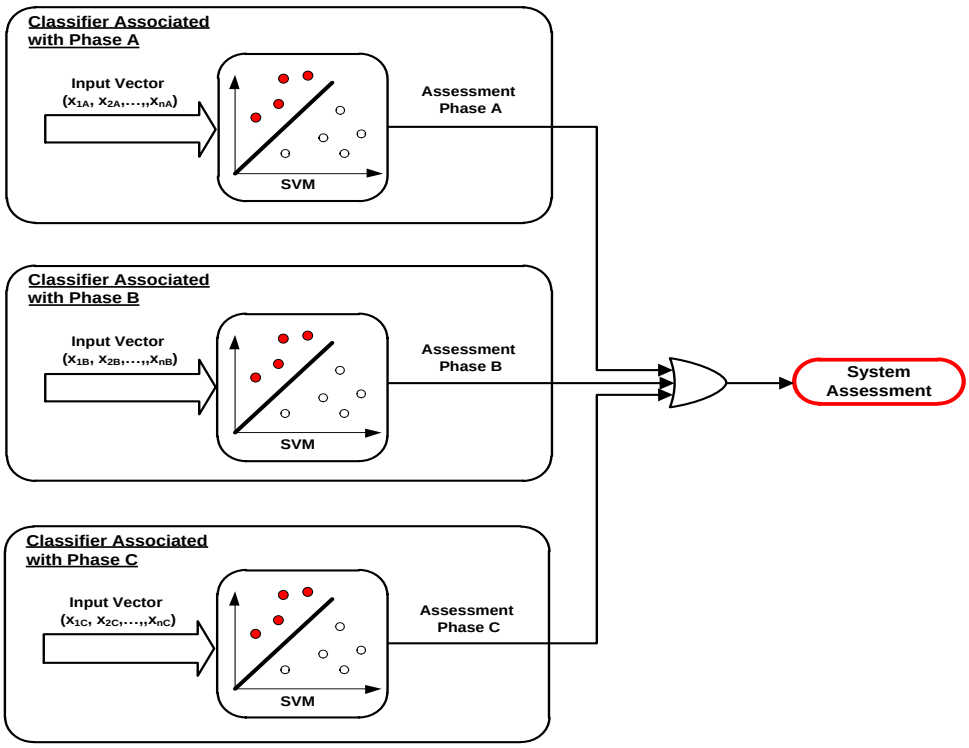

Figure 4.2 Modified transient stability status prediction scheme

4.3.2.3. Prediction results and performance

The performance of the proposed transient stability status prediction algorithm is evaluated by using the trained classifiers to predict stability status of the unseen cases in the

test data set. In this analysis, ten folds cross validation was applied. The optimal settings for the Gaussian Radial Basis Function kernel found through a grid search was $\sigma^2 = 0.1$ and the optimal value of the penalty parameter C=33.3. In order to analyze the performance, the test data was separated according to the type of fault. This allows observing how the classifier is performing under each type of faults. The results are summarized in Tables 4.2 to 4.6.

When all types of faults are considered, the stable cases were predicted as stable with 100% accuracy. In predicting the stability status of unstable cases, the highest accuracy was obtained in predicting the stability condition after single-phase to ground faults. An accuracy of 100% was obtained in this type of faults. The prediction accuracy decreased to 94.87% and 97.73% during the classification of phase-to-phase and phase-to-phase-to-ground faults respectively. For the case of three-phase to ground faults, the accuracy increased to 98.24%. Careful analysis of the misclassified cases showed that they were the marginally unstable cases and therefore misclassified as stable.

Table 4.2 Transient stability status prediction accuracy for single-phase to ground faults

Condition	**Prediction Accuracy on Testing Data**	
	Classified as Stable (%)	Classified as Unstable (%)
Stable Case	100% (219/219)	0 % (0/219)
Unstable Case	0% (0/36)	100% (36/36)

Table 4.3 Transient stability status prediction accuracy for phase-to-phase faults

Condition	**Prediction Accuracy on Testing Data**	
	Classified as Stable (%)	Classified as Unstable (%)
Stable Case	100% (173/173)	0% (0/173)
Unstable Case	5.13% (2/39)	94.87% (37/39)

Table 4.4 Transient stability status prediction accuracy for phase-to-phase–to-ground faults

Condition	**Prediction Accuracy on Testing Data**	
	Classified as Stable (%)	Classified as Unstable (%)
Stable Case	100% (137/137)	0% (0/137)
Unstable Case	2.27% (1/44)	97.73% (43/44)

Table 4.5 Transient stability status prediction accuracy for 3-phase–to-ground faults

Condition	**Prediction Accuracy on Testing Data**	
	Classified as Stable (%)	Classified as Unstable (%)
Stable Case	100% (103/103)	0% (0/103)
Unstable Case	1.75% (1/57)	98.24% (56/57)

Table 4.6 Transient stability status prediction accuracy for the entire database

Condition	**Prediction Accuracy on Testing Data**	
	Classified as Stable (%)	Classified as Unstable (%)
Stable Case	100 % (660/660)	0 % (0/660)
Unstable Case	2.84 % (5/176)	97.16 % (171/176)

4.3.3 Prediction accuracy and speed

The transient stability status prediction results presented so far indicate that overall accuracy is above 95%. Further analysis of the results show that predictions are 100% accurate when the system remains stable after the disturbance, that the scheme is very secure. When predicting the stability status after contingencies that cause transient instability, the accuracy is slightly lower, and there are few unstable cases that are incorrectly predicted. This could be due to smaller number of unstable patterns in the training database.

Since the transient stability is a very fast phenomenon that demands a corrective action within short period of time (< 1s) [30], fast detection of instability is essential. The time before loss of synchronism is dependent on the system inertia, damping and the severity of the disturbance. The frequency of a swing can vary from a few tenths of a Hz to 2 Hz [62]. If a maximum swing frequency of 1 Hz is considered, about 0.5 sec is available to predict the stability status and deliver control decision to actuators within the first swing. Observation time required in the proposed method is 0.067 ms (4 cycles) and that allows over 400 ms for measurement, telecommunication and processing delays.

Once the data (the vector of voltage magnitudes collected from 10 generator HV side terminals) is provided, the time required to classify a given unseen case was 0.034 s when used a MATLAB program on a computer with an Intel Core 2 Duo @ 2.33 GHz processor and 3 GB of RAM memory. In a real power system, monitoring of more voltages may be required depending on the system characteristics. The algorithm should be coded in a lower level programming language to increase the computational performance.

4.3.4 Effect of voltage dependent loads

As mentioned previously, prediction of transient stability status was possible due to differences in the rate of recovery of the voltage following clearing of a fault. This rate of recovery could be affected by the type of loads connected to the system, specially the voltage dependent loads. It is well known that the presence of induction motors adversely affects the transient stability of power systems. Reference [63] which discusses the disadvantages of using constant impedance representation of loads in stability studies points out that higher initial fault recovery voltages is one of the factors that could contribute to erroneous results. The voltage depressions resulting from the faults may cause tripping or change of control modes in certain loads such as induction motors and HVDC converters. When the bus voltages recover after fault clearance, these load components attempt to restore their power within the time period considered in transient stability. For this reason, it is considered that use of an appropriate load model is important in the analysis of transient stability of a power system [64].

In order to evaluate the effect of voltage dependent loads on the proposed algorithm, the constant power loads considered in the 39-bus test system were replaced by a composite load. To represent this type of load, a CLOD model available in the commercial software Power System Simulator (PSS/E) [27] was imported to TSAT model of the 39-bus test system. The reason for adopting this load model was the requirement of the simulation tool (TSAT) to have consistency in all dynamic models of the system under the same simulation platform which was PSS/E format. This load representation takes into account the effect of large and small induction machines connected to the network, as well as

fluorescent lighting, constant current and constant power loads [27]. In Figure 4.3, the main elements considered in this load representation are illustrated.

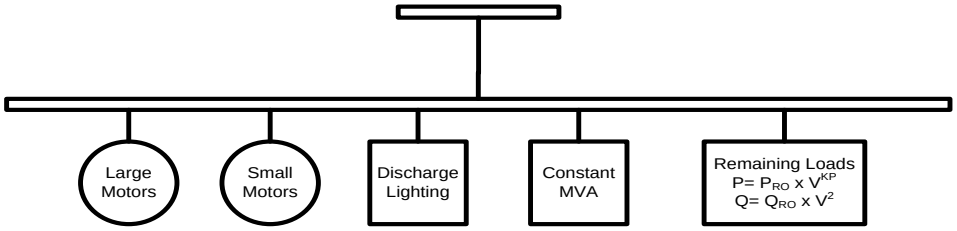

Figure 4.3 Scheme of the components considered in the dynamic model of the load

Simulations were carried out with different load compositions; the percentage of induction motor component in the load was varied from 10 to 60 %, which is considered as the range of induction motor component in typical HV substation load [64]. Figure 4.4 illustrate the effect of induction motor composition on the post-fault voltage trajectory of bus-30 of the test system after being subjected to a 3-phase to ground fault on the line connecting buses 4 and 14. The curves in Figure 4.4 clearly show that the higher the percentage of induction motor composition, the slower the recovery rate of the bus voltage magnitude. The test results presented in Table 4.7 show that this effect makes it easier to discriminate contingencies that lead to transient instability.

In Table 4.7, the overall accuracy of predicting transient stability status under different load compositions is presented. During the simulations, the percentages of discharge lighting and small induction motors were kept constant at 20% of the total load while the large induction motor composition was varied from 10 to 60% as shown in Table 4.7.

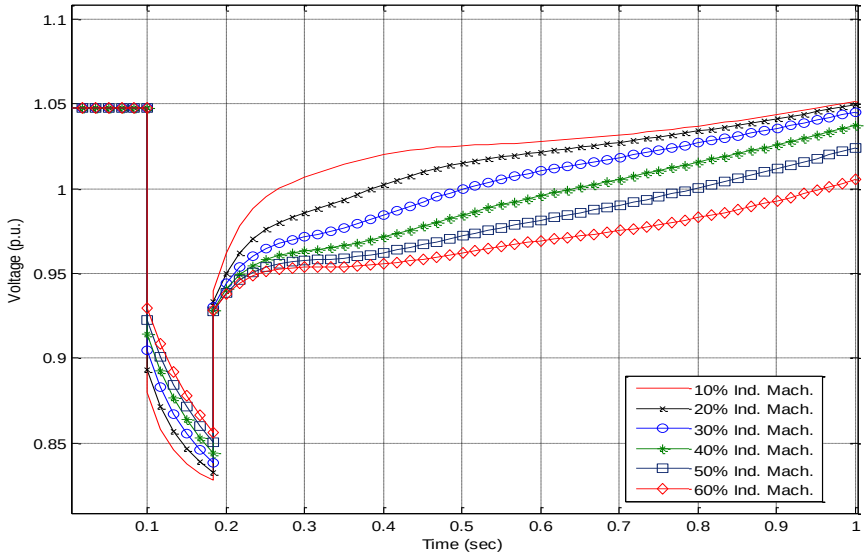

Figure 4.4 Voltage trajectories for different percentage of induction motor composition in the load

It was assumed that large induction motors are disconnected when the bus voltages drop below 0.8 p.u. and they get reconnected when the bus voltages climb back to 0.9 p.u.. The same composition was applied to all loads in the 39-bus test system. The contingencies applied were three-phase to ground faults at various locations and a typical clearing time of 5 cycles was assumed. The number of contingencies considered at a given load composition was 92. This gives a total of 552 cases when the six induction motor composition levels are considered. These new cases were not used for training the classifier. Parameters determined from the previous database (used in Section 4.3.1) were used to identify the stability status under these changes in the load composition. The accuracy of the classifier improved as the percentage of large induction motor was increased. When the composition of large induction motors was 10 and 20% the prediction accuracies were 98.52% and 99.23 % respectively. When the composition of induction motors is 30% or higher, the transient stability status prediction was 100% accurate.

Table 4.7 Effect of the load composition on the classification accuracy

Load Composition				**Overall Accuracy of Classifier (%)**
Large Induction Machines (%)	Small Induction Machines (%)	Discharge Lighting (%)	Constant Power (%)	
10	20	20	50	98.519
20	20	20	40	99.259
30	20	20	30	100.0
40	20	20	20	100.0
50	20	20	10	100.0
60	20	20	0	100.0

4.3.5 Impact of the network topology changes

Topology of a transmission network can be subjected to changes during the operation for various reasons such as equipment outages, scheduled maintenance, and other technical and economic reasons. In general, when designing the classifier different configurations should be taken into account. However, it is infeasible to consider all possibilities when generating the training data. The transient stability status prediction scheme should be able to work even with small changes to the network topology. To verify the robustness of the approach, the transient stability prediction method was tested under some topology changes. Three different scenarios were evaluated independently:

a) Generator 37 and the transmission line interconnecting Buses 25 and 26 in the test system were taken out of service,

b) The transmission line interconnecting Bus 5 and Bus 8 out of service, and

c) The transmission line interconnecting Bus 22 and Bus 23 out of service.

Such network changes are common in the day to day operation of power systems to accommodate maintenance or operational requirements. This topology change altered the pre-fault power flow and the voltage profile of the network. This also provides a new recovery characteristic after the system is subjected to a fault. The classifier trained with the original test system (the classifier used in Section 4.4.3) was used to predict the transient stability of the altered network. The contingencies considered were single-line-to-ground transmission line faults (applied at 25%, 50% and 75% of length). This type of fault was selected for representing the most common type in power network. The fault clearance times were ranged from 5-10 cycles. A total of 558 cases were generated for each scenario studied. All these cases were used as unseen cases to the prediction algorithm. The classification results are summarized in Table 4.8.

Table 4.8 Transient stability prediction under network topology changes

Scenario	**Prediction Accuracy on Testing Data**		
		Classified as Stable (%)	Classified as Unstable (%)
-Generator 37 out -Line between Bus 25 and Bus 26 out	Stable Case	99.76% (430/431)	0.23 % (1/431)
	Unstable Case	3.15% (4/127)	96.85% (123/127)
-Line between Bus 5 and Bus 8 out	Stable Case	100% (446/446)	0 % (0/446)
	Unstable Case	3.57% (4/112)	96.42% (108/112)
-Line between Bus 22 and Bus 23 out	Stable Case	100% (454/454)	0 % (0/454)
	Unstable Case	3.84% (4/104)	96.15% (100/104)

According to the results, the proposed algorithm managed to predict the transient stability with reasonable accuracy, even when the network topology was changed.

4.3.6 Effect of measurement errors

The *IEEE Standard for Synchrophasors for Power Systems* stipulates that PMUs with Level 1 compliance have to have a total vector error less than 1% [11]. Thus when using such PMUs to measure the bus voltages, the expected maximum magnitude error is 1% (in the case of total error is due to error in phasor magnitude).

In order to test the prediction performance under measurement errors, a random error between 0 and 1% was added to all the bus voltage measurements before using them as inputs to the binary classifier. The complete database which was used in Section 4.3.3 was used for this test. Initially, the algorithm was tested without using this new noisy data to train the classifier. The performance was very poor, as could be observed in Table 4.9. This test demonstrates that noisy measurements can seriously affect the prediction accuracy.

Table 4.9 Transient stability prediction accuracy with noisy inputs (using the classifier trained with training data without noise)

Condition	**Prediction Accuracy on Testing Data**	
	Classified as Stable (%)	Classified as Unstable (%)
Stable Case	72.046% (866/1202)	27.954 % (336/1202)
Unstable Case	30.975% (197/636)	69.025 % (439/636)

In investigating the ways to improve classification performance under noisy inputs, the classifier was re-trained with noisy input data before testing. Once the classifier is trained with noisy input data, the situation improved. The results presented in Table 4.10 shows a slight degradation of performance compared to the case of without noise, but it was able to predict the transient stability status with an overall accuracy of 95.83%, even when the random measurement errors are present in input signals.

Table 4.10 Transient stability prediction accuracy with noisy inputs (using the classifier trained with noisy training data)

Condition	**Prediction Accuracy on Testing Data**	
	Classified as Stable (%)	Classified as Unstable (%)
Stable Case	98.41 % (1189/1202)	1.58 % (13/1202)
Unstable Case	4.12% (43/636)	93.24 % (593/636)

4.4 Application to a power system with multiple DC infeeds

In this section, the performance of the classifier on a power system with multiple DC Infeeds is evaluated. For testing the algorithm a modified version of the New England 39-bus test network was used. The details of the modifications are presented in [61]. This new network contains two DC-links as shown in the single line diagram shown in Figure 4.5. For data generation and management, the same methodology described in Section 4.3.2.1 was used. The database of simulations was separated into training and testing data

with 75% of the cases allocated for training while the rest is reserved for testing the classification accuracy. The fault types simulated included single-line to ground, line-to-line, and line-to-line to ground as well as three-phase-to ground faults. The faults were created on all transmission lines at different locations (25%, 50% and 75% of the line length) for the base loading case. The clearing times were varied between 5 to 10 cycles.

A total of *2,137* cases were simulated using the Power System simulation tool PSCAD. As mentioned in the previous chapter, the training data set was selected by using the cross validation method. The total population was approximately divided into 4 groups of equal composition of stable and unstable cases. Three of these groups were which represents 75% of the population used to train the classifier and the remaining was used as test dataset. This process is repeated until all groups have been used as test dataset. The classification error was obtained as the average of all individual errors. The results are summarized in Table 4.11.

Table 4.11 Classifier performance for power networks with multiple HVdc-infeeds

Condition	**Prediction Accuracy on Testing Data**	
	Classified as Stable (%)	Classified as Unstable (%)
Stable Case	100 % (406/406)	0 % (0/406)
Unstable Case	3.75% (2/41)	96.25 % (39/41)

The overall accuracy is 99.55% (445 out of 447). Two out of the 41 unstable cases were wrongly classified as stable cases. Careful examination showed that these two cases are marginally unstable cases. This demonstrates that the proposed algorithm could also be used to predict the stability status in the network with multiple HVdc links.

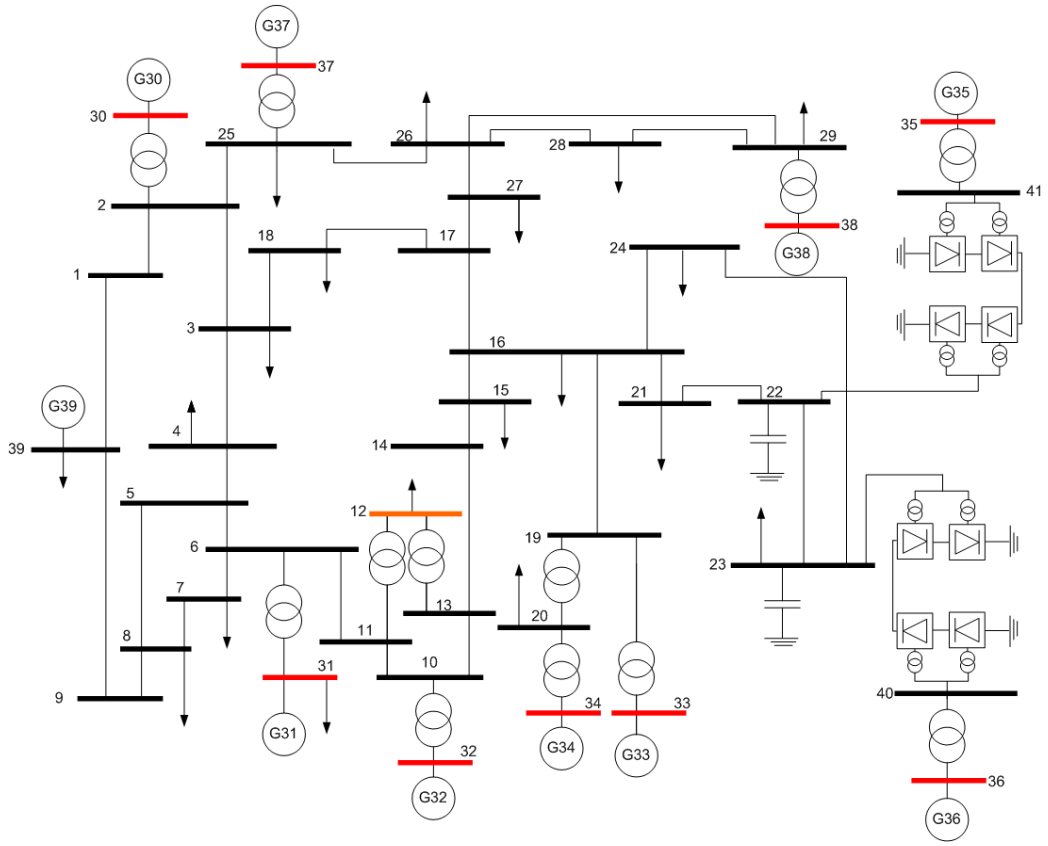

Figure 4.5 IEEE-39 bus test power system after adding multiple HVdc infeeds

4.5 Application to the Venezuelan power system

In this section, the proposed transient stability status prediction algorithm is tested on a model of the Venezuelan Power Electric Network, which is a practical example of a large AC power system. An up to date dynamic model of the Venezuelan power system was available in PSS/E format for this study. The dynamic model of the Venezuelan Electric System used for this study included all components in the power system from 4.16 kV distribution level to 765 kV extra high voltage transmission level. The PPS/E model included protection associated with generators and large motors, out-of-step tripping and load shedding schemes. However, line distance protection was not modeled.

The PPS/E model of the power system was imported to TSAT software program to perform the simulations due to flexibility of TSAT when generating a diverse set of training and testing scenarios in somewhat automated manner.

4.5.1 Main features of the Venezuelan power system

The Venezuelan power system is a highly interconnected grid with a total power generation of approximately 15,700 MW. Generation is predominantly (70%) hydro based and is located mostly in the southern region of the country along the Caroni River. The load centres are concentrated in the central and northern regions and therefore energy is transported via long transmission lines at voltages of 765 kV, 400kV and 230 kV. The modelled system comprises of 1140 major buses, out of which 7 are at 765 kV level, 28 are at 400 kV level, and 74 are 230 kV level. The rest of the buses are at subtransmission and primary distribution levels. Some of the buses are provided with static reactive power compensation (SVC) and a few transmission lines are series compensated. The Venezuelan system is also interconnected to the northern Brazilian and Colombian grids through 230 kV ac tie lines.

The main characteristics of the Venezuelan systems are summarized in Table 4.12. A simplified diagram of the Venezuela Power System is presented in Figure 4.6. Each region includes the sub transmission system below 230 kV and small generation plants. The main synchronized measurement points used to predict the transient stability are also indicated on the diagram.

Table 4.12 Salient features of the Venezuelan power system

Number of Buses	1140
Number of lines	914
Transformers	567
Number of Generators	91
Induction Motors (Large)	56
Static Voltage Compensators	2
Constant Current Loads	356
Constant MVA Loads	56
Total Power	15759 MW

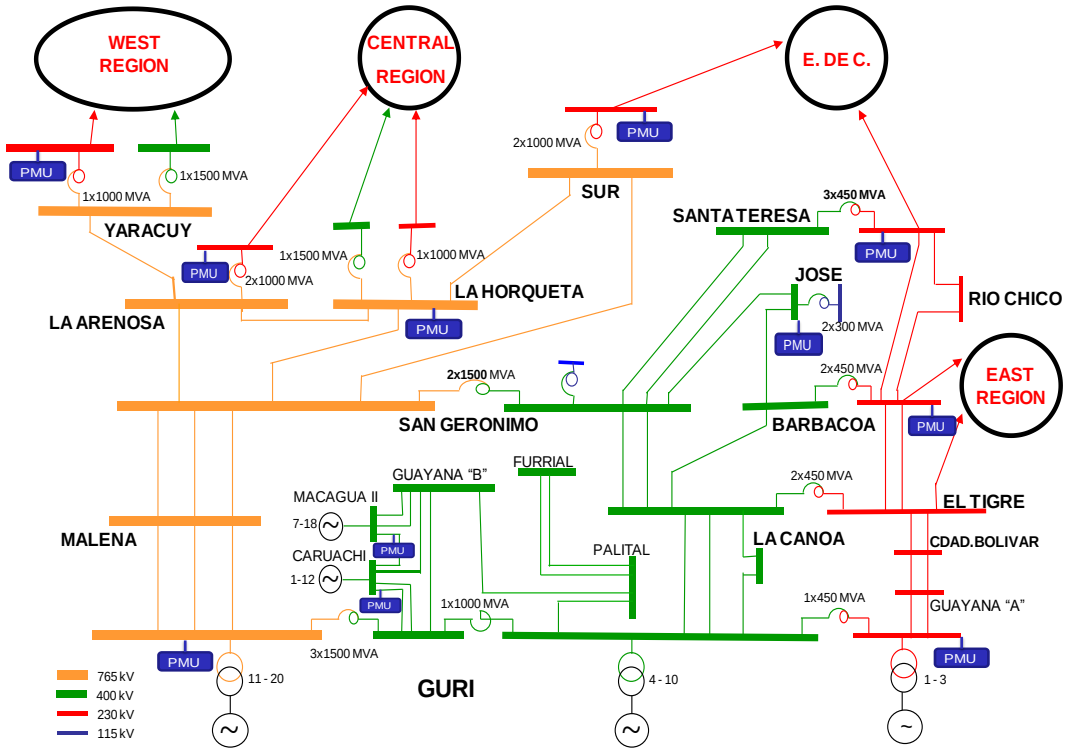

Figure 4.6 Simplified single line diagram of the Venezuelan power system

4.5.2 PMU location

In a large power system there is a large number of generators and it is neither economical nor required to monitor all of them. In this study, 15 PMUs were placed on the high voltage (230 kV, 400 kV and 765 kV) buses close to large generation/load centers. The specific locations of the PMUs were selected partly based on the familiarity of the system and the knowledge gained through stability studies. It will be shown later in this chapter that the 15 PMU locations chosen are sufficient for effective prediction of the system stability status after being subjected to a disturbance. The number and the placement of PMUs, shown on the simplified network diagram in Figure 4.6, can however be optimized using a techniques such as the one presented in [65, 66]. As indicated in [65] it may be required to incorporate expert knowledge to PMU location selection process. Some simulation examples are discussed below.

Figure 4.7 and Figure 4.8 show the voltage magnitude and rotor angle trajectories respectively for a 3 phase-to-ground fault on a transmission line interconnecting two 230 kV substations. Clearing of the fault by removing the line after 5 cycles causes transmission capacity loss of 175 MW. The fault does not cause a transient stability problem, and the voltage recovers after the fault. In Figure 4.8, which shows rotor angles of all generators in the system, it is also possible to observe that the rotor angles find a new stabilization point after the oscillations are damped out after about 3.2 sec.

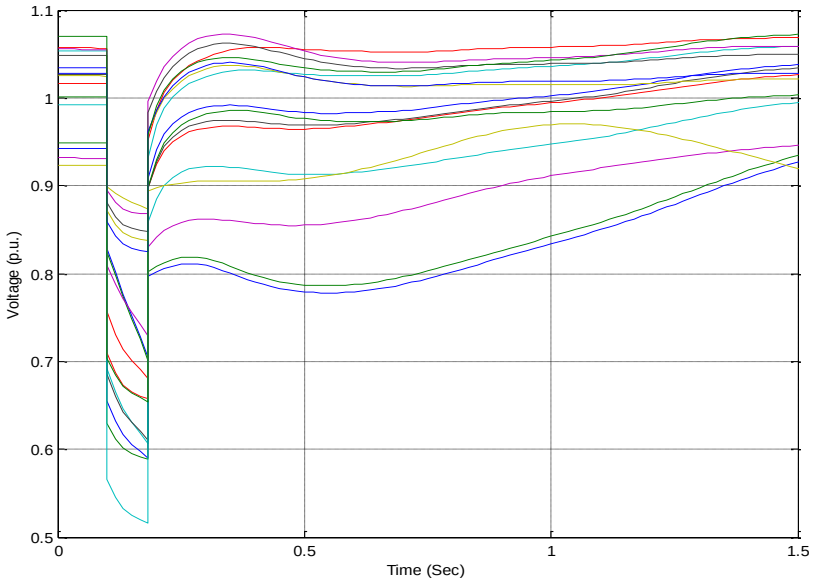

Figure 4.7 Voltage trajectories during a disturbance not leading to transient instability

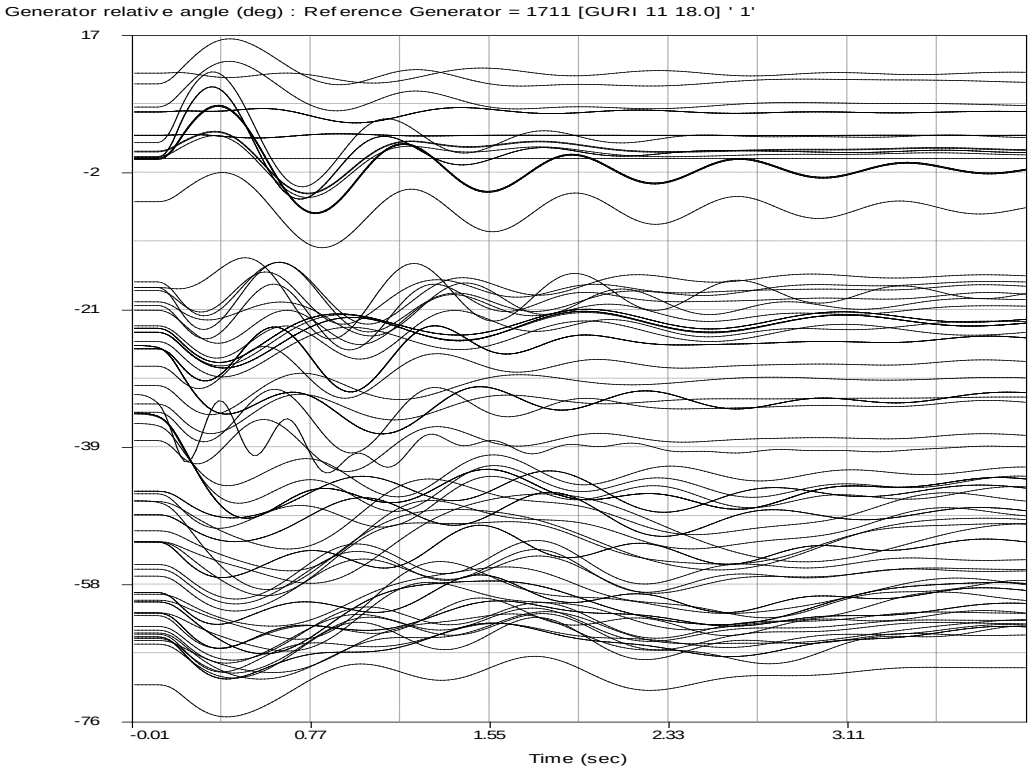

Figure 4.8 Rotor angles during a disturbance not leading to transient instability

In contrast, Figure 4.9 and Figure 4.10 show the waveforms corresponding to a different 3-phase-to-ground fault on a transmission line interconnecting two 765 kV substations Guri and Malena. This disturbance resulted in a loss of 1898.9 MW of transmission capacity. This scenario corresponds to a high loading condition with a large generation-load imbalance. This transmission line interconnects a large generation conglomerate in the Southern region with the largest states and industrial centres located in the Central region of the country. This fault is a very severe contingency and led to a condition of instability.

In Figure 4.9, a poor voltage recovery after the disturbance can be observed. Voltage magnitudes of some of the monitored buses stay below 0.6 p.u. during the post-fault period. On the other hand, the rotor angles of some critical machines accelerate against the rest of the system. These are the very small generators which range from 10-20 MW of capacity with a very small inertia in comparison to the large generators connected to the network.

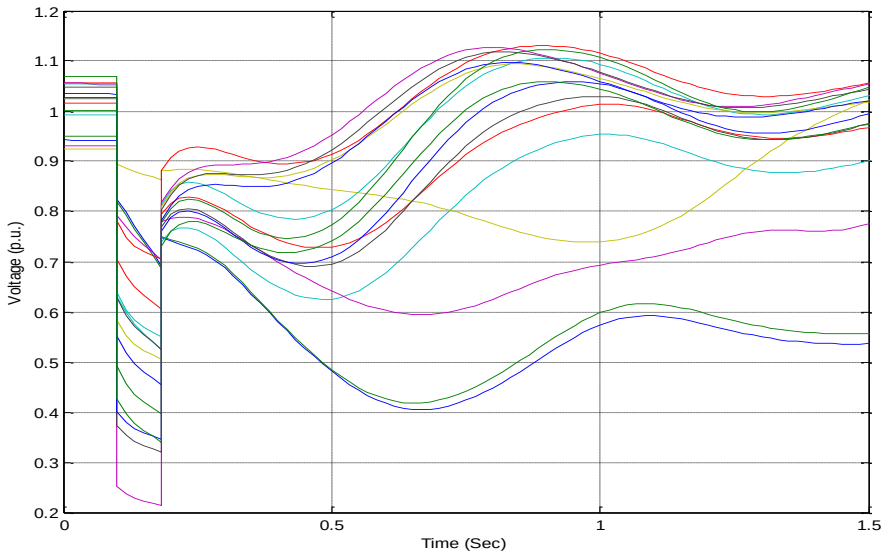

Figure 4.9 Voltage trajectories during a disturbance leading to transient instability

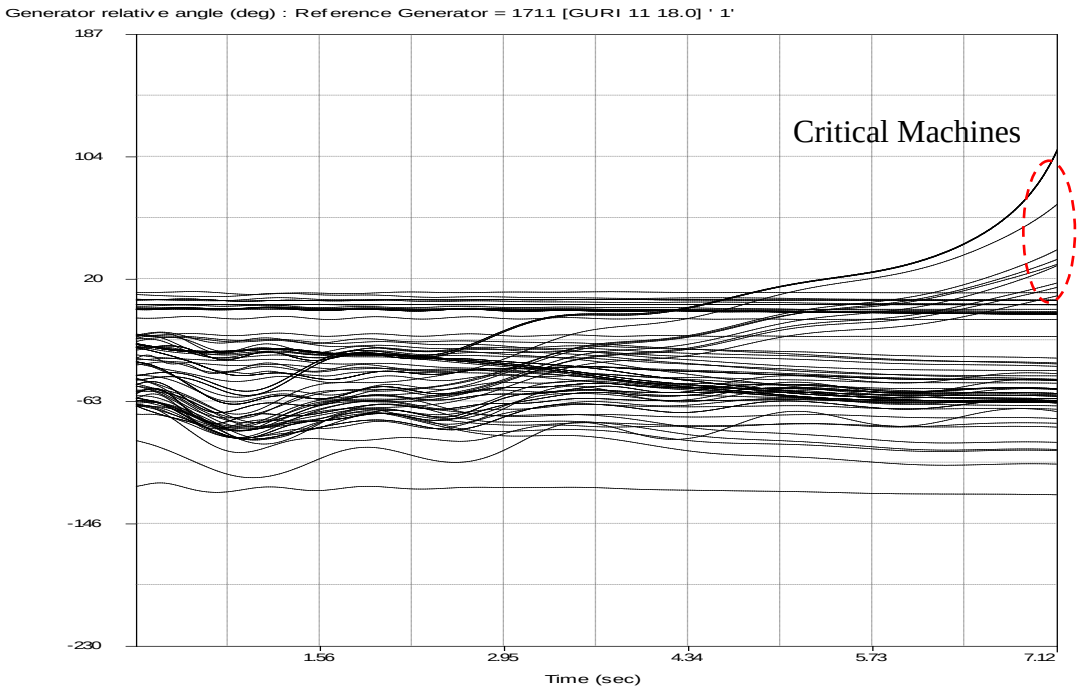

Figure 4.10 Rotor angles during a disturbance leading to transient instability

4.5.3 Design of the SVM classifier

As mentioned earlier, it was assumed that only 15 Synchronized Measurement Points are available. The selected locations include large generation centres that respond to power imbalances originated by severe contingencies. Thus the resulting SVM classifier has 60 inputs (15 buses x 4 consecutive samples). Since the system is simulated in TSAT, only the positive sequence phasors can be obtained. Thus only one classifier is needed to be trained.

In order to train the classifier simulation database was created. For each simulation case, variations of the voltage magnitudes at the synchronized measurement points (15 buses) were recorded, and at the end of the simulation, observed stability status was noted as the class label. Contingencies simulated were three-phase to ground faults on all transmission lines at 400 kV and 765 kV level. The fault clearing times were varied between 5-10 cy-

cles, to obtain a total of 402 contingencies. Similar to the methodology used for testing the transient stability predictor with the IEEE 39-bus test network, the contingencies generated in the Venezuelan System were also split into two groups. The training data set contained70% of the simulation cases representing 282 cases, and the testing data contained the remaining 120 cases, which amount to 30% of the total number of cases.

4.5.4 Prediction results and performance

The performance of the proposed transient stability status prediction algorithm is evaluated by using the trained classifiers to predict stability status of the unseen cases in the test data set. The results of the classifier performance are summarized in Table 4.13.

All stable and unstable cases considered in the test data set were predicted with 100% accuracy. This encouraging results show that the algorithm can effectively predict the first-swing stability status soon after a fault has been removed (approximately 4 cycles (66.667 milliseconds) plus communication delays).

Table 4.13 Transient stability status prediction performance on Venezuelan system

(Only the 3-phase-to-ground faults on 400 and 765 kV transmission lines are considered)

Condition	**Prediction Accuracy on Testing Data**	
	Classified as Stable (%)	Classified as Unstable (%)
Stable Case	100 % (89/89)	0 % (0/89)
Unstable Case	0 % (0/31)	100 % (31/31)

As described in Section 4.5.3, in generation of the training data, faults were applied only on the 765 kV and 400 kV transmission lines. The classifier trained with these data was tested for three-phase-to-ground faults on 230 kV transmission lines. A new test database

was created by applying faults on all 230 kV transmission lines. For the classifier, all 152 contingencies in the new test data set are unseen cases. Since the contingencies on 230 kV lines are not severe, the system was stable after all of the contingencies. Even though samples of these types of contingencies were not included in the training set, the classifier demonstrated 100% accuracy in predicting the stability status as seen in Table 4.14. This is possible due to the generalization capability SVM based classification. The ability of a hypothesis to correctly classify data not in the training set is known as its generalization. This is the outstanding feature that makes SVM a better machine learning technique over the classical ANN and DT.

Table 4.14 Transient stability status prediction performance on Venezuelan system

(3-phase–to-ground faults on 230 kV transmission lines)

Condition	**Prediction Accuracy on Testing Data**	
	Classified as Stable (%)	Classified as Unstable (%)
Stable Case	100 % (152/152)	0 % (0/152)
Unstable Case	0 % (0/0)	100 % (0/0)

This indicates the possibility of designing the transient classification system only considering the most important parts of the network (usually the higher voltage levels). This is a very important observation, because when implementing the prediction system on a per phase basis to handle the unbalanced faults, it is required to perform full three-phase simulations of the power system using a software tool such as PSCAD. It is not possible to handle thousands of nodes in EMTP type simulations. However, if it is possible to design the transient stability prediction system based on a reduced system model (which in-

cludes only the most important sections of the network), this restriction can be surmounted.

The results presented in this section prove that the proposed algorithm is applicable to a real systems and it was able to predict the possible transient instabilities in the Venezuelan power system after being subjected to a severe disturbance. The proposed method is fast, and can be implemented using only a limited set of synchronized measurements of voltage magnitudes close to generation/load centres.

4.6 Prediction of transient stability in the Manitoba Hydro power system

In this section, the accuracy of the proposed algorithm is also tested on the model of a practical example of a large power system with multiple HVdc links. This extends the extensive tests carried out on the modified IEEE 39-bus test system after the inclusion of two HVdc links. The power system considered is the Manitoba Hydro power network. Similar to the case of the Venezuelan power system, detailed dynamic models of all elements of the Manitoba Hydro power system were also available in PSS/E format. The disturbances applied to generate the training and testing database were generated using batch simulations in PSS/E. In this case, the simulations were carried out directly in PSS/E due to the complexity involved in importing numerous user customized HVdc models available in the Midcontinent Area Power Pool (MAPP) simulation case into TSAT software. This system base case model represented the Manitoba and Saskatche-

wan power transmission networks together with the interconnections to the USA and Ontario.

A simplified diagram of the Manitoba Hydro power system is shown in Figure 4.11. Most of the generation is from the hydro power plants located in the northern part of the province. Three large generating stations located on the Nelson River (Kettle, Long Spruce and Limestone) contribute about 70% of the total generation in Manitoba. The electricity generated by these power stations is transmitted to the load center located about 900 km south using two HVdc transmission lines (±450 kV and ±500 kV). For this reason, these three large generating stations are normally operated separated from the main ac grid and referred to as the Northern Collector System (NCS).

The remaining generation in the northern area, located at Kelsey, Jenpeg, and Grand Rapids, is used to serve northern loads. The excess power from these stations is transmitted south via 230 kV and 138 kV transmission lines running parallel to the HVdc transmission lines. This part of the network is referred to as the Northern AC System and operates synchronously with the main grid. There are several small hydro generating station located on the Winnipeg river in the southern part of the province close to Winnipeg. They are connected to the grid through 115 kV ac lines.

HVdc transmission lines are terminated at the converters (Bi-Pole 1 and Bi-pole2) located at Dorsey station close to Winnipeg. Manitoba Hydro system is interconnected through 230 kV transmission lines to the neighbouring Canadian provinces of Saskatchewan and Ontario. It is also interconnected to Midcontinent Area Power Pool (MAPP), USA, in the south through 500 kV and 230 kV tie lines.

Since the NCS is isolated from the main ac grid, the inertia of large generators in NCS is not available to stabilize the system after a large disturbance. However, since these machines are isolated and do not serve any ac loads, they are allowed to operate within a wider frequency range. Therefore, the generators in the NCS can tolerate sudden changes in the HVdc link power. The generators located on the Winnipeg river have small inertia. There are a number of synchronous condensers installed at the Dorsey converter station to provide reactive power support to HVdc converters and inertia to the system.

A new HVdc transmission line that links the Northern collector system to a new inverter station (Bi-pole 3) to be located at Riel, Winnipeg, is planned for improving the reliability. This new HVdc transmission system will also be used to transmit the power from several new generating plants, which are in the planning stage. The Manitoba Hydro grid is generally a very stable system. However, simulations show that with the addition of new generation on HVdc loading, prolonged faults on tie lines (when operating in power export mode) can potentially result in the hydro generators on Winnipeg river to lose the synchronism, if implemented with inadequate mitigation measures.

4.6.1 PMU placement

An approach similar to the methodology followed for the Venezuela Power grid, was used to specify the locations of the PMUs. Based on the consultations with the planning engineers at Manitoba Hydro and the knowledge gained through stability studies, 14 locations were selected for monitoring using PMUs. These PMUs were placed on the 230 kV and 500 kV buses close large generation and load centers. Also the locations that are connected to important tie lines were also included so that the effect of tie line transfers

can be monitored. Again, there is a possibility for optimizing the placement of PMUs using techniques such as the one presented in [65, 66], but that was beyond the scope of this study. The final locations determined are given in Table 4.15.

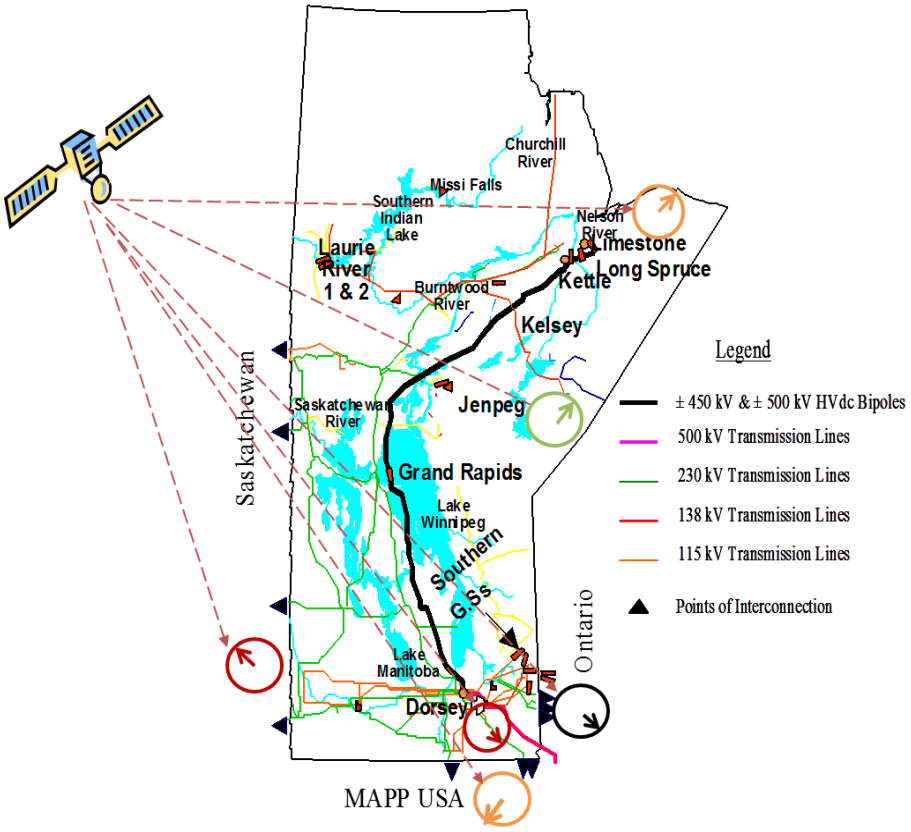

Figure 4.11 Geographical layout of Manitoba Hydro power grid

4.6.2 Design of the SVM classifier

The voltage magnitudes obtained from the 14 synchronized measurement points selected in the previous section are input to the classifier. Thus the classifier has to have 56 inputs (14 monitored buses × 4 consecutive voltage samples). In order to generate data for training and testing the classifier, simulation were carried out in PSS/E. In Manitoba Hydro network, transient stability problems are not visible for faults that are cleared by primary protection (cleared within 5-6 cycles). Transient instabilities were observed only for the

prolonged faults, which can occur due to failure of primary protection or stuck breakers. Typical unstable cases included three-phase faults on the 230 kV lines, which are cleared only after a duration of 20 cycles. In Figure 4.12, the voltage magnitude trajectories of the 14 monitored buses after being subjected to such a prolonged disturbance are shown. The particular case shown in Figure 4.12 leads to transient instability. The dashed box represents the time window where the measurement to be used in the prediction are taken.

Table 4.15 PMU locations on the Manitoba Hydro network

Location	Bus Voltage	Remarks
Dorsey	500 kV	HVdc converter station, PUM already in service
Roblin	230 kV	Monitors oscillations and imbalances between Manitoba and Saskatchewan networks
Whiteshell		Monitors the interactions between Manitoba and Ontario power networks
Ridgeway		Monitors the eastern area of Manitoba
Laverendrye		Tie lines monitoring
Lettelier		Tie lines monitoring
Ashern		Tie lines monitoring
Jenpeg		Winnipeg river power plant
Riel		Future HVdc converter station
Kelsey		Monitors northern generation power plants
Grand Rapids		Monitors northern generation power plants
Dorsey		Tie lines monitoring
Forbes	500 kV	Tie lines monitoring
Chisago		

A simulation database consisting of 192 cases were generated. As in the previous cases, variations of the bus voltages were recorded together with the final stability status after the simulation. About 70% of the data, 134 out of 192 cases were used for training the SVM classifier. The remaining 30% of the data, 58 out of 192 were saved for testing the performance.

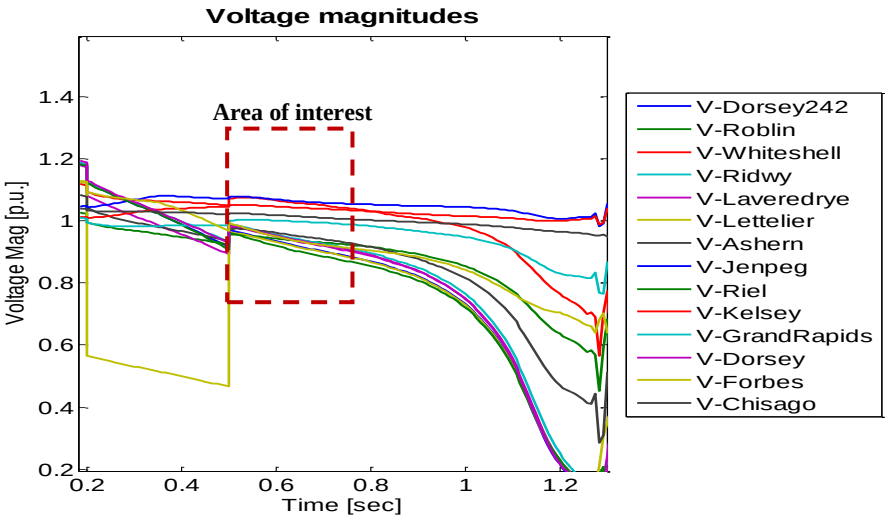

Figure 4.12 Voltage trajectories on the Manitoba Hydro system after a fault

4.6.3 Prediction results and performance

The results are summarized in Table 4.16. As observed in the previous test cases, when the system is transient stable after the fault, prediction accuracy is 100%. The slightly lower prediction accuracy (93.3%) observed for unstable cases in the Manitoba Hydro power system is somewhat misleading due to relatively small number of unstable test cases. Only one out of 15 unstable cases was incorrectly classified.

Table 4.16 Transient stability status prediction performance on Manitoba Hydro system

Condition	**Prediction Accuracy on Testing Data**	
	Classified as Stable (%)	Classified as Unstable (%)
Stable Case	100 % (43/43)	0 % (0/43)
Unstable Case	6.66 % (1/15)	93.33 % (14/15)

The results presented in Table 4.16 confirm that the proposed transient stability status prediction algorithm is applicable to real power systems with HVdc links. It was also possible to predict the possible transient instabilities in the Manitoba Hydro power system only using few PMU measurements. Additionally, the measurement points are not necessarily to be placed on generator buses. They should be placed in locations where the imbalance generation-load can be identified.

4.7 Concluding remarks

In this chapter, the transient stability status prediction scheme proposed in Chapter 3 was tested on several different power systems with different characteristics. Synchronously measured bus voltage magnitudes obtained from PMUs were input to a SVM classifier. The classifier needed to be trained with examples generated through simulations. It was shown that the method can be successfully applied under both symmetrical and asymmetrical faults: studies carried out for the IEEE 39-bus test system showed over 97% overall prediction accuracy under all types of faults. The proposed method was also shown to be robust under the presence of random measurement errors and network topology changes. The method performs well even for the power systems with HVdc transmission links as

found from the testing on the modified IEEE 39-bus test system with two HVdc links. Then the proposed method was tested on two real power systems; the Venezuelan and Manitoba Hydro power grids. Those tests showed that the proposed method can be implemented on real power systems using relatively few PMUs placed at strategic locations.

Chapter 5

Emergency control strategies using wide area synchronized measurements

5.1 Introduction

In this chapter, application of the transient stability status prediction scheme developed in Chapters 3 and 4 for initiating emergency control actions against transient instability is explored. Rather than proposing a generic scheme, emergency control actions were design for two specific power systems with vastly different characteristics. This allows exploiting control variables unique to the power system for dealing with the transient stability problems which are also largely related to characteristics of the particular system. The first example is an emergency load and generator shedding scheme for the Venezuelan power system, which is a completely ac grid. The second example is an emergency HVdc power control scheme for the Manitoba Hydro grid, which is characterized by its high reliance on HVdc transmission.

5.2 Emergency control

Special protection systems should initiate appropriate control actions when an impending transient instability is predicted. When the transient stability status prediction scheme indicates that the system is unstable, the power system is either operating in or soon moving into the *emergency state*, referred to in Figure 1.2. The system will become unstable and move into an *in extremis state* unless appropriate control actions are triggered, forcing the system to return to the *alert state*.

Different philosophies of power system emergency control are illustrated in Figure 5.1. Continuous control where the control actions are of continuous nature is applied for dealing with issues such as small disturbance rotor angle stability (steady state or small signal stability). The small disturbance rotor angle stability is usually maintained through continuous adjustment of control variables, for example excitation current of a generator or output of a FACTS device, using an appropriate feedback controller. Unlike the small disturbance rotor angle stability, the transient stability is a function of the disturbance [9]. Improvement of transient stability requires use of control actions which are large sudden changes such as shedding loads, switching of reactive power sources, system separation or tripping of generators, but of temporary in nature. Such actions are termed as discontinuous control. Most special protection systems are discontinuous controllers. Some SPSs are designed to respond to a particular conditions in the power grid, and usually known as event-based control systems. These systems monitor the power system variables and various status signals through supervisory control and data acquisition (SCADA) systems or dedicated teleprotection signals.

On the other hand, emergency control systems generally referred to as wide area control systems or WACS monitor a power system using wide area measurement technology, which includes synchrophasors obtained from PMUs. These systems detect abnormal conditions from the changes in the monitored power systems variables, and take control actions that are of discontinuous nature. They are therefore known as response based controllers. The emergency control proposed in this chapter belongs to this last category.

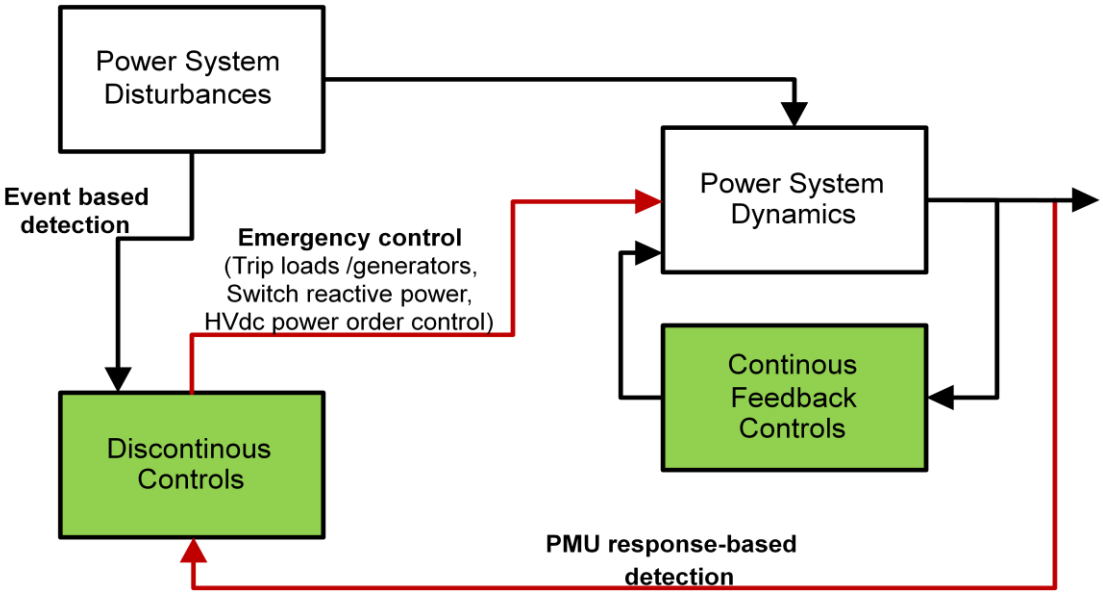

Figure 5.1 Power system stability controls (adapted from [42])

These emergency control solutions are system-dependant because they will be developed based on the available infrastructure such as HVdc links, FACTs devices, and braking resistors among others. In this chapter, two response based discontinuous emergency control strategies are presented. The first technique is designed for grids principally dependent on ac transmission. This is the case for most of the electric power grids around the world. This strategy uses fuzzy logic system to perform load shedding and generation tripping following a critical disturbance. The proposed emergency control scheme was tested on the Venezuelan power system.

5.3 Generator and load shedding scheme for the Venezuelan power system

The transient stability status prediction scheme presented earlier in Chapters 3 and 4 can determine after a fault, whether the system is going to lose the synchronism due to the disturbance. Once an imminent instability condition is predicted, some emergency actions needed to be taken to preserve the stability of the grid. If no further action is taken, then the system may break apart due to uncontrolled tripping of generators (from out of step protection) and formation of islands which are unstable.

Two of the most effective control actions that could be undertaken to reduce the kinetic energy gained during the disturbance are: (i) the tripping of generation in areas where there is a surplus of power and (ii) the shedding of loads in areas where a deficit of power exists. Generator tripping and load shedding are the fastest actions that can be taken to reduce a major power imbalance resulting from a disturbance, although these actions should be taken only as the last resort to prevent further damage. The selective tripping of generators for transmission line outages has been used extensively to improve stability [67]. The other forms of power control include generator fast valving and dynamic braking and have an effect similar to the generation tripping for stability enhancement.

The action of the WACS against transient instability requires a response within fraction of a second, thus there is no time for human operators to intervene [68]. Design of automatic control against large disturbances such as faults using conventional linear control approaches is difficult due to nonlinear nature of the power system. Fuzzy logic control offers a way of dealing with modeling problems and uncertainty by implementing lin-

guistic, informally expressed control laws derived from expert knowledge. This control theory has demonstrated to be an effective control means in a broad range of applications. Thus a fuzzy logic based approach is used for the design of the proposed emergency control scheme.

5.3.1 Structure of the control system

The complete WACS proposed is summarized in Figure 5.2. The scheme consists of three stages: (i) a disturbance detecting trigger mechanism, (ii) a stability prediction scheme and (ii) a discontinuous emergency control strategy. The near real-time measurements of the system are obtained using conventional measurement transformers and the waveforms are sampled in a PMU where the phasors of the voltages and the currents as well as the local frequency are computed. These phasor measurements are transmitted to a phasor data concentrator (PDC). It was assumed that measurements are taken at a rate of 60 phasors/second. Applications such as the proposed WACS get the required data from the PDC. A disturbance detector is employed to detect the occurrence of a fault and the instant of its clearing to initiate preparing input feature vectors for predicting the transient stability status. If the predictor indicates a transient instability, the fuzzy logic based emergency controller chooses the suitable actions and gives commands to relevant actuators.

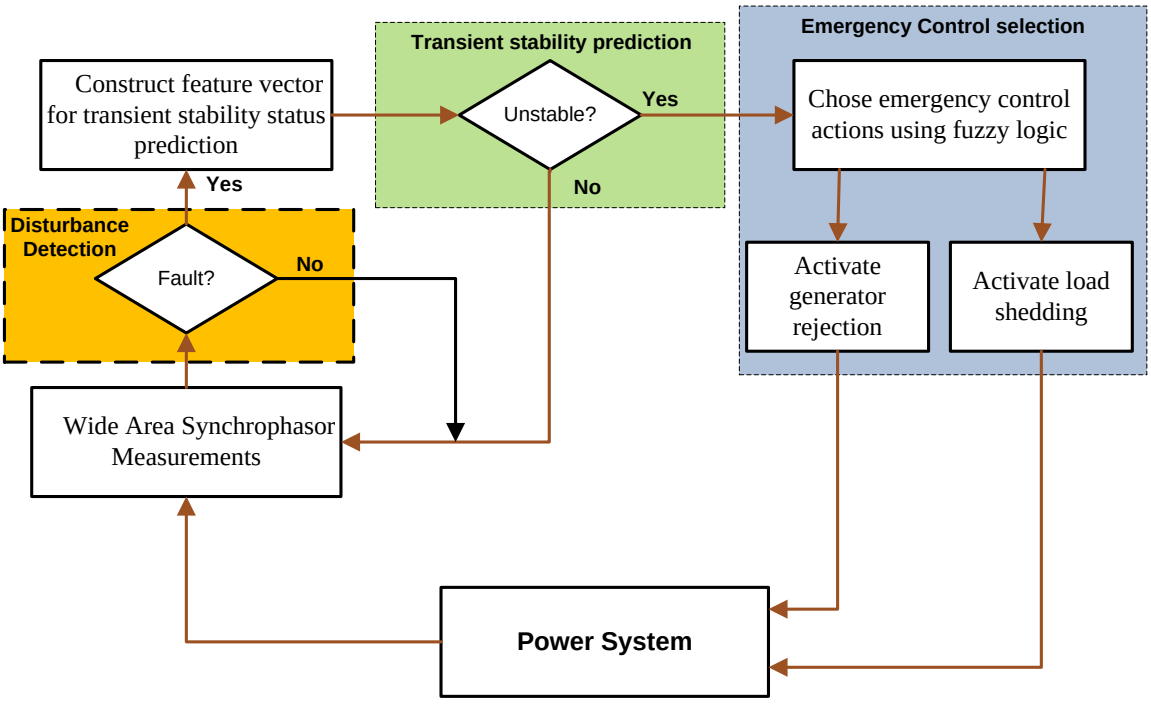

Figure 5.2 Overall structure of the wide area control system

5.3.2 Disturbance detection

Although the proposed control system monitors the power system continuously, the transient stability status prediction is activated only after detecting a major fault. Once, a major fault happens, the voltage magnitudes measured at the buses close to the fault depress. This can be used to detect the occurrence of a major fault in the system. In the disturbance detection system used in this research, shown in Figure 5.3, if the voltage magnitude in any of the monitored bus drops below 0.7 pu (V_{dip} = 0.7 pu), for more than 4 consecutives measurements (four cycles), a fault is assumed. Once the faulty element is isolated by the action of local protection, the voltage starts to recover. The fault is assumed cleared, if the voltage dip starts to recover at a rate faster than 40% (k=0.6) per measurement period at the bus where the minimum voltage was observed. When this condition is satisfied, construction of the input feature vector to be used for the SVM binary classifier

is initiated. These thresholds and time delays were determined through a trial and error approach using numerous simulation data. The thresholds found in this study should be applicable to most power systems, although slight adjustments may be necessary depending on the exact nature of the system and types of control devices (FACTS devices, synchronous condensers, among others) in the system..

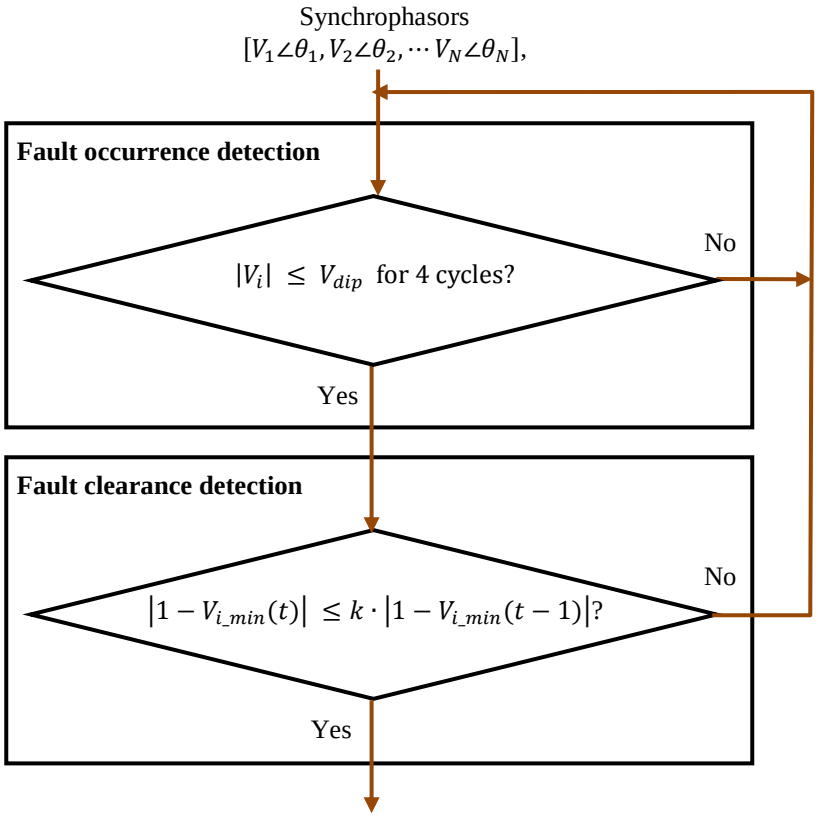

Figure 5.3 Disturbance detection logic

In the above system, only the phasor measurements were used for disturbance detection. This can be alternatively achieved using the status signals from circuit breakers or protection relays. However, this approach will require monitoring of the status of many breakers and defeat the purpose of response based special protection systems. This philosophy

is used to trigger the control schemes developed for both the Venezuelan and Manitoba Hydro power systems.

5.3.3 Fuzzy logic based emergency control

As mentioned previously, voltage magnitudes, voltage phase angles, and bus frequency all undergo changes during a disturbance leading to transient instability, and therefore are indicators that can be used as inputs of an emergency controller. PMUs can provide accurate and time tagged measurements of all these quantities. The same 15 PMUs locations determined during the testing of the transient stability status prediction stage were used in the emergency control as well [69]. The measurements at these locations demonstrated good overview of the grid and the instability conditions could be predicted with accuracy over 95%. These 15 PMUs were placed on the high voltage (230 kV, 400 kV and 765 kV) buses close large generation or load centers. Placements of PMUs are shown on the simplified network diagram in Figure 4.6.

The voltage phase angles can indicate the stress at various localities in the system. For example, in Figure 5.4(a), the phase angles monitored at several locations in the Venezuelan grid under normal operation is plotted on a vector graph. A snap shot of the phase angles of the same buses monitored during a contingency leading to transient instability are presented in Figure 5.4(b). It is possible to see the phase angles in the southern region are advancing after the disturbance indicating a possible excess of power generation in the southern area. Although phase angles are a key variable for identifying the areas where generation need to be reduced, they are slow varying compared to the voltage magnitudes and the frequency, as observed in Chapter 3. Also in case of identifying

where the load has to be reduced, the voltage phase angles are less effective. Frequency is almost always used as an indicator of stress in load shedding schemes. Deviations in the frequency (Δf) indicate the condition of unbalance of real power generation and load at the measurement point. Voltage magnitudes vary considerably and rapidly during the initial part of the disturbance can also indicate deficit of generation, although the low voltages could also mean deficit of reactive power or voltage stability problems. For example, Figure 5.4(b) shows that the magnitudes of the vectors are decreased during the disturbance in the Western region, where the majority of the loads are located. Considering mainly the speed requirements, the emergency control strategy proposed here relies only on the voltage magnitudes and bus frequencies. Even though the rate of change of frequency is also commonly used in load shedding schemes, this was not considered here since the selected input variables (frequency and voltage magnitude) combined with the fuzzy logic control give a simple but effective solution.

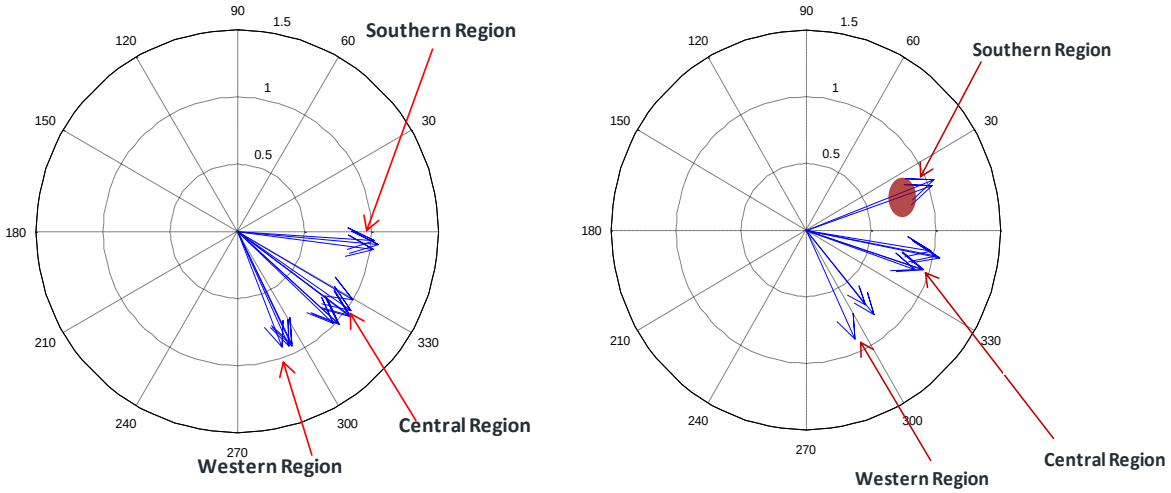

(a) (b)

Figure 5.4 a) Normal angular differences in the Venezuelan power grid, b) Angular differences during a disturbance leading to transient instability

The proposed load shedding and generator tripping scheme shown in Figure 5.5 utilizes a fuzzy inference system to determine the required emergency control actions. A separate fuzzy system is employed for each monitored area (all of them are implemented on one centrally located controller). The frequency and voltage magnitudes at that given area are acquired through wide area PMU measurements and the corresponding fuzzy values are computed. Using a fuzzy rule base, three fuzzy measures indicating the requirement for load shedding (*LS*), requirement for generator tripping (*GT*) and the requirement for no action (*NA*), are computed for each area.

The load shedding requirement (*LS* values) obtained for each monitoring point are compared and the area with the highest *LS* value, where load shedding is most needed, is selected for load shedding. Similarly, the area with the maximum generator tripping requirement is chosen for tripping generators. The requirement for no action *(NA)* is used as a restrain against load shedding or generator rejection. In this study, it was not attempted to optimally determine the exact location of load shedding in the selected area, but was depended on the existing area separation guidelines provided by the grid operator (Centro Nacional de Gestion del Sistema Eléctrico). The grid's operator provided a ranked list of circuits within the control area. These circuits have been pre-selected and a priority order has been assigned after multiple stability studies taking into account the importance of the loads served by each of the circuits. The exact load served by the circuits at time of load shedding was not considered in selection of the circuit, but multiple consecutive load shedding in stages is allowed until the system stabilizes.

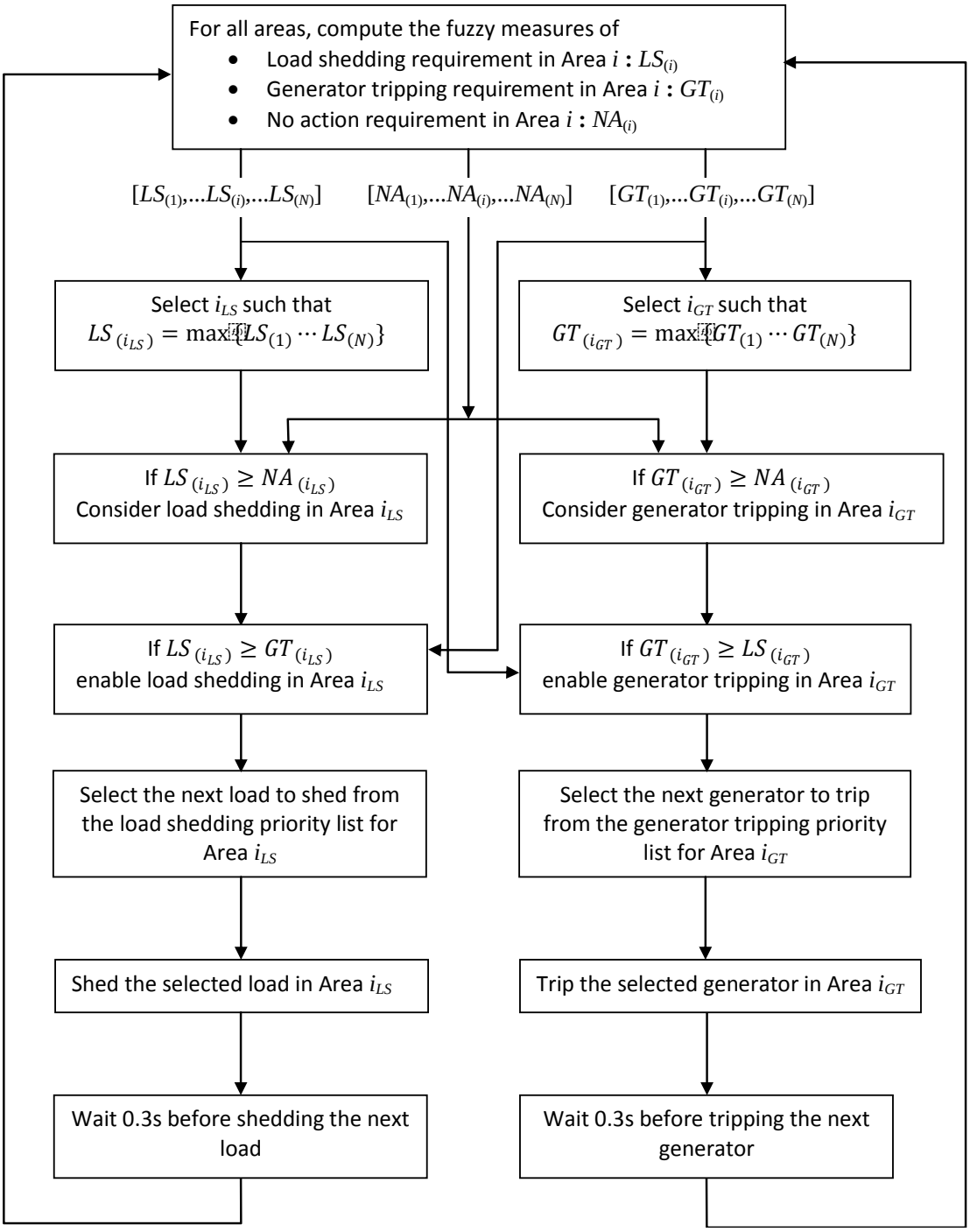

Figure 5.5 Proposed fuzzy based emergency control strategy

When it is required to shed more than one circuit, a 300 ms waiting time was added between two consecutive load shedding events as shown in Figure 5.5. A similar approach

is used for generator rejection as well. The proposed philosophy does not allow simultaneous load shedding and generation tripping within the same area.

5.3.4 Fuzzy logic system for evaluating control actions

The input signals (voltage magnitudes and bus frequency) are first characterized by linguistic variables using fuzzy set notations, through the fuzzification. The fuzzy rule base, which can be expressed using the fuzzy relation matrix or decision tables presented in Table 5.1 to Table 5.3 relate controller inputs and outputs. Usually, at a given instance, more than one fuzzy rule is applicable, and therefore, the final values of the fuzzy measures are computed by combining all applicable rules through a fuzzy inference method. This fuzzy logic controller was implemented in Matlab using Fuzzy Logic Toolbox. But it could be coded in a lower level language to improve the speed of computation in real-time implementations.

5.3.5 Fuzzification

Fuzzification is the process where the crisp quantities, for example variables measured to control a certain process, are converted to fuzzy values by using fuzzy membership functions [70]. Fuzzy membership functions recognize the uncertainties present in the crisp values. A membership function (MF) is a curve that defines how each point in the input space is mapped to a membership or fuzzy value (or degree of membership) between 0 and 1 [70]. In Figure 5.6, the input membership functions, which were used in the technique proposed in this research work, are presented. The labels corresponding to the lin-

guistic variables are: L=low, N=normal and H=high. These linguistic variables are used to construct the fuzzy rules that describe the relationship between the inputs and outputs.

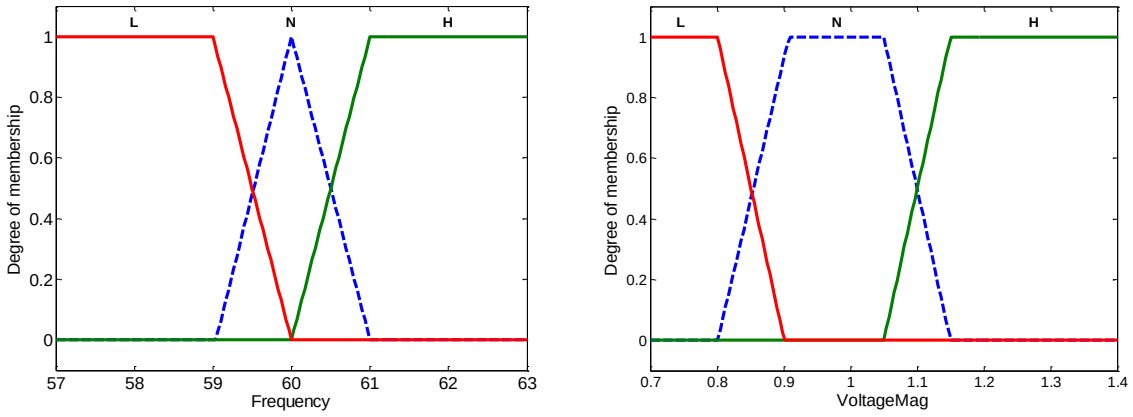

Figure 5.6 Input membership functions used in the proposed scheme

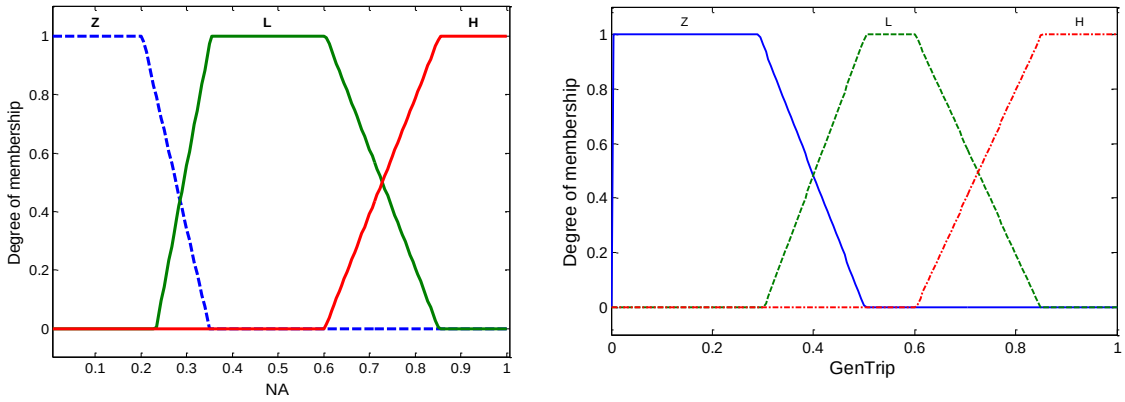

(a) (b)

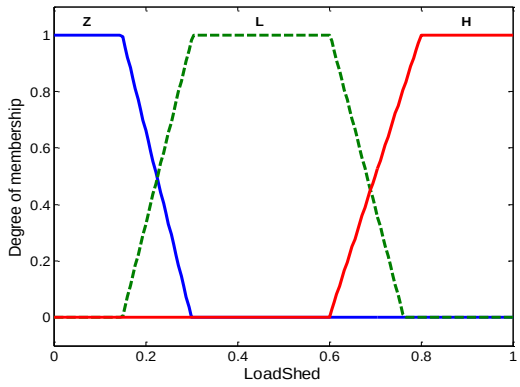

(c)

Figure 5.7 (a) Output fuzzy membership function for the non-action output, (b) Output fuzzy membership function for the Generator Trip Scheme and (c) Output fuzzy membership function for the Load Shedding

The fuzzy memberships of the outputs, those of the three possible the control actions (LS, GT, NA), are presented in Figure 5.7. The labels corresponding to the linguistic variables are: Z= zero, L= low, and H= high.

5.3.6 Fuzzy inference and defuzzification

The fuzzy inference system (FIS) tries to formalize the reasoning process of human language by means of fuzzy logic (that is, by building fuzzy IF-THEN rules). These rules will determine the output of the controller according to the fuzzified values measured in the input. The rules are of the following nature:

IF the frequency *(f)* IS low (L) and the voltage magnitude (*V*) is low (L), THEN the load shedding requirement (LS) IS high (H).

This type of rules can be presented in a compact form in a table such as Table 5.1. A set of rules is required to relate reach of the outputs. The fuzzy rule tables for the generator tripping *(GT)*, load shedding *(LS)* and no action *(NA*) requirements are presented in Table 5.1 to Table 5.3.

Table 5.1 Fuzzy rule base for calculating the requirement for load shedding

f \ **|V|**	**L**	**N**	**H**
L	H	H	L
N	L	Z	Z
H	Z	Z	Z

Where:

H = High Priority

L = Low Priority

Z= Zero Priority

Table 5.2 Fuzzy rule base for calculating the requirement for generator tripping

f \ |**V**|	**L**	**N**	**H**
L	Z	Z	Z
N	Z	Z	L
H	L	H	H

Where:

H = High Priority

L = Low Priority

Z= Zero Priority

Table 5.3 Fuzzy rule base for calculating the requirement for No-Action

f \ |**V**|	**L**	**N**	**H**
L	Z	Z	Z
N	L	H	L
H	Z	L	Z

Where:

H = High Priority

L = Low Priority

Z= Zero Priority

The product–sum type fuzzy inference, where various operations are interpreted as either product of the sum of membership function values, is used in this thesis [70]. The fuzzy operations are implemented as in Table 5.4:

Table 5.4 Implementation of fuzzy operations

Fuzzy operation	Method
AND	Product
OR	Sum (Probabilistic Sum)
Implication	Product
Aggregation	Sum (Probabilistic Sum)

This method of fuzzy inference yields smoother output compared to min–max type inference method. Several fuzzy rules leading to different consequent fuzzy sets can be activated under a given input condition. The process of obtaining a crisp value for the output, based on the membership values of all output fuzzy sets is called *defuzzification*. The most common defuzzification method is the *centroid* method or the center of area method. Based on the product–sum inference and centroid defuzzification, the output of the fuzzy control requirement is computed using: [71, 72]

$$z = \frac{\sum_{r=1}^{M} \left\{ \mu_{r_{fl}}(f) . \mu_{r_{vl}}(|v|) \right\} c_r}{\sum_{r=1}^{M} \left\{ \mu_{r_{fl}}(f) . \mu_{r_{vl}}(|v|) \right\}} \tag{5.1}$$

where M is the number of rules, and c_r is the centroid of the consequent fuzzy set of rule r $[c_r, r = 1,2, \dots, M]$. $\mu_{r_{fl}}$ and $\mu_{r_{vl}}$ are the degree of membership of the input fuzzy sets for the frequency and voltage magnitude corresponding to rule r. In the notation used for membership functions, l stands for the linguistic label of the input membership function ($l \in$ {L, N, H}). The output z in this case is the requirement for load shedding (LS), the requirement for generator tripping (GT) or the requirement for no action (NA). The fuzzy system was implemented and evaluated using Matlab Fuzzy Logic Toolbox [72].

The voltage magnitudes and frequency are gathered from the PMUs at each control point [42]. According to the measured voltage magnitude and the frequency of a monitored bus, certain rules will be applied. Based on the applicable fuzzy rules, three outputs (LS, NA, GT) are produced. This is repeated for each monitored bus, as presented in Figure 5.5. In case of the Venezuelan power system, 15 monitoring points were used.

5.4 Results and controller performance

In this section, the proposed fuzzy logic based emergency control strategy is tested on a dynamic simulation model of the Venezuelan Power Electric Network. As mentioned in the previous chapter, the PPS/E model of the Venezuelan power system was imported to the Transient Stability Assessment Tool (TSAT). In order to simulate the emergency control actions in runtime, a User Defined Model (UDM) was implemented in TSAT to perform the tripping of loads and/or generators. However, the fuzzy control system was implemented outside of TSAT, using MATLAB Fuzzy Systems Toolbox. Thus, first the simulation was run without the control action, and variations of the frequency and the voltage were obtained. Then these variations are input to the controller implemented in MATLAB. The decision of the fuzzy controller is incorporated to a second simulation run through the UDM to obtain the results with emergency control action.

The effectiveness of the emergency control strategy was validated considering a high power interchange scenario. A three-phase to ground fault was applied on a 765 kV transmission line carrying 1395.7 MW from the Southern generation centre (Guri Power Plant and Malena Station) to the northern load centers. After clearing the fault, the Western region of the grid suffers a lack of generation to supply the local loads. Although there are few small generating plants in the Western region, the electrical power output that can be delivered by those generators is curtailed due to prevailing low voltages in the Western region. In order to prevent the loss of synchronism of some of the critical machines in the Western region, some load need to be shed. The rest of the system is able to redistribute the power flow to maintain a safe operation of the system.

The voltage magnitudes and bus frequencies corresponding to this contingency are presented in Figure 5.8 . Once the fault is cleared, the overloaded buses can be clearly identified. Those are the buses supplying the loads in the Western region. The synchronous machines located at Guri 765 kV generation station experience large frequency excursions due to the export reduction originated by the lost of this important transmission line. The frequency in the Southern part reaches a maximum of 60.8 Hz before returning to the acceptable range during the subsequent oscillations. However, the frequency slowly increases.

The curves in Figure 5.8 are corresponding to the 15 locations which are monitored using PMUs, and they do not directly show transient instability. However, the top graph in Figure 5.10 which shows the rotor angles of all the generators in the system indicate that there are two generators that loose the synchronism as a result of the fault. Although the phase angles of the monitored buses do not directly indicate this, the transient stability status prediction scheme could correctly predict using only the 15 monitored bus voltage magnitudes that this contingency is leading to loss of synchronism of some of the generators. The buses which show a prolong undervoltage condition in Figure 5.8 are in the same area as these two unstable generators are located.

The power system was predicted to be unstable after taking four measurements since the clearance of the fault; however, about 100 ms delay was added to account for the communication delays and PDC processing times. Therefore, it was assumed that system was declared unstable 0.176 s after clearing the fault. The requirements for different control actions under this faulty condition, as obtained from the fuzzy logic system, are summarized in Table 5.5. These values correspond to measurements taken about 100 ms after

clearing the fault. Taking a control decision based on the measurement obtained immediately after clearing the fault is not appropriate, since the voltages are still recovering. Therefore, control decision was made based on the measurements gathered after about 100 ms from the trigger signal. This requires addition of further 100 ms delay to represent the time taken by these measurements to reach the central controller.

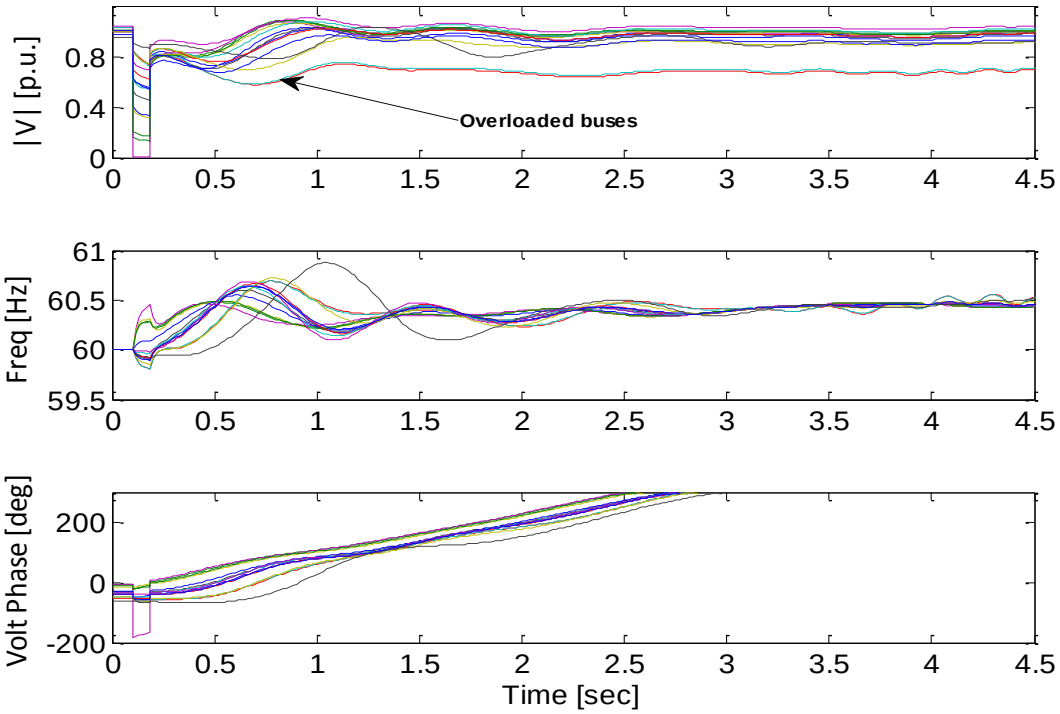

Figure 5.8 Voltage magnitude, frequency and voltage phase angles trajectories after a contingency leading to transient instability problems

The maximum value of the requirement for load shedding was given by the controller associated to bus 3 (*LS (3)* = 0.61). At the same time point, the value of the requirement for no action associated with the same bus, *NA(3)*, was 0.37. Since *LS(3)* > *NA(3)*, a decision was made to shed loads in the region close to bus 3. Then *LS (3)* is compared with *GT (3)* and since *LS(3)* > *GT(3)*, load shedding is confirmed. For this contingency, the requirement for generator tripping (*GT*) is smaller than the requirement for no action (*NA*), for

all the buses. So generator tripping is not considered as an emergency control action for any area. Further time delay of 200 ms was added before actually shedding the loads, in order to account for the time required for conveying the control decision to the breakers that actually tripping the loads and operating time of the breakers. Thus a total time delay of 400 ms was assumed from the trigger signal to the time of execution of the control action.

Table 5.5 Values of requirements for load shedding (LS), generator tripping (GT) and no action (NA)

AREA #	**1**	**2**	**3**	**4**	**5**	**6**	**7**	**8**	**9**	**10**	**11**	**12**	**13**	**14**	**15**
LS	0.59	0.53	**0.61**	0.59	0.50	0.54	0.58	0.57	0.55	0.55	0.53	0.11	0.54	0.27	0.59
GT	0.23	0.29	0.20	0.21	0.31	0.28	0.24	0.26	0.28	0.23	0.25	0.28	0.21	0.20	0.23
NA	0.35	0.37	0.37	0.38	0.39	0.36	0.34	0.33	0.33	0.40	0.42	0.77	0.44	0.73	0.35

The effect of the control action on the system's enhancement is illustrated in Figure 5.9. The two stages load rejection improved the voltage profile after the disturbance and the voltage phase angle returned to a new operating point.

The plots of variations of the rotor angles of all the generators in the Venezuelan power system shown in Figure 5.10 illustrate the effect of emergency control action. The top graph represents the case when the controller was not enabled. Two small thermal generators located in the western region (noted as the critical machines) moves out of synchronism. In the bottom plot which shows the case after emergency load shedding, these two generators stabilize after the initial oscillations.

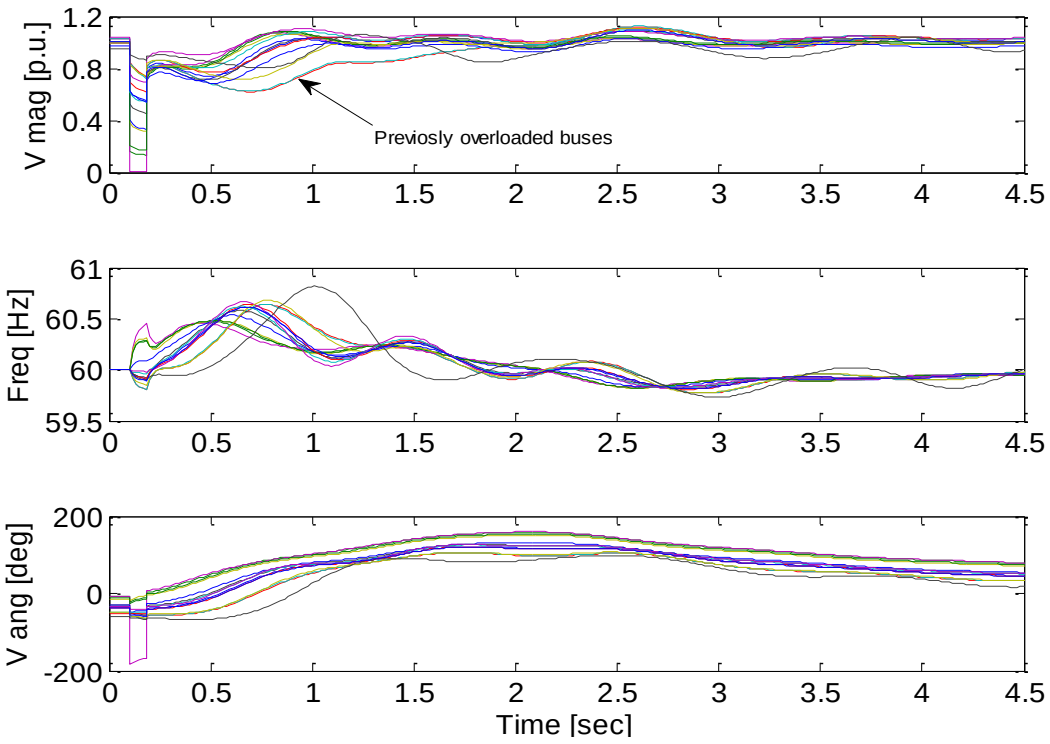

Figure 5.9 Voltage magnitude, frequency and voltage phase angles trajectories executing load shedding in the system

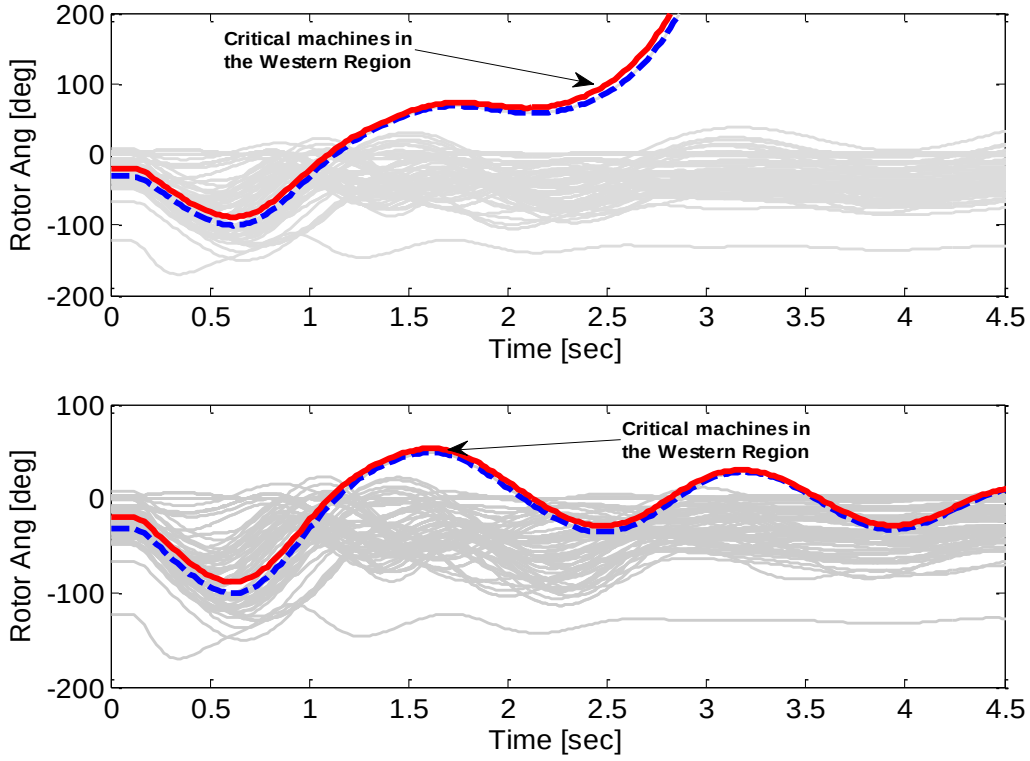

Figure 5.10 Rotor angles trajectories with and without emergency control schemes

Variations of the values of the output fuzzy measures corresponding to bus # 3 are plotted in Figure 5.11. These correspond to the variations throughout the complete disturbance. After the fault that occurs at 0.1s, the value of the fuzzy requirement for load shedding, *LS*, increases above the restrain provided by the value of fuzzy requirement for no action, *NA*. Even though the restrain *NA* is overtaken by *LS* immediately after the fault, decision on the control action is made based on their values at a point 100 ms is after the fault clearing time. Furthermore, no action will be taken unless the stability status of the system is predicted to be unstable. Once, the controller is enabled after receiving the transient instability status, the first stage of load rejection occurs at 0.5 seconds (after the 400 ms time delay described previously). The controller continues to monitor the situation after the load has been shed. After the removal of the load with the highest load shedding priority, the load shedding requirement *(LS)* still remains higher than the no action *(NA)* signal. Consequently, a second load stage is shed at 0.9 s.

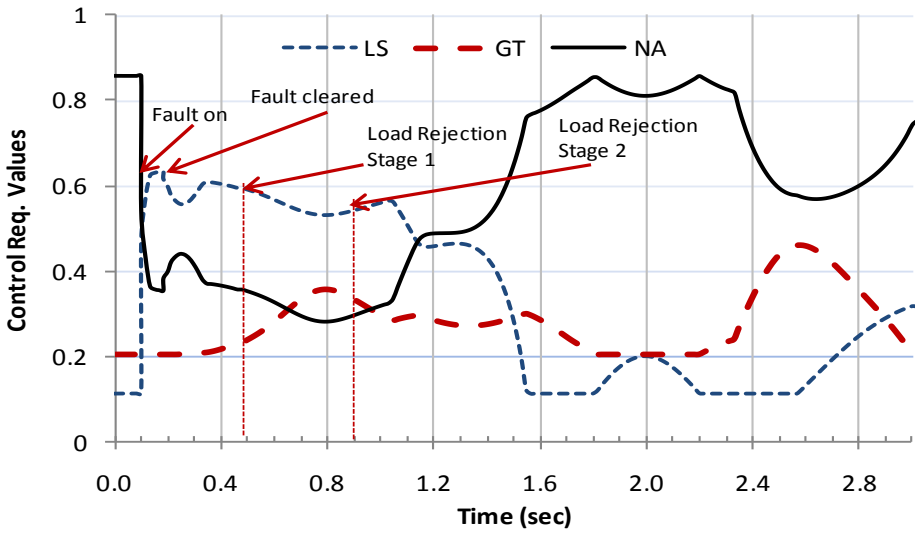

Figure 5.11 Fuzzy output for control area associated to bus # 3 (Western region)

This corresponds to the North Ring (Anillo norte), specifically the load is located at Cuatricentenario 230 kV. Following this second load shedding action the system recovers and the restrain signal *(NA)* overtakes the load shedding (*LS)* requirement.

The control requirements of area 14 for the same disturbance are presented in Figure 5.12. According to the measurements, NA (no action) remains above LS (load shedding) and GT (generator tripping) requirements in this particular area, except for a very short period. Therefore, GT and LS actions are not triggered. Although the generator tripping requirements, GT, overtook the restraint, NA, approximately around 0.7s,.this condition lasted only for a period less than 250 ms and did not result in issuing a generator tripping signal.

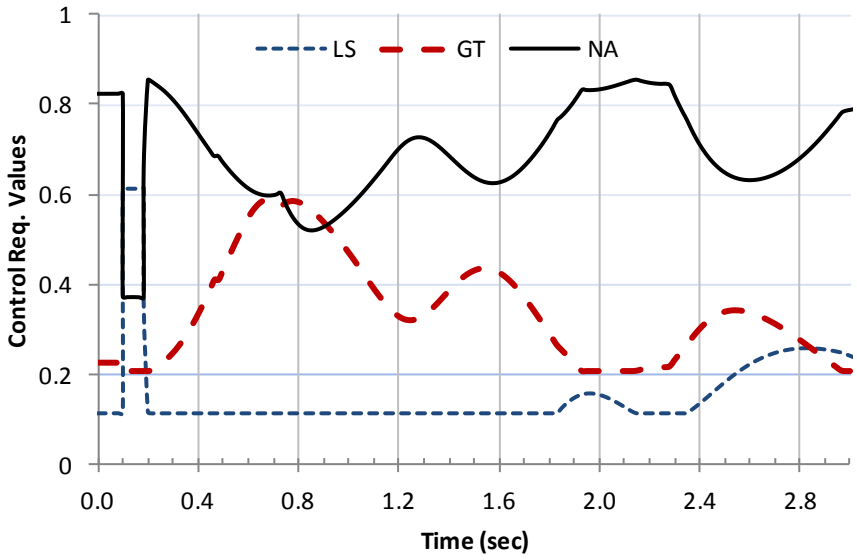

Figure 5.12 Fuzzy output for control area associated to bus # 14 (Southern region)

The buses where the load rejection might take place in the Western region are presented in Figure 5.13. This section of the system corresponds to the transmission grid connected to the main transmission buses at 400 kV of the Venezuelan interconnected system. The major loads are supplied from the Cuatricentenario substation operating at 400 kV. Once

the first stage of load shedding has taken place in the required area, the priority list is followed step by step. After shedding a load, the controller waits 0.3 s before shedding the next load, in order to allow for recalculation of fuzzy requirements to determine whether further reduction of load is necessary. In determining this delay, the 0.5 s waiting interval in the current event based system implemented in the Venezuelan grid was taken as guidance.

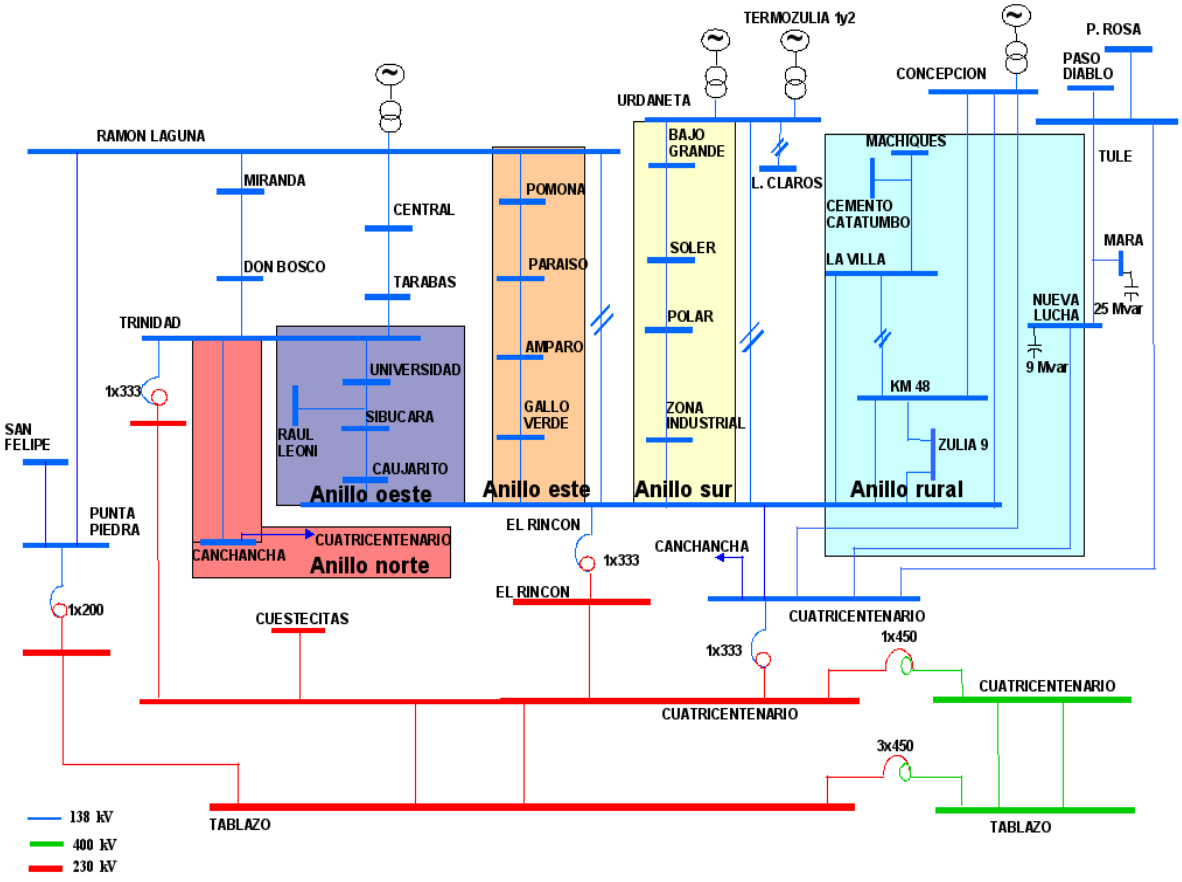

Figure 5.13 Detailed western region showing allowable load rejection areas

According to the load shedding priority list, the Anillo oeste area (West ring) in violet color was tripped out 200 ms after the load shedding is enabled by the emergency controller. This 200 ms time delay accounts for the communication and actuator delays. As discussed previously, this study scenario required two stages of load rejection. The

amount of the shed load in first stage was 79.56 MW and corresponded to the West ring. A second load rejection of 56.83 MW was needed at 0.9 seconds because the generation available is still insufficient to supply the loads According to the priority list, the second block of loads to be shed is Anillo Norte (Northern ring) shown in red color. A total load rejection of 136.39 MW was sufficient to stabilize the grid after the disturbance.

Furthermore, for this study case, generation tripping was not needed because the variations remained within the safe operation region of the machines (see Table 5.5). Once, the power was reduced, the critical machines in the Western region started swinging back to a new stability equilibrium point.

The critical machines are located in the Western Region where the load shedding took place. The reason of the acceleration of these critical machines is the severe voltage depression in the area (~ 0.7 p.u.). If conventional control actions were taken, these machines will be tripped worsening the condition. These facts demonstrate the effect of this control strategy in improving the operation of the grid and the prevention of uncontrolled operation.

5.5 HVdc power order reduction scheme for the Manitoba Hydro grid

High voltage direct current (HVdc) transmission is frequently applied for interconnecting asynchronous ac systems and transportation of electricity from remote generation resources [73]. HVdc transmission is playing an increasing role in the modern power systems. Many new HVdc projects are being built/planned in various places including the

large scale projects in China, India and Brazil. The fast controllability of power flow in HVdc links can be advantageously utilized for stabilizing the interconnected ac power systems following a large disturbance in the ac system. However, under normal operation, HVdc schemes that use line commutated converters operate in power control or current control mode. Such constant power operation is not the optimal way to support the ac network to recover from a disturbance. Some utilities with HVdc links employ special protection systems (SPS) that adjust the HVdc link power to support the ac network to overcome rotor angle and voltage stability problems [53]. In this section, application of HVdc control for enhancing the large disturbance rotor angle stability is explored. The proposed approach exploits the fast controllability of the HVdc power transmission and the near real-time measurement of the voltage and current phasors at the point where the PMUs are located.

Most special protection systems that control HVdc power are event-based systems which activate in response to a selected set of contingencies. One example is the HVdc reduction scheme currently used in Manitoba Hydro power system. As mentioned earlier, one concerned with such event based protection systems is that their complexity grows as the system changes [51]. Alternative to event-based special protection systems are the response-based special protection systems which take actions in response to abnormal situations detected through system variables such as voltages and power flows [52]. This thesis pursues the latter approach.

The emergency control approach proposed here has two stages. The first stage involves prediction of transient stability status after the disturbance based on wide area synchronized measurements [69, 74] while the second stage is to take emergency control actions,

in this case control of HVdc power, to avoid loss of synchronism and equipment overloading. The proposed algorithm is applied to Manitoba Hydro's power system which currently utilizes two long (~900 km) HVdc transmission lines to transport the electricity from hydropower stations located north of the province of Manitoba, Canada, to the main load center located in the south. A third HVdc link will be added to the Manitoba Hydro system in the near future and studies have shown that prolonged faults on several important tie lines could potentially lead to loss of synchronism of some generators, if implemented without adequate remedial measures.

5.5.1 HVdc power order control for improving transient stability

The schematic of the proposed transient instability prediction and control scheme based on wide area synchronized phasors measurements is shown in Figure 5.14. The measurements are obtained using PMUs located in different geographical areas of the grid. These phasor measurements are transmitted over telecommunication links to a PDC where they are accessed by the proposed WACS. The transient stability status prediction stage based on the support vector machine classifier will issue a permissive signal when an impending instability condition is detected [46, 69]. The transient stability status predictor has demonstrated high accuracy and very short detection time. Finally, the HVdc control stage will reduce the power injected by the link to preserve the transient stability of the system. An additional logic is included to prevent overloading of some critical elements in the system using the same measurements. These stages will be described in detail in the following subsections.

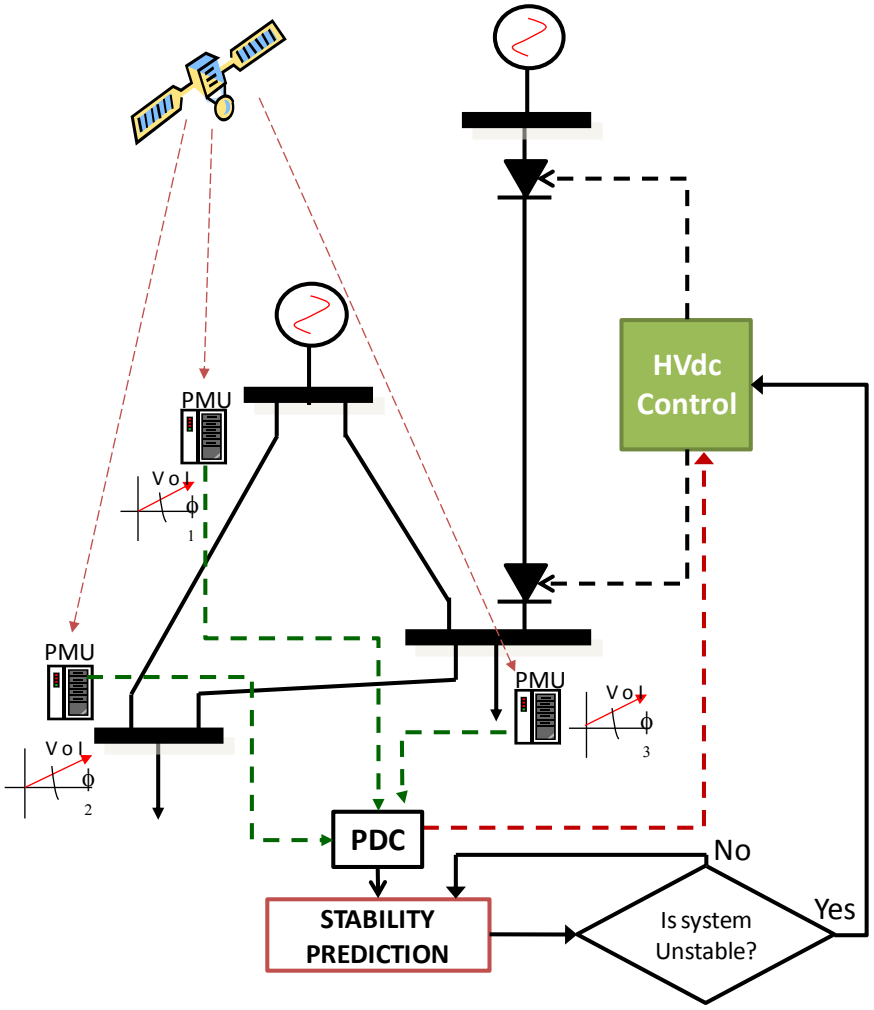

Figure 5.14 Proposed wide area control system (WACS)

5.5.2 Instability prediction stage

This was described in detail in Chapter 4. The SVM classifier based transient stability status predictor uses four consecutive synchronously measured samples of the bus voltage magnitude at the location where the imbalance generation-load can be observed. Transient stability is a very fast phenomenon and the time before loss of synchronism is dependent on the system inertia, damping and the severity of the disturbance.

In the case of Manitoba Hydro power system, the inertia is lower in comparison to conventional complete ac systems because most of the generators are interconnected to the

grid through HVdc links. For this reason, it is imperative to mitigate the consequences of the disturbances as early as possible. Observation time required in the proposed method is 0.067 ms (4 cycles) and that allows about 400 ms for measurement, telecommunication and processing delays.

5.5.3 HVdc power order control

Planning studies have indicated that transient instability conditions can arise in the Manitoba Hydro System after including the planned third HVdc link (bipole-3) due to prolonged faults (failure of primary protection) during high export scenarios. Most transient stability problems in Manitoba Hydro system originate as a result of a contingency that affects the tie lines exporting power to the neighbouring utilities, particularly to USA [75]. Therefore, when an impending transient instability condition is detected, the power transmitted across the HVdc transmission links can be quickly reduced to balance out the reduction in the power export. This is possible due to the unique features of the Manitoba Hydro power system. As described in Section 4.6, large generating stations at the sending end of the HVdc transmission system (collectively referred to as the Northern collector system) operate as an isolated gird, and are not used to serve any local loads. Therefore, the Northern collector system can withstand large transient frequency deviations up to 80 Hz due to sudden reduction in the power HVdc transmission.

Major function of the second stage of the emergency control scheme is to determine the total amount of reduction in the power transfer through HVdc links and distribute this reduction over the three HVdc links. It is possible to accurately estimate the power being transferred through a tie line using phasor measurements. If the phasors of the currents and voltages are provided at the measurement points, the complex power is readily ob-

tained [3]. The advantage of phasor measurements over conventional Supervisory Control and Data Acquisition (SCADA) Systems is the availability of measurements at a faster rate (up to every cycle) and those measurements are time tagged. Figure 5.15 present the scheme for active power computation using real-time PMU data.

A line outage can be detected when the metered power goes below a threshold for a reasonable period of time. In this thesis, when the power level goes below 0.1 MW for at least 10 consecutive cycles, it was considered a permanent change in the operation of the system. The thresholds is not assumed exactly zero to account for any noise in the power flow or inaccuracies in the measurement. This threshold is quite low in comparison to the power handled through the export tie lines. The scheme is inhibited when there is a scheduled change in the direction of the flow (change from export to import mode). This scheme avoids the need to monitoring the circuit breaker status signals, therefore, lowering the number of signals to be monitored and handled and simplifying the complexity of the logic.

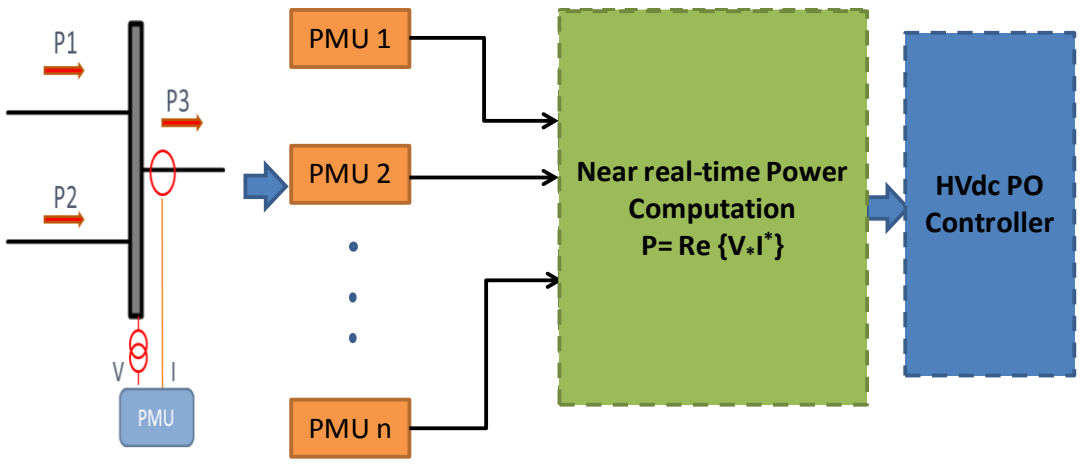

Figure 5.15 Near real-time tie line active power measurements

The scheme used for determining the required reduction in the HVdc power order is shown in Figure 5.15. Once a line is removed due to a fault, the controller compares the actual power transported (near zero MW after the tripping) with a reference magnitude, which is computed as a moving average of the pre-contingency steady state power transfer over a 500 ms time window. The power flow difference, denoted as ΔP, has to be reduced from the HVdc link to establish the power balance. The actual amount of power that needs to be reduced at the rectifier end is estimated by increasing the value of ΔP by 15% to compensate the losses across the HVdc link. Finally, the total power reduction is proportionally allocated to each bipole using (5.2).

$$\Delta P_{BPi} = 1.15 \cdot \frac{\Delta P_{measured} \cdot P_{BPi\_rated}}{P_{BP1\_rated} + P_{BP2\_rated} + P_{BP3\_rated}} \tag{5.2}$$

This is also the method employed in the existing event-based dc reduction controller of the Manitoba Hydro system for distributing the power reduction among bi-poles.

Additional logic can be incorporated to determine the course of action when more than a tie line is lost. For example, the current event based SPS in operation allows reduction of HVdc power only once for a given event or series of event. This emergency control strategy could be expanded to include emergency control against overload of key equipment such as power transformers. For example, the main interconnection between the Manitoba Hydro grid and the US utilities includes step-up transformers to increase the voltage level from 230 kV (common voltage level used for transmission in Manitoba) to 500 kV used in the interconnection.

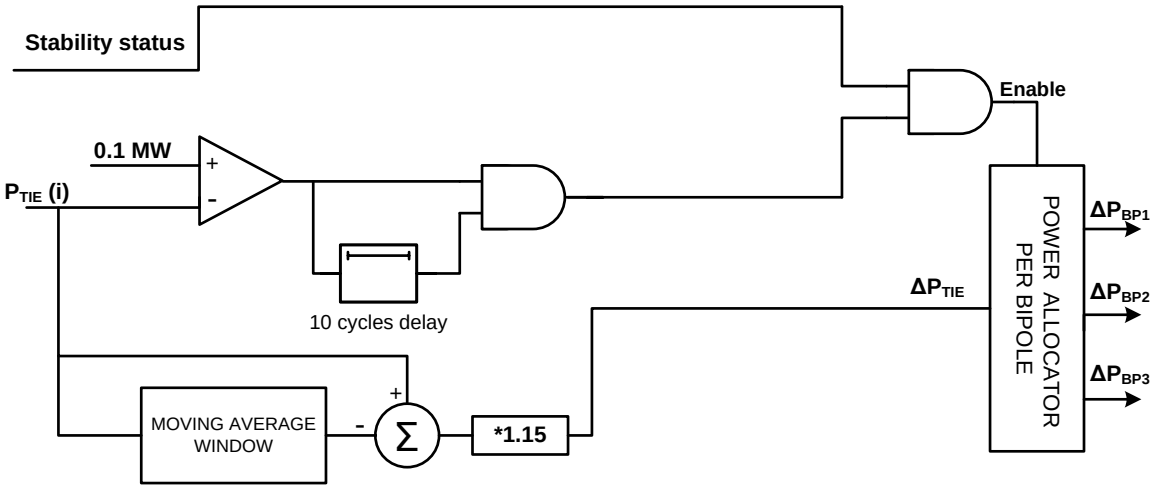

Figure 5.16 Basic control logic for the HVdc power order reduction scheme

Depending on the exporting condition, some of these transformers could be overloaded due to the power flow redistribution when another tie line is removed. This can happen, even when the contingency is not causing any transient stability issues. As a remedy, HVdc power transfer can be reduced by the amount of power transfer lost due to the removed tie line.

5.5.4 PMU locations

In Chapter 4, 14 Synchronized measurement points were used to predict the system transient stability status. These measurement points are located on some of the 230 kV and 500 kV buses close to large generation centers and main tie lines. When selecting the specific locations of the PMUs, monitoring of the important tie lines was considered. This allows the measurement of tie line power flows using the same set of PMU locations considered in Chapter 4.

5.5.5 Simulation results of emergency control performance

In this section, some examples demonstrating the operation of the proposed emergency control strategy during a sample of critical disturbances are presented. If no control actions are taken to enhance the transient stability of the grid, the synchronous generators located along the Winnipeg River tend to lose synchronism when a major tie line to USA is lost. These machines belong to the same coherent group. In Figure 5.17 the variations of phase angles at these power generating stations after a prolonged (18 cycles clearing time) three-phase-to ground fault on the Lettelier-Drayton 230 kV tie line is shown. It is clearly seen that the group is starting to split into 3 subgroups when the collapse starts to occur.

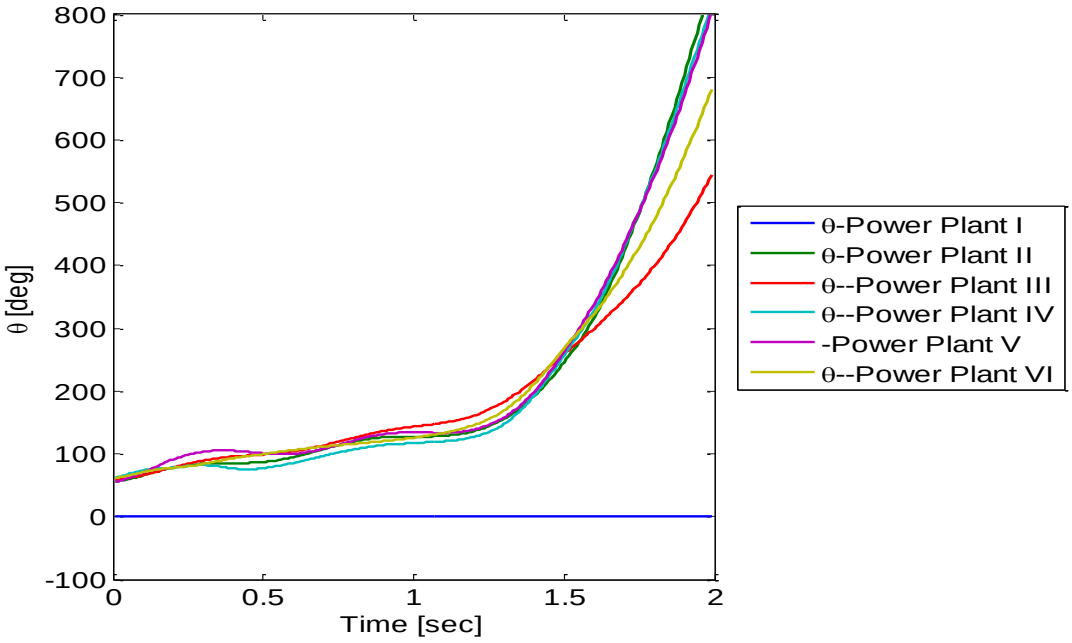

Figure 5.17 Rotor angle trajectories for the power plants located on the Winnipeg River

The corresponding power flow variations across the tie lines are presented in Figure 5.18. The fault occurs at 0.2 second and it last for 18 cycles. Prior to the fault, the faulty tie line was carrying 426.69 MW. The voltage trajectories are presented in Figure 5.19.

After clearing the fault, the input vector is constructed and used in the transient stability status prediction stage. Once, the system is predicted to be unstable, a trigger signal to take emergency control action is issued. This signal is the permissive signal to initiate the HVdc control scheme.

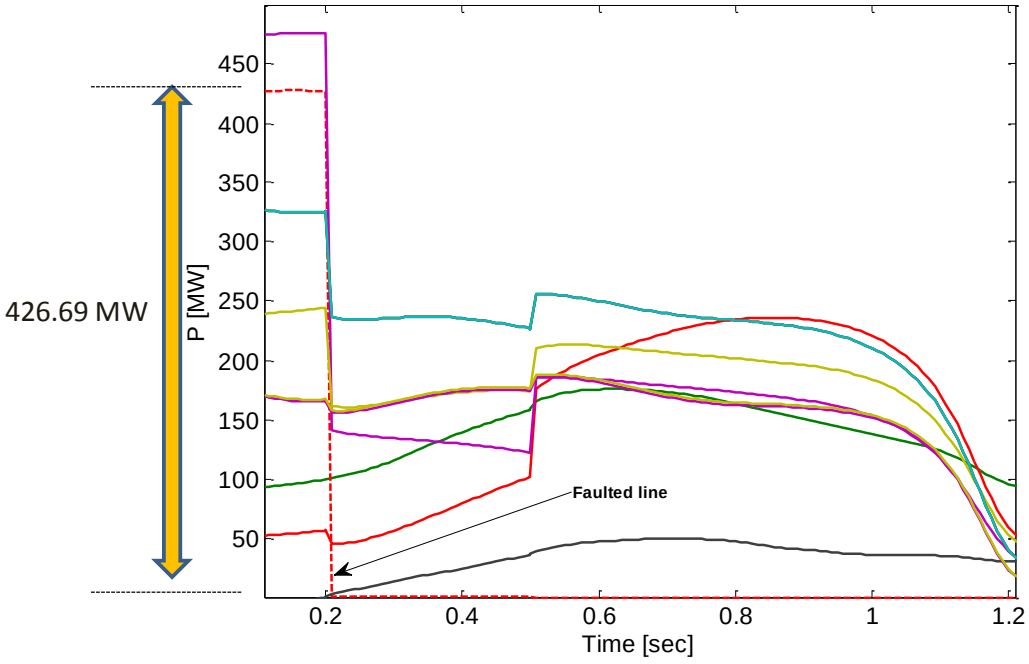

Figure 5.18 Power flow on the tie lines without the HVdc reduction

DC power reduction takes place to remove the surplus of energy that was promoting the instability. In Figure 5.20 the result of the HVdc power order reduction is presented. The disturbance applied on the given tie line causes a reduction of approximately 426.69 MW, and this requires reduction of 426.69×1.15= 490.7 MW across all three bi-poles.

The power order of bipoles 1 and 2 were reduced from 1571.8 MW to 1381.5 MW, and the power of bipole-3 was reduced from 1640.6 MW to 1490.4 MW.

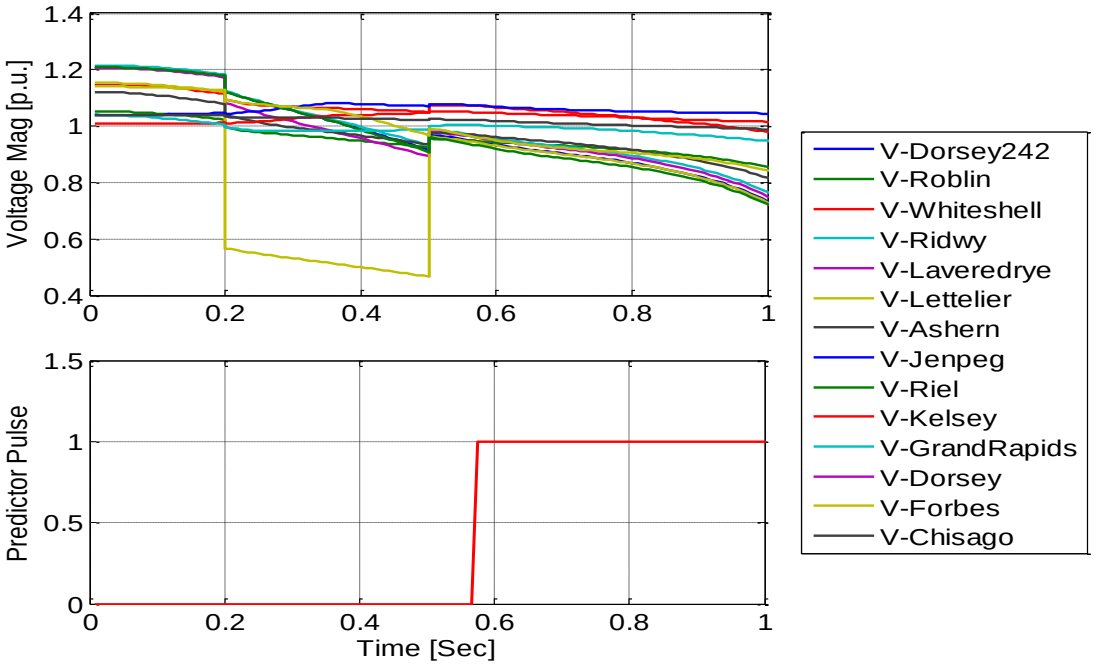

Figure 5.19 Voltage trajectory and transients stability status prediction

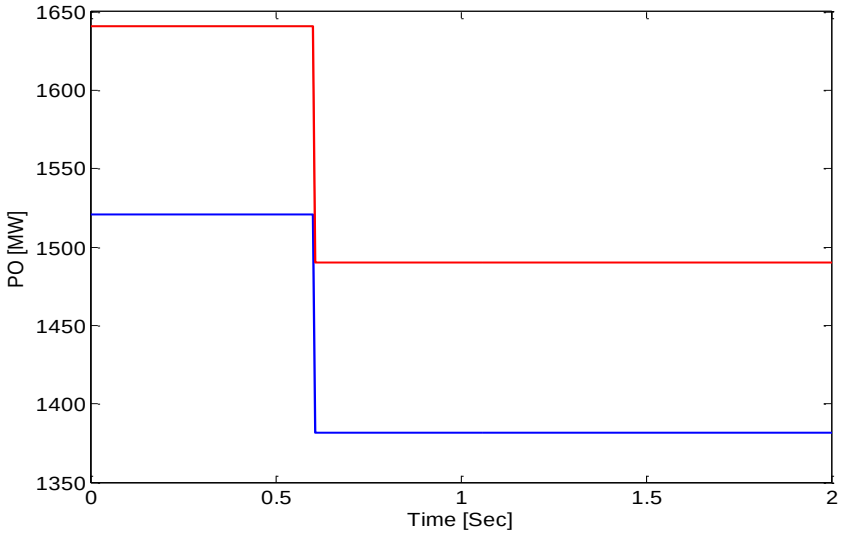

Figure 5.20 HVdc links power order reduction

The kinetic energy gained by the rotating masses of the synchronous machines is absorbed by the connected loads. The system stabilizes and settles at a new equilibrium point. The new rotor angle trajectories after enabling HVdc power order reduction are presented in Figure 5.21.The tie line power flows after reducing the HVdc Power order is shown in Figure 5.22.

The second example presented in Figure 5.23 corresponds to a prolonged (18 cycles clearing time) three-phase-to ground fault on the 230 kV tie line between Glenboro and Rugby. The transmission line was exporting approximately 140 MW to the USA when the fault occurred and the 230 kV tie line is removed due to the action of backup protection scheme for the line. After the fault is removed, the system was predicted to be transient unstable due to the surplus of power resulting from sudden rejection of the export power. Similar to the previous case, the HVdc power order reduction scheme operates and decreases the power transmitted across the bipoles by 1.15×140=161 MW.

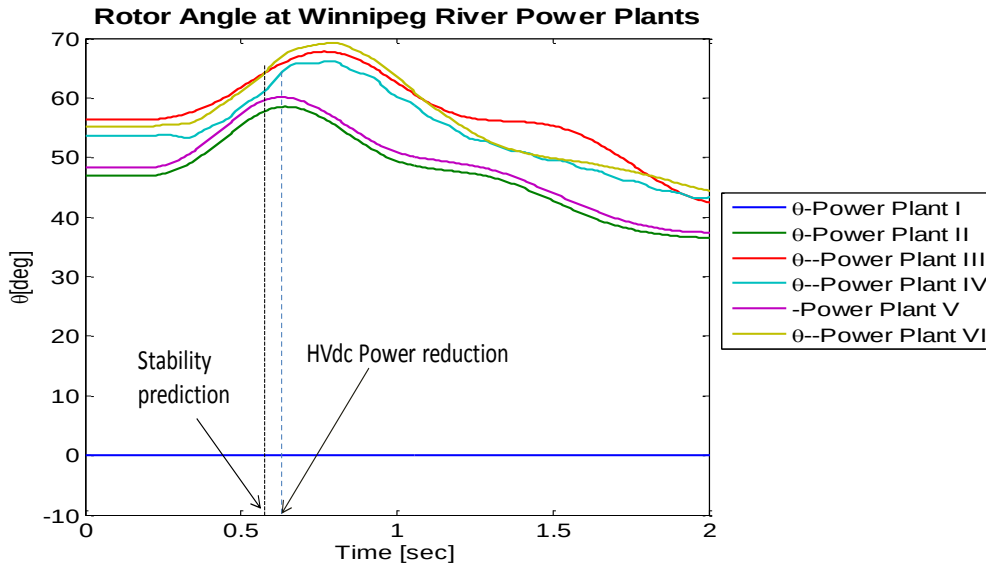

Figure 5.21 Rotor angle variations of Winnipeg River power plants after performing HVdc power order reduction

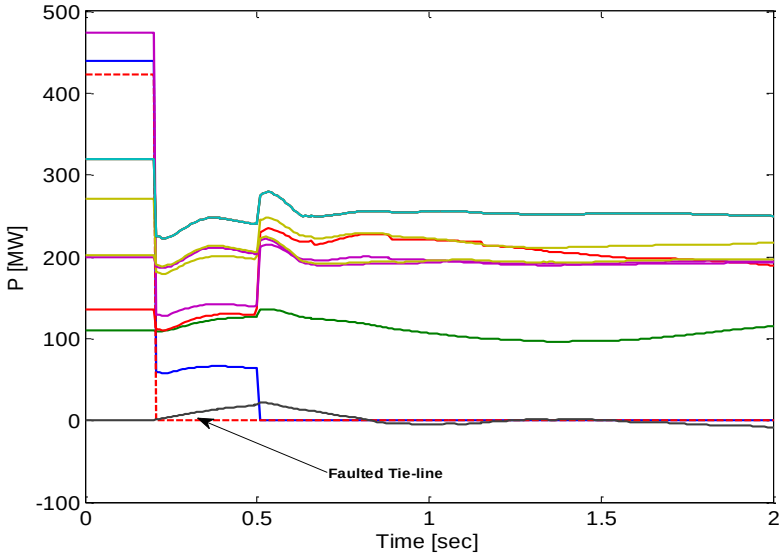

Figure 5.22 Power flow on the tie lines after performing HVdc power order reduction

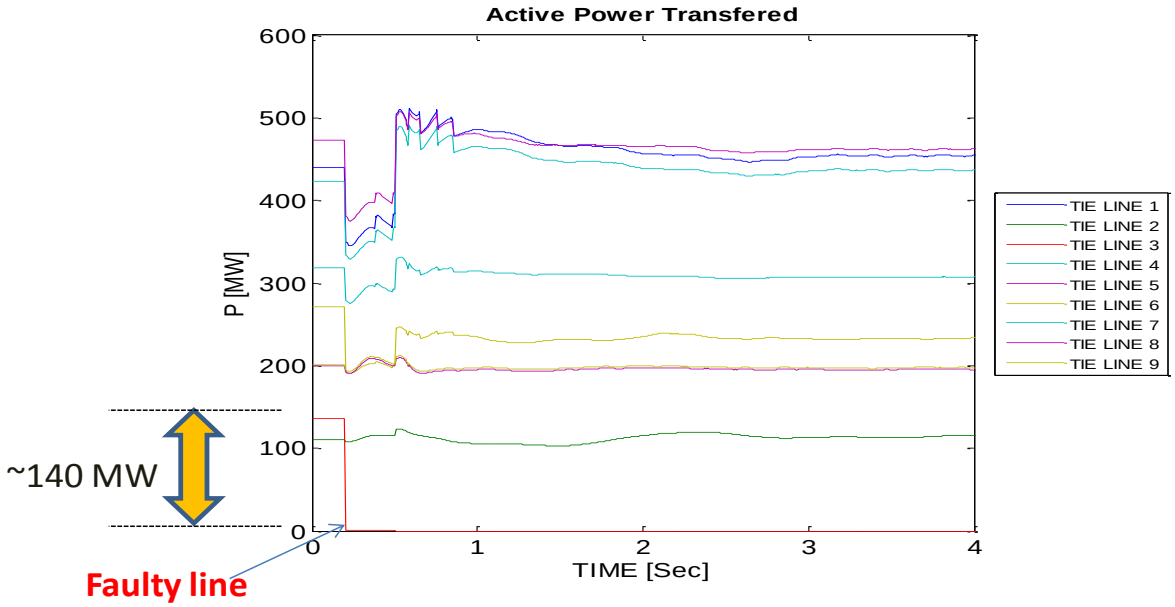

Figure 5.23 Active power transmitted across the monitored tie lines during a fault on the line Glenboro-Rugby 230 kV

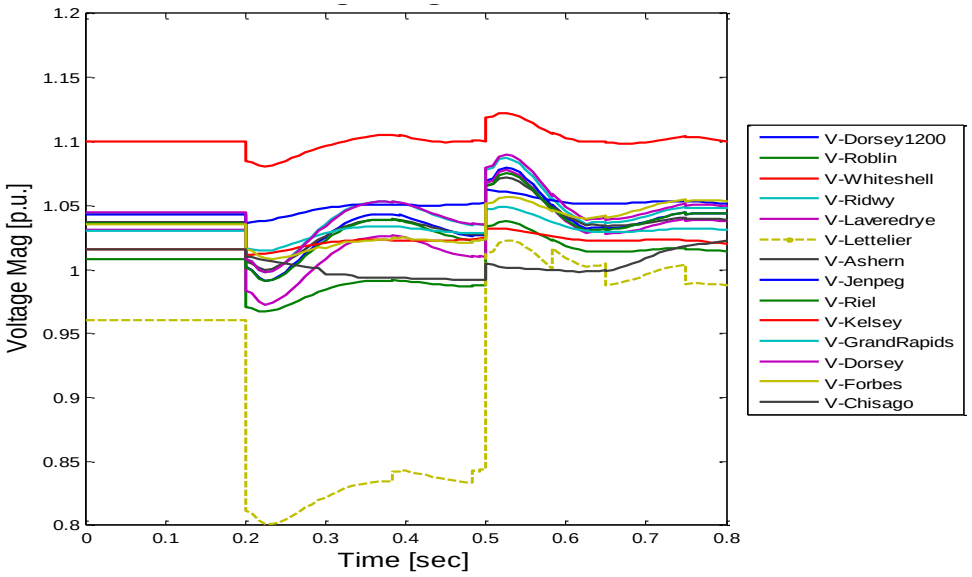

Figure 5.24 Voltage trajectories for a fault on the tie line Glenboro-Rugby 230 kV

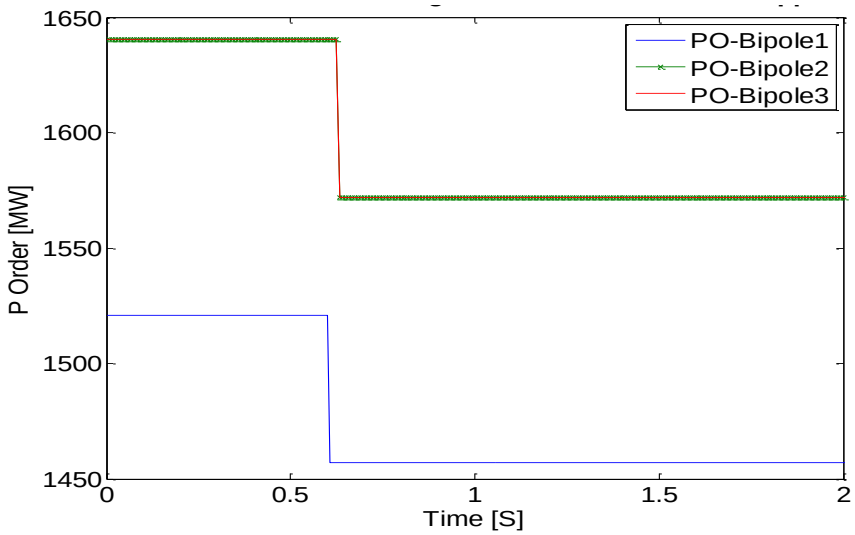

Figure 5.25 Power order at the bipoles during HVdc reduction

After reducing the power transmitted through HVdc transmission lines, the critical machines swing back to a new stable operating state. This is illustrated in Figure 5.26. These phase angles at the synchronous machines reach a maximum of 64 electrical degrees and settle to a new operating state at a level lower than the pre-fault value.

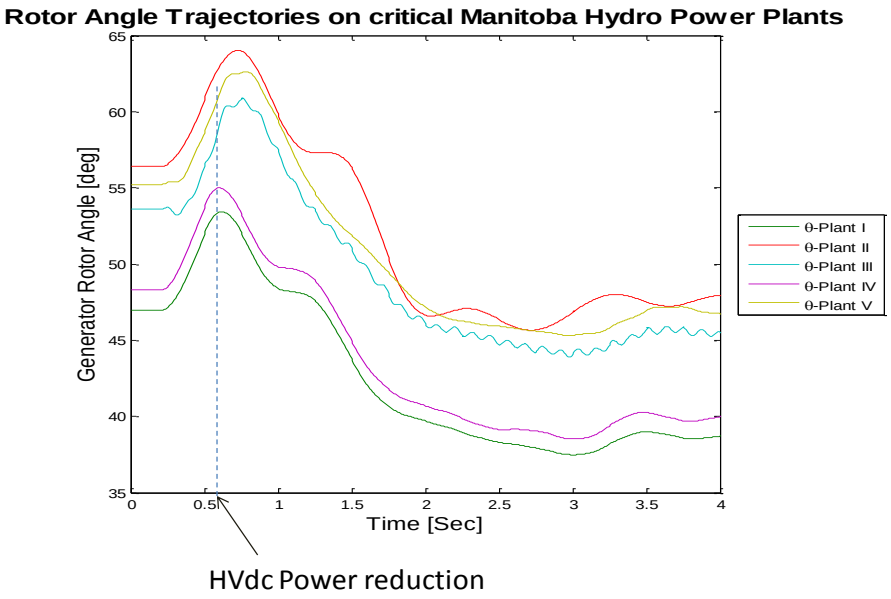

Figure 5.26 Rotor angles after performing HVdc power order reduction

5.6 Concluding remarks

Two emergency control strategies based on near real-time Synchronized Wide Area Measurements were demonstrated. The near real-time measurements provided by the phasor measurement units permit the development and deployment of new response base control strategies. The results presented in this research show that emergency control based on synchrophasor measurements can effectively enhance the transient stability of a power network. Both the fuzzy logic-based load shedding and generator rejection scheme as well as the measurement based HVdc power order reduction scheme could preserve the transient stability of the grid after subjecting to major disturbances. Response based emergency control using wide area synchrophasor measurements offers simpler and effective solutions to transient stability problems.

Chapter 6

Conclusions and Contributions

This chapter presents the conclusions of the research, summarizes the main contributions, and suggestions directions for future research in the area of wide area measurement based transient stability control.

6.1 Conclusions

In this thesis, the problem of predicting the transient stability status of a power system after a major disturbance was investigated. Additionally, how these predictions can be utilized to develop emergency control against transient instability was explored. The main hypothesis behind the research was that variations of measurable power system variables immediately after a fault provide sufficient information to predict the transient stability status, as well as to determine the required emergency control actions. The research proved the hypothesis and showed that transient stability status can be predicted well before it becomes apparent from the divergence of the generator rotor angles, using the voltage magnitudes acquired through wide area synchronized measurements. This allows design of emergency controllers that can take remedial measures sufficiently early to prevent system instabilities.

In Chapter 2 the literature on transient stability assessment methods widely used in dynamic security assessment was reviewed to decide whether these methods could be further developed to predict the transient stability status in a near real-time environment. Time domain simulation, transient energy function based direct methods and hybrid methods as well as machine learning-based approaches were reviewed. It was concluded that approaches based on machine learning methods has the best potential for developing a solution for the problem considered. However, the powerful features of time domain simulation such as accuracy and modeling capabilities is essential for applying machine learning-based methods.

A framework for predicting transient instability condition of a power system using synchronized measurements provided by phasor measurements units (PMU) was proposed in Chapter 3. The proposed approach utilizes binary classifier trained using examples to distinguish the stable and unstable events based on the input features, which in this case are the measurements taken immediately after the disturbance. Support Vector Machines is a classification technique that works well for this application. After investigation of the performance with different predictor variables on a 39-bus test power system, it was shown that the magnitudes of the fundamental frequency voltage phasors are the best features to predict the stability status of a power system after being subjected to a critical disturbance. Traditionally used indicators such as rotor angles require longer time to confirm a transient instability situation. System wide voltage magnitudes measurements can be used to accurately predict the transient stability status using a window of measurement as short as four cycles.

In order to determine the functional relationship between the transient stability status and the bus voltage magnitudes using support vector machine classifier, a transient stability database generated using time domain simulation was used. Preparation of a comprehensive transient stability simulation database covering credible contingencies and loading conditions is a key requirement for the success. The assessment of the proposed technique using an extensive database generated using New England 39-bus test system showed that the proposed method is sufficiently fast and accurate to be implemented as a real-time application based on Wide Area Measurements: the proposed scheme could predict the system transient stability status after 4 cycles from the clearing of a fault, with over 97% accuracy. The developed algorithm demonstrated robust performance under presence of asymmetrical faults, voltage dependent loads as well as with small unseen changes in the network topology. The method can work satisfactorily with noisy input signals, if the classifier is trained using noisy signals. The proposed transient stability prediction scheme can be applied to power systems with different configurations as evident from its performance on the modified 39-bus power system with two HVdc infeeds.

The proposed transient stability status prediction scheme can be designed and applied to large power systems. This was verified applying the algorithm to two real power system networks, the Venezuelan and Manitoba Hydro power grids. The transient stability status prediction algorithm demonstrated high prediction accuracy and confirmed its suitability for real-time stability assessment in realistic power system.

The purpose of the transient instability condition prediction is to enable activation of emergency control actions sufficiently at an early stage to prevent outages. The challenge is the selection of appropriate post-contingency corrective actions to avoid loss of syn-

chronism, based on the wide area measurements made within few tens of milliseconds after the fault. This is achievable as demonstrated by the two response based discontinuous control strategies were proposed in Chapter 5. The first scheme consists of a fuzzy logic based load shedding and generator tripping controller for the Venezuelan power system, which is a completely ac system dominated by 765 kV ac transmission system. The second scheme designed for the Manitoba Hydro power system uses the fast controllability of HVdc link to rapidly control the power supplied by the HVdc link after loss of a tie line exporting a large amount of power. This action prevents critical machines from losing synchronism in this low inertia system dominated by HVdc transmission. The sample simulation cases presented in the Chapter 5 demonstrated possibility of deploying response based wide area control systems for preserving transient stability after a large disturbance.

6.2 Contributions

The main contributions of the research work presented in this thesis are as following:

- Ascertaining that the magnitudes of bus voltage phasors, taken immediately after clearing a fault can be used to predict the transient stability status after the fault. This finding is an alternative to the traditional approach of using generator rotor angles for determining transient instabilities.
- Development of an algorithm for predicting the transient stability status of a power system after being subjected to a fault based on the SVM classification technique.

- Verification of the performance of the proposed transient stability prediction approach by applying it to various test systems, including two large power systems of contrasting characteristics.
- Investigation of the sensitivity of the proposed transient stability prediction scheme to verity of conditions such as asymmetrical faults, voltage sensitive loads, network topology changes and measurement noise.
- Development and demonstration of a novel wide area synchronized measurement based emergency control scheme to enhance the transient stability of the Venezuelan power system under an impending transient instability condition. The proposed fuzzy logic based load shedding and generator tripping scheme highlighted the importance of the transient stability status prediction as an early trigger for such emergency control.
- Development and demonstration of a response based HVdc reduction scheme for enhancing the transient stability of the Manitoba Hydro power system after subjecting to prolong fault affecting the tie line flows. The control actions are analogous to the existing event based special protection scheme, but decisions are made based on the phasor measurements and triggered by the transient stability status prediction scheme.

These contributions have led to the following publications in journals and conferences:

- **F. R. Gomez**, A. D. Rajapakse, U. Annakkage, and I.T. Fernando, “Support Vector Machine-Based Algorithm for Post-Fault Transient Stability Status Prediction

Using Synchronized Measurements". *IEEE Transactions on Power Systems*, Nov. 2010, Vol. 21, Pages 1856-1863.

- A. D. Rajapakse, **F. R. Gomez**, K. Nanayakkara, P. A. Crossley, and V.T. Terzija, "Rotor angle instability prediction using post-disturbance voltage trajectories," *IEEE Transactions on Power Systems*, vol. 25, no. 2, pp. 947–956, May 2010.
- **F. R. Gomez**, A. D. Rajapakse and U. Annakkage, "Transient Stability Assessment Algorithm based on Post-Fault Recovery Voltage Measurements". *IEEE Electrical Power and Energy Conference 2009*, Montreal, Quebec, Canada, October 2009.
- A. D. Rajapakse, **F. R. Gomez**, O.M.K.K. Nanayakkara, P.A. Crossley, and V.V. Terzija, "Rotor Angle Stability Prediction Using Post-Disturbance Voltage Trajectory Patterns", IEEE PES General Meeting, Calgary, Canada, July 26-30, 2009.

The following publication is currently under preparation:

- **F. R. Gomez**, A. D. Rajapakse, U. Annakkage, and I.T. Fernando, "Emergency Control Strategies for Transient Stability Enhancement based on Wide Area Synchronized Measurements", to be submitted to IEEE Transaction on Power Systems.

6.3 Suggestions for future research

The area of research presented in this thesis is still at infancy stage and there are a wide range of aspects that need to be further studied.

The application of this novel early transient stability prediction scheme relies on the synchronized measurement of voltage magnitudes at different locations of the system for using as predictors to a SVM based binary classifier. The prediction accuracy depends on the integrity of the input data and development of methods to deal with missing and erroneous data is essential. Such developments can be incorporated to PDC technology. A possible next step for confirming the accuracy and performance of this SVM based transient stability status prediction algorithm is to test the application on a Real Time Digital Simulator (RTDS). The power system with wide area measurement can be simulated on the real-time simulator and the signals can be sampled from the I/O of RTDS and fed to the predictor to assess its performance. More advanced testing can be done by feeding the synthetic phasor data generated by real time power system simulator to PMUs connected though a communication network. This modeling requires the determination of dynamic system equivalents to reduce the power system under study so that it could be modeled using a reasonable number of real-time simulation racks.

Additionally, to prevent the misclassification of marginally unstable cases and maximizing the accuracy of the proposed scheme, repeated predictions using an expanding data window could be implemented. This is on the assumption that use of more consecutive samples measured data for constructing the input vector results in more reliable prediction. However, this need to be verified through further studies.

In this thesis, load shedding, generation tripping and HVdc power reduction were employed as the emergency control strategies to improve the transient stability. In the case of the fuzzy logic based emergency control scheme, the simultaneous load shedding or generation tripping in different control areas of the system needs to be optimized. In case

of HVdc power control, instead of simply reducing, the HVdc power can be controlled in a manner helping to damp the power swings.

Other options for emergency control such as use of FACTS devices and controlled separation need to be investigated. It is interesting to perform an extensive study to compare and select the different emergency control strategies to secure the integrity of a power system after a catastrophic disturbance.

Appendix A

- Test system data: New England 39-bus system

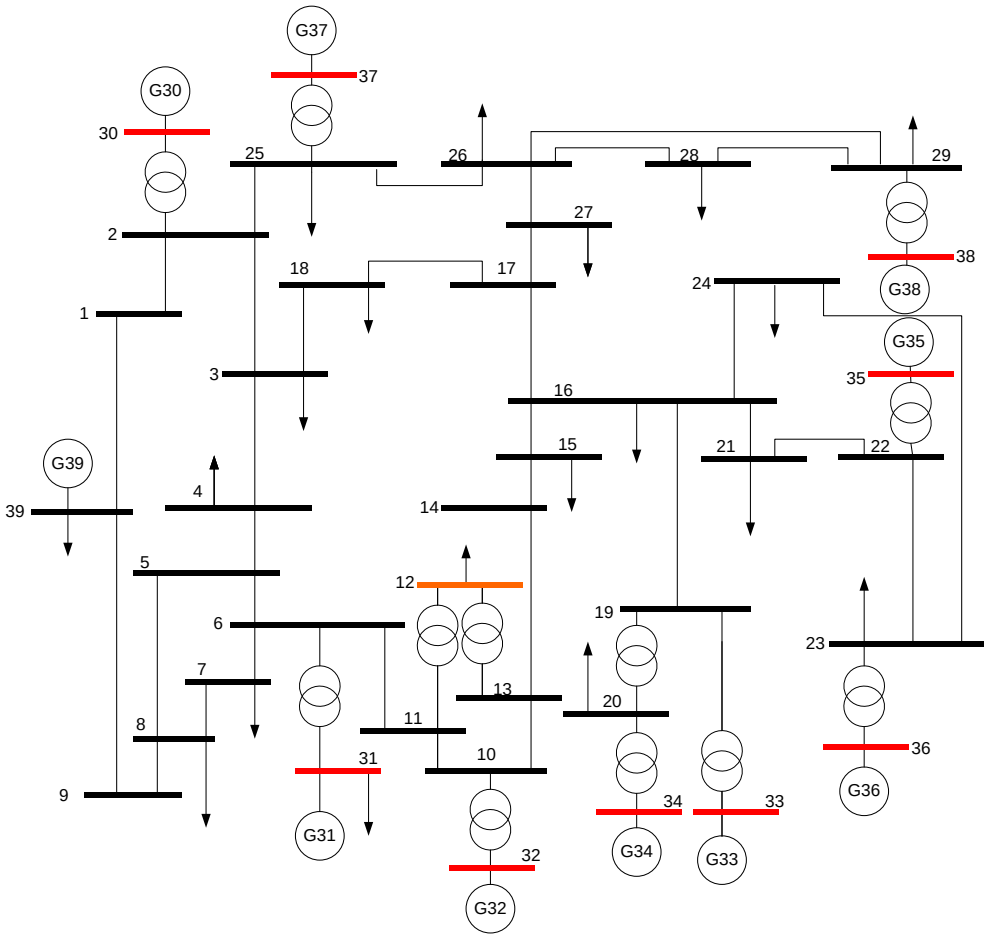

i. Power flow data for the 39-bus test system

Bus	Type	Voltage [PU]	Load		Generator	
			P(MW)	Q(MVAR)	P (MW)	Q (MVAR)
1	PQ	-	0.0	0.0	0.0	0.0
2	PQ	-	0.0	0.0	0.0	0.0
3	PQ	-	322.0	2.4	0.0	0.0
4	PQ	-	500.0	184.0	0.0	0.0
5	PQ	-	0.0	0.0	0.0	0.0
6	PQ	-	0.0	0.0	0.0	0.0
7	PQ	-	233.8	84.0	0.0	0.0
8	PQ	-	522.0	176.0	0.0	0.0
9	PQ	-	0.0	0.0	0.0	0.0
10	PQ	-	0.0	0.0	0.0	0.0
11	PQ	-	0.0	0.0	0.0	0.0
12	PQ	-	7.5	88.0	0.0	0.0
13	PQ	-	0.0	0.0	0.0	0.0
14	PQ	-	0.0	0.0	0.0	0.0
15	PQ	-	320.0	153.0	0.0	0.0
16	PQ	-	329.0	32.3	0.0	0.0
17	PQ	-	0.0	0.0	0.0	0.0
18	PQ	-	158.0	30.0	0.0	0.0
19	PQ	-	0.0	0.0	0.0	0.0
20	PQ	-	628.0	103.0	0.0	0.0
21	PQ	-	274.0	115.0	0.0	0.0
22	PQ	-	0.0	0.0	0.0	0.0
23	PQ	-	247.5	84.6	0.0	0.0
24	PQ	-	308.6	-92.0	0.0	0.0
25	PQ	-	224.0	47.2	0.0	0.0
26	PQ	-	139.0	17.0	0.0	0.0
27	PQ	-	281.0	75.5	0.0	0.0
28	PQ	-	206.0	27.6	0.0	0.0
29	PQ	-	283.5	26.9	0.0	0.0
30	PV	1.0475	0.0	0.0	250.0	-
31	PV	0.9820	9.2	4.6	521	-
32	PV	0.9831	0.0	0.0	650.0	-
33	PV	0.9972	0.0	0.0	632.0	-
34	PV	1.0123	0.0	0.0	508.0	-
35	PV	1.0493	0.0	0.0	650.0	-
36	PV	1.0635	0.0	0.0	560.0	-
37	PV	1.0278	0.0	0.0	540.0	-
38	PV	1.0265	0.0	0.0	830.0	-
39	PV	1.0300	1104.0	250.0	1000	-

ii. Branch data for the 39-bus test system respect to a base of 100 MVA

From Bus	To Bus	R (PU)	X (PU)	B (PU)	From Bus	To Bus	R (PU)	X (PU)	B (PU)
1	2	0.0035	0.0411	0.6987	13	14	0.0009	0.0101	0.1723
1	39	0.0010	0.0250	0.7500	14	15	0.0018	0.0217	0.3660
2	3	0.0013	0.0151	0.2572	15	16	0.0009	0.0094	0.1710
2	25	0.0070	0.0086	0.1460	16	17	0.0007	0.0089	0.1342
3	4	0.0013	0.0213	0.2214	16	19	0.0016	0.0195	0.3040
3	18	0.0011	0.0133	0.2138	16	21	0.0008	0.0135	0.2548
4	5	0.0008	0.0128	0.1342	16	24	0.0003	0.0059	0.0680
4	14	0.0008	0.0129	0.1382	17	18	0.0007	0.0082	0.1319
5	6	0.0002	0.0026	0.0434	17	27	0.0013	0.0173	0.3216
5	8	0.0008	0.0112	0.1476	21	22	0.0008	0.0140	0.2565
6	7	0.0006	0.0092	0.1130	22	23	0.0006	0.0096	0.1846
6	11	0.0007	0.0082	0.1389	23	24	0.0022	0.0350	0.3610
7	8	0.0004	0.0046	0.0780	25	26	0.0032	0.0323	0.5130
8	9	0.0023	0.0363	0.3804	26	27	0.0014	0.0147	0.2396
9	39	0.0010	0.0250	1.2000	26	28	0.0043	0.0474	0.7802
10	11	0.0004	0.0043	0.0729	26	29	0.0057	0.0625	1.0290
10	13	0.0004	0.0043	0.0729	28	29	0.0014	0.0151	0.2490

iii. Dynamic data

Gen No	T'_{do}(s)	T''_{do}(s)	T'_{qo}(s)	T''_{qo}(s)	H(s)	X_d(PU)	X_q(PU)	X'_d(PU)	X'_q(PU)	X''_d(PU)	X_l(PU)
30	10.2	0.05	1.5	0.06	42	0.1	0.069	0.031	0.008	0.025	0.0125
31	6.56	0.05	1.5	0.06	30.2	0.295	0.282	0.0697	0.17	0.05	0.035
32	5.7	0.05	1.5	0.06	35.8	0.2495	0.237	0.0531	0.0876	0.045	0.0304
33	5.69	0.05	1.5	0.06	28.6	0.262	0.258	0.0436	0.166	0.035	0.0295
34	5.4	0.05	0.44	0.06	26	0.67	0.62	0.132	0.166	0.05	0.054
35	7.3	0.05	0.4	0.06	34.8	0.254	0.241	0.05	0.0814	0.04	0.0224
36	5.66	0.05	1.5	0.06	26.4	0.295	0.292	0.049	0.186	0.04	0.0322
37	6.7	0.05	0.41	0.06	24.3	0.29	0.28	0.057	0.0911	0.045	0.028
38	4.79	0.05	1.96	0.06	34.5	0.2106	0.205	0.057	0.0587	0.045	0.0298

BUS	T_R	K_A	T_A	V_{RMAX}	V_{RMIN}	K_E	T_E	K_F	T_F	E_1	$S_E(E_1)$	E_2	$S_E(E_2)$
38	0	40	0.02	10.5	-10.5	1	1.4	0.03	1	4.257	0.62	5.676	0.85
37	0	5	0.02	1	-1	0	0.528	0.085	1.26	3.191	0.072	4.255	0.282
36	0	40	0.02	6.5	-6.5	1	0.73	0.03	1	2.8	0.53	3.8	0.74
35	0	5	0.02	1	-1	0	0.471	0.075	1.2	3.587	0.064	4.782	0.251
34	0	40	0.02	10	-10	1	0.785	0.03	1	3.927	0.07	5.236	0.91
33	0	5	0.06	1	-1	0	0.5	0.08	1	2.868	0.08	3.824	0.314
32	0	5	0.06	1	-1	0	0.5	0.08	1	2.342	0.13	3.123	0.34
31	0	6.2	0.05	1	-1	0	0.405	0.057	0.5	3.036	0.66	4.049	0.88
30	0	5	0.06	1	-1	0	0.25	0.04	1	3.54	0.08	4.728	0.26

Bibliography

[1] "U.S.-Canada Power System Outage Task Force. *Final Report on the August 14, 2003 Blackout in the United States and Canada: Causes and Recomendations*," April 2004.

[2] M. Zima, M. Larsson, P. Korba, C. Rehtanz and G. Andersson, "Design Aspects for Wide-Area Monitoring and Control Systems," *Proceedings of the IEEE,* vol. 93, pp. 980-996, 2005.

[3] S. C. Savulescu, *Real-time stability assessment in modern power system control centers*. Hoboken, N.J.: John Wiley & Sons, Inc., 2009.

[4] A. G. Phadke and J. S. Thorp, *Synchronized Phasor Measurements and Their Applications* 2008.

[5] P. Kundur, J. Paserba, V. Ajjarapu, G. Andersson, A. Bose, C. Canizares, N. Hatziargyriou, D. Hill, A. Stankovic, C. Taylor, T. Van Cutsem and V. Vittal, "Definition and classification of power system stability IEEE/CIGRE joint task force on stability terms and definitions," *Power Systems, IEEE Transactions on,* vol. 19, pp. 1387-1401, 2004.

[6] T. E. DyLiacco, "The Adeptive Realiability Control Systems," *IEEE Transactions on Power Appratus and Systems,* vol. 86, pp. 517-531, May 1967.

[7] L. H. F. a. K. Carlsen, "Operating under Stress and Strain," *IEEE Spectrum,* p. 48, 1978.

[8] P. Kundur, N. J. Balu and M. G. Lauby, *Power system stability and control*. New York: McGraw-Hill, 1994.

[9] P. M. Anderson, A. A. Fouad, Institute of Electrical and Electronics Engineers. and Knovel (Firm). (2003). *Power system control and stability (2nd ed.)*. Available: http://www.knovel.com/knovel2/Toc.jsp?BookID=2108

[10] A. G. Phadke, "Synchronized phasor measurements in power systems," *Computer Applications in Power, IEEE,* vol. 6, pp. 10-15, April 1993.

[11] "IEEE Standard for Synchrophasors for Power Systems," *IEEE Std C37.118-2005 (Revision of IEEE Std 1344-1995)*, pp. 0_1-57, 2006.

[12] G. Š. D.S.Kirschen, "Why Investments do not Prevent Blackouts," *The Electricity Journal,* vol. 17, pp. 29-36, 2004.

[13] F. F. Song, Bi, T.S., and Yang, Q.X, "Study on Wide Area Measurement System based Transient Stability Control for Power Systems," *IPEC Power Engineering Conference,* vol. 2, pp. 757-760 2005.

[14] D. Karlsson and S. Lindahl, "Wide area protection and emergency control," in *Power Engineering Society General Meeting, 2004. IEEE*, 2004, p. 5 Vol.1.

[15] H. Dongchen and V. Venkatasubramanian, "New Wide-Area Algorithms for Detection and Mitigation of Angle Instability using Synchrophasors," in *Power Engineering Society General Meeting, 2007. IEEE*, 2007, pp. 1-8.

[16] L. Wehenkel, T. Van Cutsem and M. Ribbens-Pavella, "An Artificial Intelligence Framework for On-Line Transient Stability Assessment of Power Systems," *Power Engineering Review, IEEE,* vol. 9, pp. 77-78, May 1989.

[17] L. Wehenkel, M. Pavella, E. Euxibie and B. Heilbronn, "Decision tree based transient stability method a case study," *Power Systems, IEEE Transactions on,* vol. 9, pp. 459-469, Feb. 1994.

[18] D. J. Sobajic and Y.-H. Pao, "Artificial Neural-Net Based Dynamic Security Assessment for Electric Power Systems," *Power Engineering Review, IEEE,* vol. 9, pp. 55-55, Feb. 1989.

[19] S. Rovnyak, S. Kretsinger, J. Thorp and D. Brown, "Decision trees for real-time transient stability prediction," *Power Systems, IEEE Transactions on,* vol. 9, pp. 1417-1426, Aug. 1994.

[20] Z. Qin, J. Davidson and A. A. Fouad, "Application of artificial neural networks in power system security and vulnerability assessment," *Power Systems, IEEE Transactions on,* vol. 9, pp. 525-532, Feb. 1994.

[21] L. S. Moulin, A. P. A. da Silva, M. A. El-Sharkawi and R. J. Marks, II, "Support vector machines for transient stability analysis of large-scale power systems," *Power Systems, IEEE Transactions on,* vol. 19, pp. 818-825, May 2004.

[22] C. Jensen, M. El-Sharkawi and R. Marks, "Power System Security Assessment Using Neural Networks: Feature Selection Using Fisher Discrimination," *Power Engineering Review, IEEE,* vol. 21, pp. 62-62, Nov 2001.

[23] A. E. Gavoyiannis, D. G. Vogiatzis, D. R. Georgiadis and N. D. Hatziargyriou, "Combined support vector classifiers using fuzzy clustering for dynamic security assessment," in *Power Engineering Society Summer Meeting, 2001. IEEE*, 2001, pp. 1281-1286 vol.2.

[24] G. C. Ejebe, C. Jing, J. G. Waight, V. Vittal, G. Pieper, F. Jamshidian, P. Hirsch and D. Sobajic, "Online dynamic security assessment in an EMS," *Computer Applications in Power, IEEE,* vol. 11, pp. 43-47, 1998.

[25] P. W. S. a. M. A. Pai, *Power System Dynamics and Stability,* 1997.

[26] "TSAT (Transient Security Assessment Tool) Manual," *Powertech Labs Inc.*, 2004.

[27] S. P. T. I. PTI. (2007, PSS/E Program Operation Manual.

[28] P. M. Anderson, *Analysis of faulted power systems*. New York: IEEE Press, 1995.

[29] L. L. Grigsby, *Power System Stability and Control*: CRC Press, 2007.

[30] M. Pavella, D. Ernst and D. Ruiz-Vega, *Transient stability of power systems : a unified approach to assessment and control*. Boston: Kluwer Academic Publishers, 2000.

[31] A. Rahimi and G. Schaffer, "Power System Transient Stability Indexes for On-Line Analysis of ``Worst-Case" Dynamic Contingencies," *Power Engineering Review, IEEE,* vol. PER-7, pp. 44-45, 1987.

[32] Y. Xue, T. Van Cutsem and M. Ribbens-Pavella, "A simple direct method for fast transient stability assessment of large power systems," *Power Systems, IEEE Transactions on,* vol. 3, pp. 400-412, 1988.

[33] Y. Xue, T. Van Custem and M. Ribbens-Pavella, "Extended equal area criterion justifications, generalizations, applications," *Power Systems, IEEE Transactions on,* vol. 4, pp. 44-52, 1989.

[34] M. A. Pai, *Energy function analysis for power system stability*. Boston: Kluwer Academic Publishers, 1989.

[35] A. L. Bettiol, Y. Zhang, L. Wehenkel and M. Pavella, "Transient stability investigations on a Brazilian network by SIME," in *Advances in Power System Control, Operation and Management, 1997. APSCOM-97. Fourth International Conference on (Conf. Publ. No. 450)*, 1997, pp. L1-L6 vol.1.

[36] S. Abe, *Support vector machines for pattern classification*. London: Springer, 2005.

[37] K. Chen and L. Wang, *Trends in neural computation*. Berlin ; New York: Springer, 2007.

[38] V. S. Cherkassky and F. Mulier, *Learning from data : concepts, theory, and methods*, 2nd ed. Hoboken, N.J.: IEEE Press : Wiley-Interscience, 2007.

[39] C. J. C. Burges, "A tutorial on Support Vector Machines for Pattern Recognition," *Kluwer Acedemic Publishers*, 1998.

[40] P. M. Anderson and B. K. LeReverend, "Industry experience with special protection schemes," *Power Systems, IEEE Transactions on*, vol. 11, pp. 1166-1179, 1996.

[41] Y. Ohura, M. Suzuki, K. Yanagihashi, M. Yamaura, K. Omata, T. Nakamura, S. Mitamura and H. Watanabe, "A predictive out-of-step protection system based on observation of the phase difference between substations," *Power Delivery, IEEE Transactions on*, vol. 5, pp. 1695-1704, 1990.

[42] C. W. Taylor, D. C. Erickson, K. E. Martin, R. E. Wilson and V. Venkatasubramanian, "WACS-Wide-Area Stability and Voltage Control System: R&D and Online Demonstration," *Proceedings of the IEEE*, vol. 93, pp. 892-906, 2005.

[43] G. G. Karady, A. A. Daoud and M. A. Mohamed, "On-line transient stability enhancement using multi-agent technique," in *Power Engineering Society Winter Meeting, 2002. IEEE*, 2002, pp. 893-899 vol.2.

[44] V. Vittal, W. Kliemann, Y. X. Ni, D. G. Chapman, A. D. Silk and D. J. Sobajic, "Determination of generator groupings for an islanding scheme in the Manitoba Hydro system using the method of normal forms," *Power Systems, IEEE Transactions on*, vol. 13, pp. 1345-1351, 1998.

[45] I. Kamwa, S. R. Samantaray and G. Joos, "Development of Rule-Based Classifiers for Rapid Stability Assessment of Wide-Area Post-Disturbance Records," *Power Systems, IEEE Transactions on*, vol. 24, pp. 258-270, 2009.

[46] A. D. Rajapakse, F. R. Gomez, K. Nanayakkara, P. A. Crossley and V. T. Terzija, "Rotor Angle Instability Prediction Using Post-Disturbance Voltage Trajectories," *IEEE PES Transactions on Power Systems*, 2009.

[47] S. M. Rovnyak, C. W. Taylor and Y. Sheng, "Decision trees using apparent resistance to detect impending loss of synchronism," *Power Delivery, IEEE Transactions on*, vol. 15, pp. 1157-1162, 2000.

[48] N. Amjady and S. F. Majedi, "Transient Stability Prediction by a Hybrid Intelligent System," *Power Systems, IEEE Transactions on*, vol. 22, pp. 1275-1283, 2007.

[49] K. Yamashita and H. Kameda, "Out-of-step prediction logic for wide-area protection based on an autoregressive model," in *Power Systems Conference and Exposition, 2004. IEEE PES*, 2004, pp. 307-312 vol.1.

[50] B. Jayasekara and U. D. Annakkage, "Derivation of an Accurate Polynomial Representation of the Transient Stability Boundary," *Power Systems, IEEE Transactions on,* vol. 21, pp. 1856-1863, 2006.

[51] I. C. Report, "Dynamic Performance Characteristics of North American HVDC Systems for Transient and Dynamic Stability Evaluations," *Power Apparatus and Systems, IEEE Transactions on,* vol. PAS-100, pp. 3356-3364, 1981.

[52] I. Kamwa, R. Grondin and Y. Hebert, "Wide-area measurement based stabilizing control of large power systems-a decentralized/hierarchical approach," *Power Systems, IEEE Transactions on,* vol. 16, pp. 136-153, 2001.

[53] M. G. Adamiak, A. P. Apostolov, M. M. Begovic, C. F. Henville, K. E. Martin, G. L. Michel, A. G. Phadke and J. S. Thorp, "Wide Area Protection; Technology and Infrastructures," *Power Delivery, IEEE Transactions on,* vol. 21, pp. 601-609, 2006.

[54] K. E. Martin, "Synchrophasor Standards Development - IEEE C37.118 & IEC 61850," in *System Sciences (HICSS), 2011 44th Hawaii International Conference on*, 2011, pp. 1-8.

[55] A. G. Phadke and J. S. Thorp, *Computer Relaying for Power Systems*. New York: Wiley, 1994.

[56] A. G. Phadke and B. Kasztenny, "Synchronized Phasor and Frequency Measurement Under Transient Conditions," *Power Delivery, IEEE Transactions on,* vol. 24, pp. 89-95, 2009.

[57] C. W. Taylor, "The future in on-line security assessment and wide-area stability control," in *Power Engineering Society Winter Meeting, 2000. IEEE,* 2000, pp. 78-83 vol.1.

[58] M. Shahraeini, M. H. Javidi and M. S. Ghazizadeh, "Comparison Between Communication Infrastructures of Centralized and Decentralized Wide Area Measurement Systems," *Smart Grid, IEEE Transactions on,* vol. 2, pp. 206-211, 2011.

[59] E. E. Osuna, "Support vector machines : training and applications," Thesis Ph. D. --Massachusetts Institute of Technology Sloan School of Management 1998., 1998.

[60] V. Kecman, *Learning and soft computing : support vector machines, neural networks, and fuzzy logic models*. Cambridge, Mass.: MIT Press, 2001.

[61] K. Nanayakkara, "Test Network with Multiple HVDC Infeeds for Wide Area Protection Studies," Thesis Master of Science., Department of Electrical and Computer Engineering, University of Manitoba, 2009.

[62] X. Qing-Qiang, J. Suonan and G. Yao-Zhong, "Real-time measurement of mean frequency in two-Machine system during power swings," *Power Delivery, IEEE Transactions on,* vol. 19, pp. 1018-1023, 2004.

[63] W. Hongbin, C. Hsiao-Dong and C. Byoung-Kon, "Slow voltage recovery response of several load models: Evaluation study," in *Power and Energy Society General Meeting - Conversion and Delivery of Electrical Energy in the 21st Century, 2008 IEEE*, 2008, pp. 1-6.

[64] "Load representation for dynamic performance analysis [of power systems]," *Power Systems, IEEE Transactions on*, vol. 8, pp. 472-482, 1993.

[65] P. S. SrinivasaReddy, L. Ramesh, S. P. Chowdhury and S. Chowdhury, "Power system PMU placement - a comparative survey report," in *Information and Communication Technology in Electrical Sciences (ICTES 2007), 2007. ICTES. IET-UK International Conference on*, 2007, pp. 249-255.

[66] I. Kamwa and R. Grondin, "PMU configuration for system dynamic performance measurement in large multi-area power systems," in *Power Engineering Society Summer Meeting, 2002 IEEE*, 2002, p. 239 vol.1.

[67] L. H. Fink, "Emergency Control Practices A report prepared for the System Control Subcommittee of the Power System Engineering Committee by the Task Force on Emergency Control," *Power Engineering Review, IEEE*, vol. PER-5, pp. 29-30, 1985.

[68] D. A. Pierre, "A Perspective on Adaptive Control of Power Systems," *Power Systems, IEEE Transactions on*, vol. 2, pp. 387-395, 1987.

[69] F. R. Gomez, A. D. Rajapakse, U. D. Annakkage and I. T. Fernando, "Support Vector Machine-Based Algorithm for Post-Fault Transient Stability Status Prediction Using Synchronized Measurements," *Power Systems, IEEE Transactions on*, vol. PP, pp. 1-1, 2010.

[70] D. Driankov, H. Hellendoorn and M. Reinfrank, *An introduction to fuzzy control*, 2nd, rev. ed. Berlin ; New York: Springer, 1996.

[71] G. Chen and T. T. Pham, *Introduction to fuzzy sets, fuzzy logic, and fuzzy control systems*. Boca Raton, FL: CRC Press, 2001.

[72] S. N. Sivanandam, S. Sumathi and S. N. Deepa, *Introduction to fuzzy logic using MATLAB*. Berlin ; New York: Springer, 2007.

[73] C. C. Diemond, J. P. Bowles, V. Burtnyk, M. A. Lebow, E. G. Neudorf, D. Povh, E. C. Starr, C. W. Taylor and R. A. Walling, "AC-DC economics and alternatives-1987 panel session report," *Power Delivery, IEEE Transactions on,* vol. 5, pp. 1956-1979, 1990.

[74] A. D. Rajapakse, F. Gomez, K. Nanayakkara, P. A. Crossley and V. V. Terzija, "Rotor Angle Instability Prediction Using Post-Disturbance Voltage Trajectories," *Power Systems, IEEE Transactions on,* vol. 25, pp. 947-956, 2010.

[75] I. T. Fernando, "Future HVDC System Performance - A Measure of Manitoba Hydro System Robustness to Triple Bipole Commutation Failure Resulting from AC Faults," Manitoba Hydro2008.